Stress singularities in classical elasticity–I: Removal, interpretation, and analysis

GB Sinclair

Department of Mechanical Engineering, Louisiana State University, Baton Rouge, LA 70803-6413

This review article has two parts, published in separate issues of this journal, which consider the stress singularities that occur in linear elastostatics. In the present Part I, after a brief review of the singularities that attend concentrated loads, attention is focused on the singularities that occur away from such loading, and primarily on 2D configurations. A number of examples of these singularities are given in the Introduction. For all of these examples, it is absolutely essential that the presence of singularities at least be recognized if the stress fields are to be used in attempts to ensure structural integrity. Given an appreciation of a stress singularity's occurrence, there are two options open to the stress analyst if the stress analysis is to actually be used. First, to try and improve the modeling so that the singularity is removed and physically sensible stresses result. Second, to try and interpret singularities that persist in a physically meaningful way. Section 2 of the paper reviews avenues available for the removal of stress singularities. At this time, further research is needed to effect the removal of all singularities. Section 3 of the paper reviews possible interpretations of singularities. At this time, interpretations using the singularity coefficient, or stress intensity factor, would appear to be the best available. To implement an approach using stress intensity factors in a general context, two types of companion analysis are usually required: analytical asymptotics to characterize local singular fields; and numerical analysis to capture participation in global configurations. Section 4 of the paper reviews both types of analysis. At this time, methods for both are fairly well developed. Studies in the literature which actually effect asymptotic analyses of specific singular configurations will be considered in Part II of this review article. The present Part I has 182 references. [DOI: 10.1115/1.1762503]

1 INTRODUCTION

1.1 Objective and scope

Stress singularities are not of the real world. Nonetheless, they can be a real fact of a stress analysis. Then it is essential to take them into account if the analysis is to be of any real use. The primary objective of this review is to assist in this regard. That is, in the first instance, to aid in the all-important task of recognition of a singularity's presence, then, in the second instance, to aid in removal or interpretation.

Throughout this review we take *stress singularities* as involving stresses which, in themselves, are unbounded. Specifically, we are concerned with when such singularities can occur in the linear elastic regime. This is a key regime since elastic response physically precedes plastic flow, so that introducing plasticity does not remove the singular character in any true sense.[1] To keep the scope of the article within reasonable limits, we further restrict attention to materials which are homogeneous, or piecewise so, and isotropic. We also focus on loading which is quasi-static. For such classical elasticity fields, two classes of singular configurations may be distinguished: those wherein singularities occur under concentrated loads, and those wherein they occur away from any concentrated loading. For either, it is important to recognize the presence of stress singularities and to appreciate their nature. In what follows we give examples of both, then turn our attention to the latter because it typically presents greater difficulties to the stress analyst.

1.2 Examples of stress singularities under concentrated loads

Concentrated loading configurations induce singularities directly by applying finite stress resultants (eg, forces, moments) over regions with vanishingly small areas (eg, points, lines). As such they may be termed *singular loads*: Table 1 exhibits the singular character of the stresses for a basic set of such loads.

Transmitted by Editorial Advisory Board Member R. C. Benson

[1]We expand on this point in Section 2.1.

Table 1. Basic singular loads of classical elasticity

Load type	3D stress state at load ($r\to 0$)	2D stress state at load ($r\to 0$)
Isolated force	ord(r^{-2})	ord(r^{-1})
Doublet state	ord(r^{-3})	ord(r^{-2})

In Table 1, r is the distance from the point of application of a singular load, and we have employed the ord notation. For a function $f(r)$, here this has

$$f(r)=\text{ord}(r^{-\gamma}) \quad \text{as} \quad r\to 0 \tag{1.1}$$

if

$$r^{\gamma}f(r)=c\neq 0 \quad \text{as} \quad r\to 0 \tag{1.2}$$

where γ and c are constants. The traditional large order O notation, in contrast, admits the possibility that $c=0$. Provided nonzero loads are being applied, c cannot be everywhere zero for the stresses in Table 1.

Examples of solutions for isolated force problems in three dimensions are: the point load in the infinite elastic medium by Kelvin (Thomson [1]), the normal point load on the surface of an elastic half-space of Boussinesq [2], the tangential point load on a half-space surface of Cerutti [3], and point loads within a half-space in Mindlin [4]. A convenient compendium of these closed-form solutions may be found in Poulos and Davis [5], Section 2.1. Inspection of these solutions demonstrates compliance with the order of singularity for point loads given in Table 1. Analogous solutions exist for isolated force problems in two dimensions, namely: the line load in an infinite elastic medium in Michell [6], the normal line load on the surface of an elastic half-space of Flamant [7], the tangential line load on a half-space surface in Boussinesq [8], and line loads within a half-space in Melan [9].[2] These may be found ibid, Section 2.2, and also demonstrate compliance with their singular order given in Table 1.

Examples of doublet states are indicated in Fig. 1. The first of these (Fig. 1*a*) illustrates a means of obtaining a concentrated moment M. This moment is produced by taking the limit as $\delta\to 0$ where δ is the horizontal separation of two vertical forces of magnitude $F=M/\delta$. The second arrangement (Fig. 1*b*) is a dual of the first and realizes no resultant force or moment in the limit as $\delta\to 0$, yet does have a nontrivial stress field if F is ord(δ^{-1}): As a consequence, it requires a generalization of the usual notion of a load in terming it a "singular load." The third arrangement (Fig. 1*c*) is a center of compression produced by superposing the second in an angular array: It, too, represents a load in a generalized sense. A precise definition of doublet states in general is given in Sternberg and Eubanks [11]. Some closed-form solutions for doublet states in three dimensions may be found in: Love [12] Article 132, Sternberg and Eubanks [11], Turteltaub and Sternberg [13], Chowdhury [14], and Chen [15]. Closed-form solutions for doublet states in two dimensions are available in Love [12] Article 152, and Timoshenko and Goodier [16] Articles 36 and 42. The stresses in all of these solutions comply with their respective orders of singularity given in Table 1.

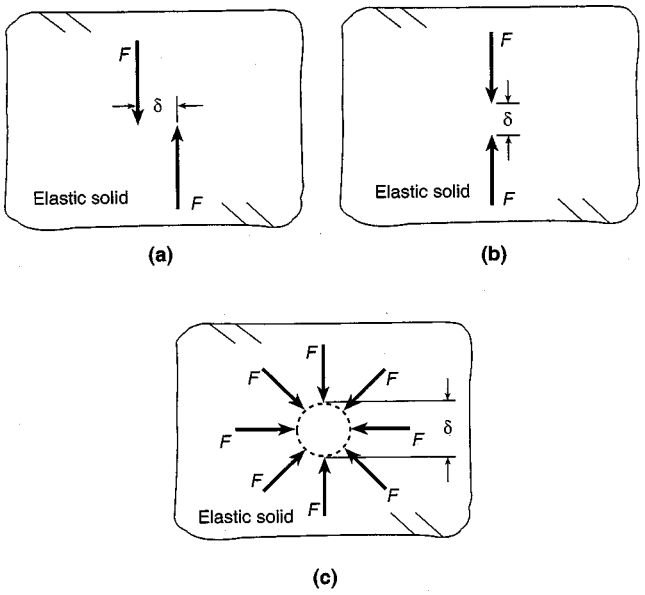

Fig. 1 Some limiting configurations for doublet states: *a*) concentrated moment, *b*) force doublet without a moment, *c*) center of compression

The nature of the singularities displayed in Table 1 is, to a degree, that expected. For a point force, integration of the tractions acting on the surface of a small sphere of radius r centered on the point of application produces a product of stresses with r^2: Hence the stresses can be expected to behave like r^{-2} if a finite force is to result in the limit as $r\to 0$. Similarly for a line load, one anticipates stresses which behave like r^{-1}. And the doublet states, being derivable by differentiation of corresponding isolated loads, then behave as r^{-3} and r^{-2} in three dimensions and two dimensions, respectively. However, some care needs to be exercised if these expectations are to be realized in the limit by a sequence of finite stress fields acting over regions of finite extent—a limiting process for producing singular loads that is physically appealing. Sternberg and Eubanks [11] gives a clear account of the sort of restrictions required on the finite stress distributions used in the limiting process: These restrictions have since been refined in Turteltaub and Sternberg [13]. In essence, Sternberg and Eubanks establish that it is insufficient to simply have the distributed fields be statically equivalent to the end stress resultant sought (as Kelvin originally proposed for his problem). If one merely makes this requirement, then it is possible, for example, to add a doublet state of the kind in Fig. 1*b* to a point load problem, thereby changing the dominant singularity of the latter without altering the force exerted. One means of avoiding this additional field for the point force example is to require all the distributed stresses in the underlying limiting sequence be unidirectional; alternative restrictions for the point load, as well as effective requirements for other singular loads, are given in Sternberg and Eubanks [11] and Turteltaub and Sternberg [13]. Provided proper attention is paid to the generating se-

[2]An error in one of the formulas given in Melan [9] is corrected in Kurshin [10].

quence of the distributed loads acting on successively smaller regions, all of the singular loads included in Table 1 have unique stress fields with singularities as indicated therein.

In practice, concentrated loads usually serve as Green's functions in stress analysis. That is, they are superposed to achieve a desired regular distribution of applied loads. Often, this superposition is undertaken via numerical analysis. A demonstration of their use in this way occurs in integral equation approaches, such as the boundary integral equation method which currently enjoys fairly wide application in elastic stress analysis. In this role, it is of value to understand the singular nature of the concentrated loads involved in order to design efficient quadrature schemes for their numerical integration. However, these integrations typically result in finite stresses. Then, one is not faced with the challenge of drawing physical inferences, with respect to structural integrity, from nonphysical singular fields. On other occasions, though, singular loads can be used to model highly localized loading, such as under a knife edge in the three-point-bend specimen of fracture mechanics (eg, at point P_1 in Fig. 2*a*). In this instance, if a line load is introduced, it is merely as one of a set of three which effect an applied moment for the crack. As such, it is not the feature of greatest interest, locally, with respect to potential failure—the crack tip is (P_2 in Fig. 2*a*).[3] Again, one is not faced with interpreting local fields at singular loads. On the other hand, one must attempt this task for the crack, with its classical, inverse-square-root, stress singularity. Indeed, in general this is the case for the second class of singular configurations recognized here. Accordingly we focus on stress singularities which occur away from any concentrated loading throughout the remainder of this review.

1.3 Examples of other stress singularities

Some illustrative examples of this class of singularity are depicted schematically in Fig. 2. The corresponding orders of stress singularity present are set out in Table 2.

The first example (Fig. 2*a*) is the aforementioned cracked elastic plate under three-point bending, with its attendant, inverse-square-root, stress singularity reflecting the stress intensification at the crack tip (ie, at P_2). For the case of a crack in a large elastic plate under transverse tension, such a singularity can be extracted from the corresponding solution for the elliptical hole on passing to the limit as the hole becomes a mathematically sharp slit. The fields required to take this limit were first provided in Kolossoff [17] (see also Kolossoff [18]), and subsequently derived in Inglis [19]. That the same singularity results for crack tips in general, and for the crack tip in the three-point-bend specimen of Fig. 2*a* in particular, can be discerned from Williams' seminal paper [20]. In this paper, the asymptotic character of elastic stresses in angular plates or wedges under extension is revealed: Letting the angle of the ''free-free'' wedge go to 2π in Williams [20] recovers singular stresses as in Table 2.

[3]If instead the stresses under the knife edge were of greatest concern, better models than a line load are available, as we demonstrate subsequently.

Table 2. Some elastic stress singularities away from singular loads

Singular point, Fig. 2 ($r=0$)	Local configuration description	Singular stresses at point ($r\to 0$)
P_2	Crack tip in three-point-bend specimen	ord($r^{-1/2}$)
P_2	Interface crack tip in bend specimen	ord($r^{-1/2}\cos(\eta \ln r)$) & ord($r^{-1/2}\sin(\eta \ln r)$), see Eq. (1.3) for η
P_3	Tire at pothole edge under icy conditions	ord($r^{-1/2}$)
P_3	Adhering nylon tire at pothole edge	ord($r^{-1/2}\cos(\eta \ln r)$) & ord($r^{-1/2}\sin(\eta \ln r)$), see Eq. (1.4) for η
P_4	Edge of piston ring pressed into cylinder wall	ord($r^{-0.23}$)
P_5	Reentrant corner in stress-free keyway	ord($Tr^{-1/3}$) ord($Fr^{-0.46}$) & ord($Fr^{-0.09}$)
P_6	Edge of adhering rubber tire on pavement	ord($r^{-0.41}$)
P_7	Circumference of an epoxy-steel interface	ord($r^{-1/3}$)
P_8	Edge of a rough heavy block on an elastic slab	ord($\ln r$)
P_9	Edge of a smooth steel chisel on a wooden block	ord($\ln r$)
P_{10}	Submodel node with displacement shape functions as boundary conditions	ord($\ln r$)

As a modification to the first example, we consider the plate now to be comprised of two distinct elastic materials instead of a single one. The two are perfectly bonded together on an interface extending straight ahead of the crack (indicated by the dashed line in Fig. 2*a*). Adding the further discontinuity of an abrupt change in material properties renders the crack-tip stress singularity more nonphysical, with the inverse square root having multipliers, $\cos(\eta \ln r)$ and $\sin(\eta \ln r)$, which oscillate an infinite number of times in the limit $r\to 0$ when $\eta \neq 0$. Herein η is a material constant given by

$$\eta = \frac{1}{2\pi}\ln\frac{\mu_1+\kappa_1\mu_2}{\mu_2+\kappa_2\mu_1} \tag{1.3}$$

where μ is the shear modulus, $\kappa = 3-4\nu$ or $(3-\nu)/(1+\nu)$ for plane strain or plane stress, ν being Poisson's ratio, and the subscripts distinguish the different materials on each side of the interface crack. Observe that if the materials are taken to be one and the same, $\eta = 0$ and there is no oscillatory multiplier, as in our original example. Otherwise, typically interface cracks have oscillatory, inverse-square-root, stress singularities, as first shown in Williams [21].

A related pair of examples concerns a tire, under light load, where it meets a relatively stiff pavement at the sharp edge of a pothole (a section through such an arrangement is sketched in Fig. 2*b*, wherein P_3 is the point of interest). If the pavement is icy, and thereby lubricated, the situation is as if the tire were an elastic half-space being indented by a flat, frictionless, rigid strip. The solution to this problem was first given in Sadowsky [22], and exemplifies the inverse-square-root stress singularity listed in Table 2. That the singular character here is the same as for the crack in a homogeneous material can be argued as follows. First we note that, for a

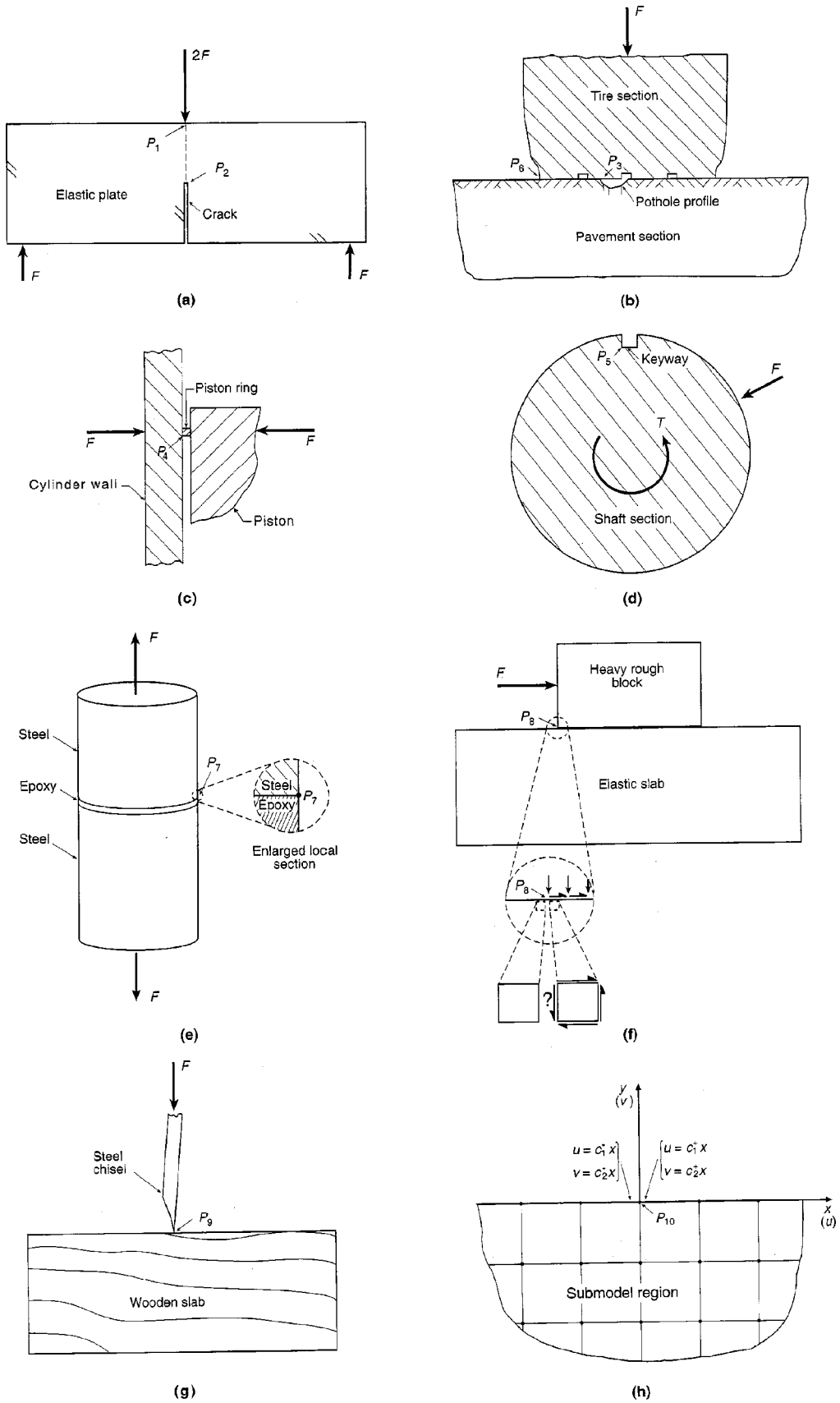

Fig. 2 Some singular configurations: *a*) three-point-bend test piece of fracture mechanics, *b*) section through a tire on a relatively rigid pavement, *c*) section through a piston with a ring pressed into a cylinder wall, *d*) section of a shaft with a stress-free keyway under torsion and lateral loading, *e*) adhesive butt joint under tension, *f*) rough heavy block sticking to an elastic base, *g*) steel chisel just starting to indent a wooden slab, *h*) displacement shape functions as submodel boundary conditions

2D elastic half-space, the constant displacement due to the rigid strip can be recovered by a rigid body translation. Hence, we need only consider homogeneous conditions under the strip, together with stress-free conditions outside the strip. But these conditions under the strip are the same as symmetry conditions. Thus the half-space can be reflected on itself to produce a full space with a pair of stress-free cracks outside of where the strip punch acts.

For the second of our examples concerning the arrangement in Fig. 2*b* at P_3, we consider the pavement to be dry and the tire to stick to it perfectly. Now the in-plane situation for the section of Fig. 2*b* is as if the tire were being indented by a flat, adhering, rigid strip. The solution to this problem was first furnished in Abramov [23], and contains the inverse-square-root stress singularity, with its oscillatory multipliers, listed in Table 2. This is the same singularity as for the interface crack, except that now η is given by Eq. (1.3) with $\mu_2 \to \infty$ therein. That is,

$$\eta = \frac{1}{2\pi} \ln \kappa \tag{1.4}$$

Recall that $\kappa = 3 - 4\nu$ for the plane strain state applicable here: So as to avoid $\eta = 0$, Table 2 specifies a nylon tire ($\nu = 0.4$) rather than rubber ($\nu = 0.5$) for this case of adhesive contact. Asymptotically, the configuration can be treated using the ''clamped-free'' conditions for a wedge of angle π in Williams [20], if one sets ''σ'' $= \nu$ in Eq. (17) therein so as to correspond to a state of plane strain. The same singularity results.

A further contact example is that of a lubricated piston ring pressed into a cylinder wall as indicated in Fig. 2*c*. This configuration is axisymmetric rather than being as previous examples which entail states of plane strain. However, as first argued in Zak [24], a plane strain analysis still applies. Then, if the ring is taken to be relatively rigid compared to the cylinder, the same inverse-square-root singularity results as for an indentation with a flat, frictionless, rigid strip (Fig. 2*c* at P_4). Alternatively, if the more realistic assumption is made that the ring is comprised of the same material as the cylinder, the weaker singularity of Table 2 results. This singularity can be identified by solving the pertinent eigenvalue equation in Dempsey and Sinclair [25]. It is weaker because now the deformation of the ring is being included.

For the example of a stress-free keyway in a shaft under torque T and transverse load F (Fig. 2*d*), multiple singularities are present (Table 2). For the torque, the singularity active at the 90° reentrant corner (ie, at P_5) is weaker than if a crack is subjected to torsion, having an exponent of 1/3 compared to 1/2. This singularity was first identified in Thomson and Tait [26], Section 710. For the transverse load, two singularities typically participate. The stronger one is associated with loading which is symmetric about the bisector of the angle at the reentrant corner, the weaker with antisymmetric. Both are weaker than the singularity at a crack, a reentrant corner of zero angle in effect. The two singularities for this right-angled reentrant corner are included in Brahtz [27]. Alternatively, they may be obtained using the ''free-free'' conditions in Williams [20], on taking a wedge angle of $3\pi/2$. In general, as the angle at a reentrant corner increases, singularity strength reduces. Eventually, when a stress-free corner opens all the way up to a half-space, singular stresses are removed.

The disappearance of stress singularities once corners are no longer reentrant need not be the case when the boundary conditions are mixed, as is demonstrated in our next example. This concerns the tire again (Fig. 2*b*), but now where it meets the pavement at its outside edge (ie, at P_6). If the tire adheres perfectly to the relatively rigid pavement, locally this configuration becomes a right-angled corner in plane strain with one face being free of stress, the other completely fixed. The singularity in this instance is characterized in Knein [28]. Alternatively, it may be obtained using the ''clamped-free'' conditions in Williams [20] for a wedge angle of only $\pi/2$, provided these are adapted to a state of plane strain. For rubber ($\nu = 0.5$), the stress singularity of Table 2 results (there is a minor round-off error in the singularity exponent in Knein [28]). While this is weaker than that of a crack, it is nonetheless quite comparable in strength.

A similar situation occurs for the butt joint under tension of Fig. 2*e*. Herein the points of interest are where the interface between the epoxy adhesive and steel adherend meets the outside free surface (eg, P_7). As for the piston ring, this configuration is axisymmetric but nonetheless plane strain analysis still applies. Again then, since steel is relatively rigid compared to epoxy, a ''clamped-free'' right-angled corner in plane strain is appropriate and can be treated via Williams [20]. Taking 3/8 as a reasonable estimate of Poisson's ratio for epoxy, this gives the singularity of Table 2. The reduction in strength here from that of the rubber corner is due to the lower value of ν. Indeed, there is no singularity for such corners when $\nu = 0$.

Our last three examples give rise to the weakest type of stress singularity in elasticity, the logarithmic singularity. The first example concerns a heavy rough block, under a lateral force, sticking to a horizontal elastic surface (Fig. 2*f*). If one assumes that the normal stresses produce a discontinuity in the surface shear (ie, at P_8, as indicated in the close-up), then a log singularity in the stresses occurs, with a coefficient that is proportional to the magnitude of the shear stress discontinuity. This result is given in Kolossoff [18]. Alternatively, it can be constructed using auxiliary fields to those in Williams [20]. These fields may be found in Dempsey and Sinclair [29]. While the normal stress discontinuity produces no stress singularity, any shear stress discontinuity on an elastic half-plane does. To see an indication of why this is so, consider the shear stress components on the two little square elements outlined by broken lines in the close-up of Fig. 2*f*. The left one is in force and moment equilibrium if it has no shears on its boundaries. The right one, constant shears. Where they meet, there is an incompatibility in shear stress which cannot be accommodated by any regular elasticity fields known to date.

The second example concerns a piece of wood, just starting to be indented but not yet cut, by a sharp chisel made of relatively rigid steel (Fig. 2*g*). Assuming the contact to be frictionless and ignoring any anisotropy in the wood, the

log-singularity stress field induced at the cutting edge (ie, at P_9) may be found in Sneddon [30], Section 48.4. Again, alternatively it can be constructed using the auxiliary fields in Dempsey and Sinclair [29]. This log singularity features a coefficient which depends on the chisel tip angle and is proportional to the elastic moduli of the wood. It also has a displacement field which is more physically applicable to initial knife-edge loading than that of a line load, being free of unbounded vertical displacement and overlapping horizontal ones.

The third example concerns the use of displacement shape functions as boundary conditions in submodeling in finite element analysis (as suggested in ABAQUS [31], and ANSYS [32]). Along a smooth submodel boundary, spurious log singularities can be introduced. An example involving four node elements is shown in Fig. 2*h*. Therein a log singularity occurs at the node at P_{10} whenever there is a discontinuity in the derivatives of either of the boundary displacements, u and v on $y=0$. That is, whenever the constants are such that $c_1^- \neq c_1^+$ or $c_2^- \neq c_2^+$. Fields are given in Sinclair and Epps [33].

1.4 What to do about stress singularities

The foregoing serves to demonstrate some of the variety of singular configurations and stress singularities possible in classical elasticity. The natural question which then arises is what is to be done about these and like configurations in attempting to ensure structural reliability? In the first instance, it is vital that the stress analyst at least recognize when a stress singularity is present.[4]

That there is a singularity present is not always immediately obvious. This is especially so in the stress analysis of actual engineering components, since frequently the complexity of such configurations necessitates numerical treatment, often via finite element analysis (FEA). Under these circumstances, one does not have available analytical solutions whereby singular character is detectable simply by observation. Nevertheless, it remains essential that the presence of any singular stress field be appreciated.

Consider the alternative. A scenario such as follows is then quite possible. On Monday, you complete a first FEA of a component subjected to cyclic loading. The maximum stresses found are a factor of two less than the endurance stress of the component's material. You conclude that the component has indefinite life, or at least long life. On Wednesday, you check your FEA with a refined grid. The peak stresses are now comparable to the endurance. You are in somewhat of a quandary as to how much life the part really has. Hence, on Friday you complete a further FEA on a still more refined mesh. Now you get stresses that are a factor of two greater than the endurance level. The component's life now is, apparently, distinctly limited. Life for you is somewhat disconcerting: Such a workweek does not make for a great weekend. More importantly, such a structural appraisal has nothing to do with the component's actual structural reliability: In the presence of a singularity, any sufficiently refined numerical analysis predicts failure when peak stresses are compared against some finite stress criterion, irrespective of what is physically happening. Under such circumstances, the participation of the singular stresses must first be recognized if any real use is to be made of the analysis. The main aim of this review is to aid in achieving such recognition.

That said, we next turn our attention to the important and challenging task of interpreting singular stress fields once it is apparent that they are active. In taking up this challenge, we begin by considering the simplifications made in classical elasticity since we expect singularities to be a product of the modeling in the theory, infinite stresses not being possible physically. Three such simplifying assumptions or linearizations can be identified in the classical theory of elasticity. The first linearization has that the relationship between stresses and strains is linear; that is, the stresses do not exceed the limits of elastic material response. The second linearization has that the strains depend linearly on the displacement gradients; that is, the displacement gradients are small. The third linearization has that all loads act on the undeformed shape throughout the entire loading process; that is, the deflections are small. The singular stress fields of classical elasticity are in violation of all three of these assumptions. Yet they do comply with all of the field equations of elasticity, as may be established by simply substituting them into these equations. This seemingly paradoxical situation results from the fact that, once an assumption is made in the theory of elasticity and equations so simplified, compliance with the assumption becomes unpoliced by the theory itself. This allows singular stress fields to comply with the field equations of classical elasticity, but remain in defiance of the underlying and unpoliced assumptions of elasticity. Such a situation requires some care if one is to be successful in interpreting these fundamentally wayward fields in a physically meaningful fashion.

To demonstrate the difficulty of interpreting results when they lie outside of admissible responses in a theory, consider the following beam example taken from Frisch-Fay [34]. On page one of his monograph, Frisch-Fay considers a horizontal cantilever beam of length 2.54 m (100 inches), with a bending stiffness of 2.87 Nm^2 (1000 $\mathrm{lbf\,in}^2$), subjected to a vertical concentrated end load of 4.45 N (1 lbf). Treating this beam within the context of classical beam theory for small deflections, Frisch-Fay obtains a prediction of a vertical tip deflection of 8.47 m (333 inches), or more than three times the beam's original length. This result suggests strains of the order of 300% and the possibility of gross yielding and even ductile rupture. Subsequently, on page 39 of Frisch-Fay [34], the same beam is analyzed within the context of nonlinear beam theory for large deflections. This analysis results in a vertical deflection of 2.06 m (81 inches), together with a horizontal deflection of 1.42 m (56 inches), and stress and strain fields that can now comply with the underlying as-

[4]We have not included, in the examples of Table 2, the yet stronger, ord(r^{-1}), singularity occurring at dislocations of the Volterra type (see, eg, Love [12], Appendix to Chapters VIII, IX, or Timoshenko and Goodier [16], Articles 34, 117). These fields are used as Green's functions, and by some theoreticians in an attempt to model microstructure. We omit discussion of them primarily because we expect users to be fully cognizant of the singular character present.

sumptions of the theory. The beam's length is essentially unchanged, in contrast to the earlier and potentially quite misleading prediction. It follows that, in this instance, all one can reasonably directly conclude from the prediction of classical, small-deflection, beam theory is that the deflection is large, too large to be quantitatively predicted by the theory. In essence, the same situation holds with respect to the singular stress fields of classical elasticity. Typically, they are correct qualitatively in implying large stresses, yet quantitatively they cannot be relied upon for the magnitude of these stresses. Other less direct interpretations must be made in order to quantify the implications of stress singularities.

The preceding example also illustrates a possible strategy for dealing with stress singularities: namely, improving the modeling in the underlying theory so that physically sensible outcomes are predicted. This is what nonlinear beam theory did in the example, albeit at the expense of turning a linear theory into a less tractable nonlinear one. Arguably, even at the expense of requiring greater analytical effort, such improvements in the physical modeling represent the ultimate of ''interpretations'' of singular stress fields. Accordingly, we consider various means that might effect such improvements next, in Section 2. Currently, not all configurations are amenable to complete amelioration of their singular stress fields via the various means identified. Hence, in Section 3 we review interpretations that can be made when singular behavior persists. Then we return to our primary intent of helping a stress analyst appreciate when a stress singularity can occur, and what its singular character can be. We begin this activity in Section 4 with a description of some methods, both analytical and numerical, for determining the nature and participation of stress singularities. We then close Part I of this review with some concluding remarks. Part II will follow with a review of contributions in the literature that have actually carried out characterizations of possible local singular stresses for a variety of elastic configurations. Throughout both parts, there are portions of the text that are tutorial in nature. Because a significant amount of today's stress analysis is carried out in industry and, in the main, by engineers with bachelor's degrees, a serious effort has been made to write these tutorial portions so that they can be understood by such stress analysts.

2 RIDDING CONFIGURATIONS OF NONPHYSICAL STRESS SINGULARITIES

2.1 Possible avenues for removing singularities

In some instances, removing singularities is straightforward. For example, the logarithmic singularities induced by the use of displacement shape functions as boundary conditions on submodels in finite element analysis (eg, P_{10} of Table 2 and Fig. 2*h*). These can be removed simply by fitting nodal displacements in the global FEA preceding the submodel with curves that are once continuously differentiable, then using intervening values in submodel boundary conditions (eg, by fitting a cubic spline as in Kondo and Sinclair [35]). In essence, all that is required here is an appreciation of the introduction of singularities by a poor choice of boundary conditions which have extraneous discontinuities. Then removing such discontinuities removes the singularities.

In other instances, smoothing discontinuities might also appear to remove singularities. For example, rounding the tip of a crack (as at P_2 of Table 2 and Fig. 2*a*), or rounding the corner in a keyway (as at P_5 of Table 2 and Fig. 2*d*), does produce finite stresses. This tactic for the latter example was suggested in Thomson and Tait [26] circa 1867, so such an approach is definitely not new. However, in instances such as these two wherein the stress singularities reflect real stress concentrations, such smoothing is questionable.

How so? For the example of the crack, certainly there are no singular stresses with any root radius that is greater than zero. However, we know that for a root radius that is zero we get the physical absurdity of infinite stresses. This raises the question of just how physically relevant are the finite but extremely large stresses that can result from extremely small root radii. Moreover, crack tips can have extremely small root radii, so the question is not moot. And similar concerns apply to rounding of the keyway corner.

The real removal of stress singularities requires that we can be confident that the unbounded stresses are being replaced by physically sensible ones. For the crack and like configurations, this really means we want finite sensible stresses when root radii actually go to zero. Only then can we be reasonably confident of the physical relevance of stress fields for root radii near but not zero.

At first thought, opportunities for achieving the removal of singularities when root radii are zero would appear to stem from relaxing the constraints implicit in the linearizations of classical elasticity listed earlier. Perhaps the most natural to consider in this regard is relaxing the assumption that the stresses remain below their elastic limits and, thereby, entertaining the possibility of plastic flow. Such a relaxation is quite often implied in the literature to be the appropriate recourse to take when singularities occur in elasticity. Indeed, if one insists upon perfectly plastic material response after elastic, unbounded stresses can be removed. Nonetheless, introducing plasticity does not really effect a resolution of the difficulties with elastic stress singularities, as we explain next.

To begin, introducing plasticity begs the question of how to remove singularities for configurations involving materials that are not ductile. Leaving this omission aside, even for ductile materials it is not really appropriate. To see this, consider what happens physically as loading progresses. At the outset, loads are small. In fact, for any actual configuration comprised of a material with $\sigma_Y > 0$, σ_Y being the yield stress, there exists a sufficiently light loading so that, physically, no yielding whatsoever is produced. Yet, if the configuration of interest has an elastic stress singularity, the theory predicts yielding for any nonzero load, no matter how small. Given the physical inappropriateness of the initial response of plastic fields derived from singular elastic ones, it is not reasonable to assume that these fields correct themselves as plastic flow increases. Accordingly, one cannot rely on these fields to accurately capture the physics of the situation.

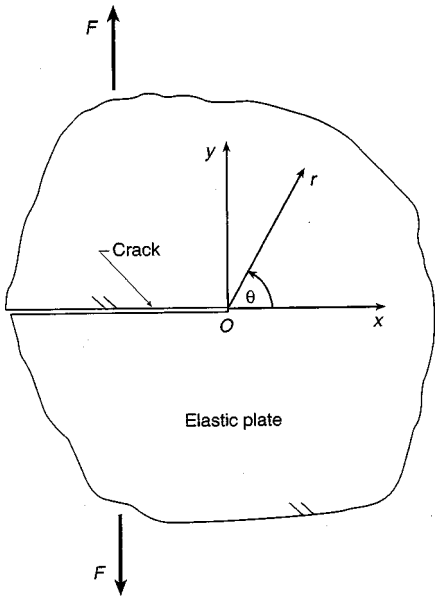

Fig. 3 Tensile crack in a hardening material

There is a further impediment to the use of such estimates of elasto-plastic response in structural integrity considerations. If the material being considered hardens at all after yielding, the stresses can be expected to remain singular, though with the strength of their singular behavior typically being abated. That this is so for the case of a crack is shown in Cherepanov [36], Hutchinson [37], and Rice and Rosengren [38], within the context of total deformation theory of plasticity. By way of specific example, we consider a tensile crack tip (Fig. 3) in a material which hardens in accordance with the model put forward in Ramberg and Osgood [39]. A law for uniaxial tensile stress σ_t versus tensile strain ε_t for such a model is

$$\frac{\varepsilon_t}{\varepsilon_Y}=\frac{\sigma_t}{\sigma_Y}+\frac{1}{500}\left(\frac{\sigma_t}{\sigma_Y}\right)^{n_\varepsilon} \tag{2.1}$$

wherein σ_Y continues as the yield stress and $\varepsilon_Y=\sigma_Y/E$ is the corresponding strain, with E being Young's modulus and n_ε the strain hardening exponent. Then, from Hutchinson [37] using the coordinates of Fig. 3, the normal stress and strain ahead of the crack within deformation theory behave in accordance with

$$\sigma_y=O(x^{-1/(n_\varepsilon+1)}),\quad \sigma_y\varepsilon_y=O(x^{-1}),\quad \text{as}\quad x\to 0^+ \tag{2.2}$$

on $y=0$. For $n_\varepsilon=1$, the classical inverse-square-root singularity of elasticity is recovered. For $1<n_\varepsilon<\infty$, the stress singularity is weaker but nonetheless persists. Hence it is futile to compare such stresses directly with finite material values such as the ultimate stress or the endurance stress (recall the previous discussion in the Introduction).

For the special and physically atypical case of perfect plasticity post yield ($n_\varepsilon\to\infty$), the crack-tip stresses are constrained to be finite but still cannot be compared in a meaningful way with material values. This is because the stresses always locally attain the limiting value set by the perfect plasticity irrespective of load level, provided it is not zero. Thus, if this value or a lesser stress is chosen as a failure criterion, failure is always predicted: If, on the other hand, a higher stress value is taken, failure is never predicted. Such stress-based predictions have no reliable correlation to what is physically happening. Furthermore, one cannot rely upon a strain criterion for this special type of material response, since the strains remain singular—see the second of Eqs. (2.2), from Hutchinson [37] (the same result may be found in Cherepanov [36] and Rice and Rosengren [38]).

Other geometries share the persistence of singular behavior when treated via deformation theory, though not all comply with the second of (2.2): see Chao and Yang [40], Rudge and Tiernan [41], Zhang and Joseph [42], and references therein. It follows that introducing yielding and plastic flow when a singularity is already present in the elastic response does not remove the singularity in any real sense.

Alternatively, one could consider relaxing the assumption of small displacement gradients and, thereby, entertaining the possibility of large strains. Again, though, initially it is always possible to have actual load levels which are light enough so that only small strains are induced physically, rather than large. This raises questions as to how important it is to include a large strain representation at such load levels. Observe, though, that in contrast to plasticity, the nonlinear contributions attending large strain representations *are present* at low load levels, even if they are relatively small. Consequently, absent analysis, it is not clear how much relaxing the small displacement gradient assumption may remove/alleviate singular stresses.

Turning to analysis then, the general finding is that large strain treatments do typically improve the physical appropriateness of singular fields, and even on occasion remove them, but nonetheless result in the persistence of a number of singularities. For the crack, results of this nature were first indicated in Wong and Shield [43], then established for more general circumstances in the two successive papers, Knowles and Sternberg [44,45]. Geubelle and Knauss [46] provides a recent large strain treatment of cracks demonstrating persistence of singular behavior, together with a review of the area.[5] There and elsewhere, the r^{-1} behavior as $r\to 0$ of the crack-tip stress-strain product is found to continue to be present (cf, the second of Eqs. (2.2)). On the other hand, a large strain treatment of the interface crack can remove the nonphysical oscillatory multiplier of the stress singularity noted in the Introduction for P_2 of Table 2 and Fig. 2*a* (see Geubelle and Knauss [47] and references therein). It can also remove the oscillatory nature of the singularity for the adhesive flat punch noted for P_3 of Table 2 and Fig. 2*b* (Knowles and Sternberg [48]). Furthermore, it does remove the entire singularity for the butt joint noted for P_7 of Table 2 and Fig. 2*e* (Ru [49]). However, it does not remove singularities for other bimaterial wedges (Ru [49]), nor for reentrant corners (Duva [50]). In sum, while introducing large strain analysis

[5]Some of these references term themselves "finite strain" treatments. This term is to underscore the contrast with the infinitesimal strains of classical elasticity: It does not imply bounded strains at the crack tip.

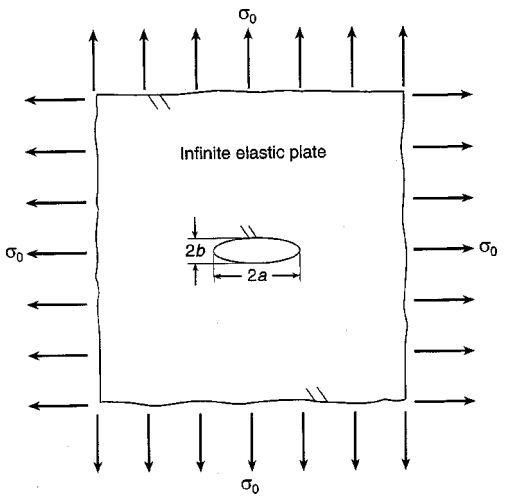

Fig. 4 Genesic Griffith crack configuration

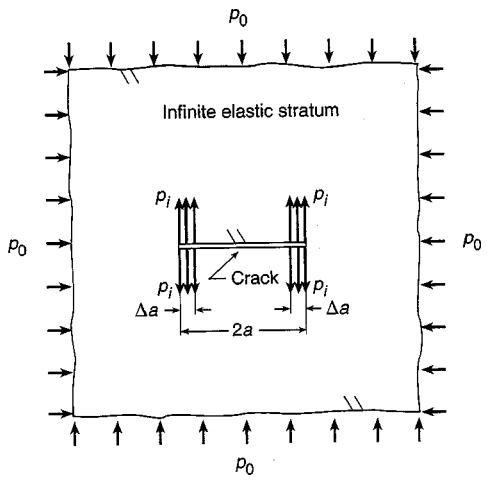

Fig. 5 Pressurized crack configuration

improves the physical appropriateness of singular fields to a degree, this relaxation fails to fully remove them.

The remaining option for relaxation within the simplifications of classical elasticity is the small deflection assumption. That is, removing the assumption that the loads act in their entirety on the undeformed state. Relaxation of this assumption can be performed by applying loads incrementally as deformation proceeds: In some sense, one may interpret nonlinear beam theory as an implementation of such an approach. Griffith was first to do this for a crack in an infinite plate under all-round tension σ_0 (Griffith [51]). He formed his crack of length $2a$ as the limit as the semiminor axis, b, of an elliptical hole goes to zero (Fig. 4). For classical elasticity, the maximum stress for the elliptical configuration used in the limiting process occurs at the ends of the major axis. This peak value σ_{max}, is given by (from Inglis [19])

$$\sigma_{max}=K_T\sigma_0, \quad K_T=2a/b \tag{2.3}$$

In (2.3), K_T is the stress concentration factor. On passing to the limit of a crack ($b\to 0$), K_T blows up reflecting the stress singularity so generated. In Griffith's incremental treatment wherein loading is gradually applied, the corresponding result is

$$K_T=\frac{E}{\sigma_0}\ln\left(\cosh\frac{2\sigma_0}{E}+\frac{a}{b}\sinh\frac{2\sigma_0}{E}\right) \tag{2.4}$$

where E remains Young's modulus and a state of plane stress is assumed.[6] An analogous treatment for the ellipse tending to a crack under uniaxial tension yields similar results. That is, stresses are ord($\ln b$) as $b\to 0$ instead of ord(b^{-1}) as in Eq. (2.3). Nevertheless, they are still singular.

A further example of the effects of relaxing the small deflection assumption may be obtained on revisiting the piston ring configuration in the Introduction (P_4 of Table 2 and Fig. 2*c*). Once the ring is allowed to deform along with the cylinder wall, the power singularity of Table 2 leads to interpenetration or overlapping of material outside of the original contact region. If, instead, the two are allowed to contact further without interpenetration, the power singularity is reduced to a log singularity which is similar to that for the chisel indentation configuration (P_9 of Table 2 and Fig. 2*g*). While this is a weaker singularity, nevertheless it is singular. Thus, this last relaxation also fails to really remove singular character once it exists in a classical elasticity solution.

All told, none of the foregoing relaxations fully remove stress singularities when they exist in classical elasticity. Not to say that elasto-plastic/large strain/large deflection analysis may not be appropriate on occasion once the removal is effected, but that by themselves such analyses do not effect the removal. Needed is a different approach.

What other options are there for improving the modeling so that stress singularities are replaced with physically sensible stresses? The answer lies in the boundary conditions enforced, both as direct requirements and as auxiliary constraints. We consider some problems where singular stresses are alleviated via this approach next.

2.2 Canceling crack-tip singularities: Barenblatt's approach

We begin our consideration of the effects of more physically appropriate boundary conditions with *cracked* configurations because of their central role in solid mechanics in general, and fracture mechanics in particular. For such configurations, it is possible to negate singularities produced by loading remote from the crack with those due to tractions acting on the crack flanks. Barenblatt credits Khristianovitch as being first to notice this in his paper with Zheltov in 1955. In Zheltov and Khristianovitch [54], a large rock stratum comprised of an oil bearing shale is considered with a view to determining when a pressurized flaw within the stratum might fracture. The stratum is under all-round pressure p_0 while the faces of the flaw near its tips are subjected to a relatively high internal pressure of p_i (Fig. 5). The configuration is treated as 2D and elastic. Then, if the extent of the regions over which p_i acts, Δa, is taken to be an appropriate fraction of the total

[6]Mansfield [52] derives the same result as Eq. (2.4). The actual theory used in all of these incremental elasticity analyses is an approximate rate-of-deformation theory (see Truesdell [53]).

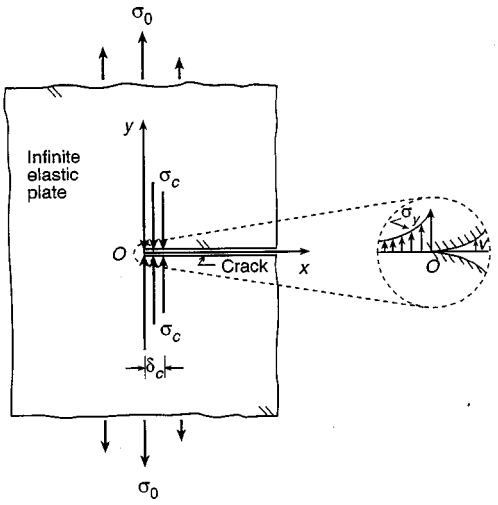

Fig. 6 Barenblatt's crack tip

flaw width, $2a$, the compressive stress singularity due to p_0 is cancelled by the tensile stress singularity due to p_i. More precisely, if

$$\frac{\Delta a}{2a}=\sin^2\left(\frac{\pi p_0}{4p_i}\right) \quad (p_i>p_0) \tag{2.5}$$

then there is no singularity for the configuration of Fig. 5.[7]

Subsequently, Barenblatt appreciated the fuller implications of Zheltov and Khristianovitch [54] (Barenblatt [56]): An extensive account of his resulting research, together with a comprehensive bibliography of related work, may be found in Barenblatt [57]. To extend the applicability of Zheltov and Khristianovitch's model, Barenblatt introduces cohesive normal stresses to replace the applied pressure p_i. Essentially, he argues as follows:

i) that the heights of cracks are small relative to their lengths so that they can be approximated by mathematically-sharp slits.
ii) that under such circumstances, the immediate proximity of the crack flanks at the crack tip ensures that intermolecular cohesive stresses act between the flanks.
iii) that the distribution of such cohesive stresses can be adjusted so that the corresponding compressive singular stress field completely negates any tensile singular stress field due to far-field loading.

Barenblatt assumes that the extent of the near-tip zone in which cohesive stresses are applied is small relative to the overall crack length. Indeed, in a first implementation of his ideas for a specific crack configuration in Barenblatt [57], he considers a semi-infinite crack with a finite cohesive zone (Fig. 6): Hence, in effect, his cohesive zone is infinitesimal compared to the crack length. Even so, the cancellation of singularities can be effected, as shown next.

First, take rectangular Cartesian coordinates x, y, with origin O at the crack tip, as in Fig. 6. Then let σ_0 be representative of the applied far-field tensile traction parallel to the y-axis: These tractions need not be uniform but are to be symmetric about $y=0$. Next, define the coefficient of the singularity due to σ_0, the stress intensity factor K_{I}, in accordance with usual practice. To wit,

$$K_{\mathrm{I}}=\lim_{x\to 0^-}\sqrt{2\pi x}\,\sigma_y \Big|_{y=0} \tag{2.6}$$

wherein σ_y is the normal stress component in the y-direction induced by σ_0 alone. Now apply a pair of tensile line loads to the crack flanks which are equal and opposite. These line loads tend to close the crack. If their strength is F per unit thickness and they act on the crack flanks at a distance x from the crack tip, the associated stress intensity factor, K_{I}', is negative and given by (Tada, Paris, and Irwin [55], p 3.6)

$$K_{\mathrm{I}}'=-F\sqrt{\frac{2}{\pi x}} \tag{2.7}$$

Introducing cohesive stresses $\sigma_c=\sigma_c(x)$ by replacing F by $\sigma_c dx$, then integrating, gives the negative stress intensity induced by the closing tractions: Equating the result to K_{I}, the factor due to the far-field loading σ_0, then renders the configuration singularity free. That is, there is no crack-tip singular stress field if

$$K_{\mathrm{I}}=\sqrt{\frac{2}{\pi}}\int_0^{\delta_c}\frac{\sigma_c dx}{\sqrt{x}} \tag{2.8}$$

where δ_c is the extent of the cohesive zone. Under this condition, the crack opening profile forms a cusp (see close-up of Fig. 6), with a crack opening displacement, ν on $y=0$ $(x>0)$, of the form

$$\nu\Big|_{\substack{y=0\\x>0}}=\frac{1+\kappa}{6\mu}\sigma_c\Big|_{x=0}\left[\left(\frac{x^3}{L}\right)^{1/2}+O(x^{5/2})\right] \quad \text{as } x\to 0^+ \tag{2.9}$$

wherein μ and κ are as previously (Eq. (1.3) et seq), and L is a normalizing length. The companion tensile stress ahead of the crack tip is given by

$$\sigma_y\Big|_{\substack{y=0\\x<0}}=\sigma_c\Big|_{x=0}\left[1-\left(\frac{|x|}{L}\right)^{1/2}+O(x^{3/2})\right] \quad \text{as } x\to 0^- \tag{2.10}$$

Clearly the crack-tip stress of Eq. (2.10) is free of singularities.

In addition to introducing cohesive stresses and assuming the region over which they act is small, Barenblatt makes a further ad hoc assumption regarding their distribution. This second assumption has that the maximum possible value of the right-hand side of Eq. (2.8) at failure does not depend upon the applied loading σ_0, and is always the same for a given material. He terms the right-hand side of Eq. (2.8) at failure a material's ''modulus of cohesion'' to reflect his assumption that it is a material property. This simplifying assumption obviates the need to determine explicitly the distri-

[7]The result in Eq. (2.5) follows directly from the singularity coefficients given in Tada, Paris, and Irwin [55] on pp 5.1, 5.13.

bution of cohesive stresses within the cohesive zone, not an easy task at the time of Barenblatt [56,57]. However, it has two serious drawbacks.

First, an immediate consequence of the assumption is that the stress intensity factor at fracture due to any applied loading such as σ_0 is also a material property, because it equals in magnitude that due to cohesive stresses. Essentially, therefore, the stress intensity factor due to applied loading becomes the key parameter controlling fracture. This is the *same fracture criterion* as used in models where *singularities are present* (see subsequent Sections 3.1 and 3.3).[8] Hence, while Barenblatt does indeed cancel singularities for cracks by introducing the concept of cohesive crack-flank stresses, the manner in which he does so leads to an approach which is equivalent to that practiced when singularities are active as far as fracture goes. Accordingly, Barenblatt's approach cannot realize any practical improvement in fracture prediction as a result of negating crack-tip stress singularities.

Second, the assumption is not realistic. To explain, consider its analogue in elasticity in general. Taking the stress intensity factor at failure resulting from cohesive stresses as a material property would be akin to taking local stress resultants in elasticity as material properties. This is not so. In elasticity, it is the elastic moduli that are the material properties. While local stress resultants can depend on the values of such material properties, they can also depend on loading and geometry and so are not material properties themselves. With cohesive stresses, then, it is the cohesive stress-separation laws that are material properties, not the stress intensity factors that can attend these laws.

It is possible to extend Barenblatt's approach and cancel singularities with cohesive stresses in other otherwise singular configurations, albeit with the same drawbacks. For example, the keyway configuration in the Introduction (P_5 of Table 2 and Fig. 2*d*). It is not clear, though, how it could be extended to all of the other examples in the Introduction.

In sum to date then, modifying the field equations of elasticity would not seem to offer any real means of removing stress singularities. On the other hand, what we learn from Barenblatt [57] is that incorporating cohesive stresses into boundary conditions can remove singular behavior. Cohesive stresses have also been used in this way to render models of dislocations free of singularities: Such models have been put forward in Peierls [60] and other papers (see Hirth and Lothe [61], Chapter 8). It would therefore appear that cohesive stresses might play a major role in the alleviation of singularities. Moreover, cohesive stresses are fundamental to solid mechanics, being the underlying source of constitutive relations. In contrast, it is not obvious that there is any fundamental justification for making assumptions regarding their distributions. Consequently, we next look to consider an approach for including cohesive stress action without such assumptions.

[8]Willis [58] and Goodier [59] provide alternative arguments that, as a result of his assumptions, Barenblatt's approach reduces to the same as for cracks with singularities present.

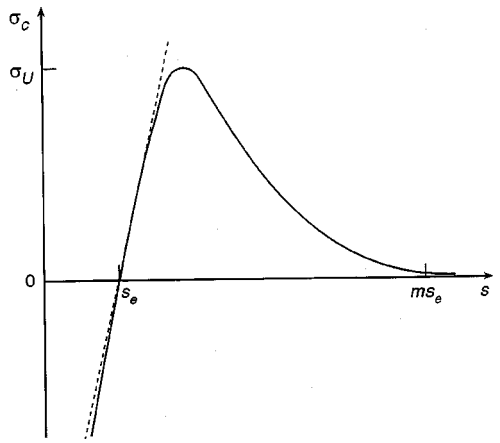

Fig. 7 Schematic of cohesive stress-separation law

2.3 Removing singularities via boundary conditions: Introducing cohesive stresses

In the approach adopted here, we endorse Barenblatt's argument that when surfaces come into extremely close proximity with one another, cohesive stresses have to act. We also follow Barenblatt in taking this interatomic action to be modeled with boundary conditions in continuum mechanics, thereby facilitating analysis. We do not, though, accept any of Barenblatt's assumptions concerning cohesive stress distributions. Rather, we introduce cohesive stresses via cohesive stress-separation laws and let these laws interact with the configuration of interest to determine cohesive stress distributions. Initially, we treat cracks with the approach, then we treat other singular configurations.

To begin, the nature of the cohesive stresses to be used merits further discussion. A *cohesive stress-separation law* for the normal stress at a single point on the surface of one elastic half-space as it is being removed from a second is sketched in Fig. 7. The initial response there exhibits a steep, nearly linear, increase in cohesive stress σ_c with separation s above the equilibrium value s_e. Thus, as s first exceeds s_e,

$$\sigma_c = k_e(s - s_e) \tag{2.11}$$

where k_e is the separation stiffness near equilibrium (the dashed line slope in Fig. 7). After reaching an ultimate value σ_U, σ_c gradually decays to zero as s becomes large. The overall character of the cohesive stress versus separation response is similar to that for the attractive force versus separation response for an isolated pair of atoms or molecules. In fact, physically it is the result of an integration or combination of such force-separation responses.

Carrying out such integrations via first-principle calculations is a challenging analytical task. However, for the first part of the curve—the linear stress-separation law—we can simply estimate the response of the accumulation of atoms or molecules directly. To do this, we obtain and fit the bulk response in experiments so as to back out cohesive law stiffnesses. For example, to use a uniaxial tension test to determine k_e of Eq. (2.11), reconsider Fig. 2*e* with the epoxy replaced by linear springs that are supposed to replicate the

initial cohesive law for steel. Then matching the response from the springs with that for a solid steel bar gives

$$k_e = E/s_e \tag{2.12}$$

For Fig. 2*e*, E would be Young's modulus for steel: In general, E is Young's modulus for whatever material is involved. Hence for uniaxial tension, our initial cohesive law is Eq. (2.11) with k_e as in Eq. (2.12). A consequence of this means of estimating k_e is that the initial cohesive law passes what might be termed a ''patch test'' and is consistent with the surrounding continuum.

The foregoing is a possible, even if somewhat crude, procedure for estimating k_e in the elastic regime since material defects in bulk specimens do not have a marked influence on response in this regime. At higher stresses, though, we cannot employ such an inverse approach because material defects do produce significant effects. For present purposes, however, the remainder of the curve is not critical since we are primarily concerned with elastic response. Accordingly, we adopt the highly idealized assumption of a perfect, defect-free, brittle material. Then there do exist estimates from solid-state physics of a material's ultimate stress (see, eg, Cherepanov [62], p 36, which gives $\sigma_U \approx E/10$). We can also set the area under the curve—the work of adhesion—to twice the surface energy, another material property for which estimates can be obtained (ibid). Regarding the decay rates as $s \to \infty$, we can just directly integrate that associated with pair-wise atomic or molecular forces, ignoring other interactions. For example, the potential of Lennard-Jones [63] for van der Waals' forces at large separations has them decaying as $1/s^7$ as $s \to \infty$: Direct integration then gives σ_c decaying as $1/s^3$ as $s \to \infty$ (see, eg, Israelachvili [64], Section 10.2). Such a derivation does not properly account for interaction and shielding effects, but suffices here.

The choice of k_e so that it is consistent with the k_e implicit in the elastic constitutive relations of the surrounding continuum offers some attributes in elastic stress analysis. A demonstration thereof follows on reconsidering the problem of a circular hole in an elastic plate under all-round far-field tension (Fig. 4 with $a=b$ therein). The classical solution to this problem is given in Lamé [65], Article 80. It features a $K_T = 2$ for the hoop stress at the hole's edge (see Eqs. (2.3) with $a=b$). However, in this solution, if one sits at the edge of the hole then takes the limit as the hole disappears, one obtains the physically anomalous result of the persistence of this stress concentration even when the plate becomes whole without a hole. What is needed to remove this anomalous result is the recognition that *cohesive tractions must act* on the hole surface as it closes. When the hole is very small, the associated cohesive stress-separation law takes the form of Eq. (2.11). Then, provided the stiffness therein is taken so as to be consistent with the elastic constitutive relations of the surrounding continuum, a state of uniform biaxial tension is recovered throughout the plate when the hole disappears (Sinclair and Meda [66]).[9]

[9]This assumes there is no activation energy or other impediment to closing the hole. If there were, the closing cohesive law would have to be modified. Nonetheless, a cohesive law would still have to act as the hole closes.

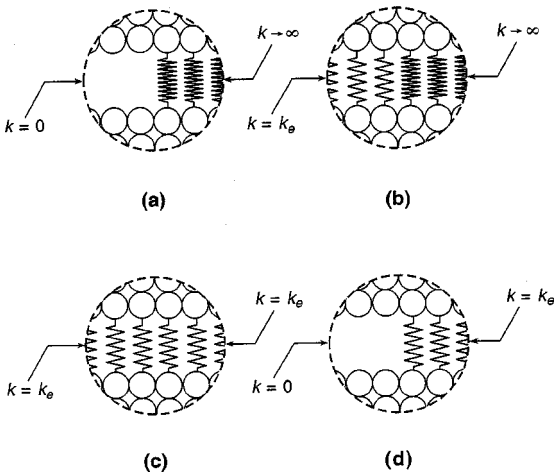

Fig. 8 Sketches of atomic or molecular ''springs'' at a sharp crack-tip for various boundary conditions: *a*) classical stress-free conditions, *b*) Barenblatt's cohesive stress conditions, *c*) consistent cohesive stress conditions, *d*) alternate cohesive stress conditions

While the foregoing describes a greatly simplified approach for determining cohesive stress-separation laws, it suffices for the discussion that follows here. We next compare various treatments of the symmetrically loaded mathematically sharp crack with and without such cohesive laws.

The traditional conditions on the crack plane for the stress-free mathematically sharp crack under symmetric (Mode I) loading are:

$$\sigma_y = \tau_{xy} = 0, \quad \text{for } x<0$$

$$v = 0, \quad \tau_{xy} = 0, \quad \text{for } x>0 \tag{2.13}$$

where the x and y rectangular coordinates are as in Fig. 3, σ_y and τ_{xy} are normal and shear stress components in these coordinates, and v is the displacement in the y-direction. In contrast, recognizing that for the mathematically sharp crack cohesive stresses must act as Barenblatt did, then inserting them via Eq. (2.11), the conditions on the crack plane are:

$$\sigma_y = k_e(\nu^+ - \nu^-), \quad \tau_{xy} = 0, \quad \text{for } x<0$$

$$\nu = 0, \quad \tau_{xy} = 0, \quad \text{for } x>0 \tag{2.14}$$

where ν^+ is the displacement of the upper crack flank, υ^- that of the lower (ie, $\nu^{\pm} = \nu$ at $y = \pm s_e/2$). Setting $k_e = 0$ in Eqs. (2.14) give Eqs. (2.13). In effect, therefore, traditional conditions overlook the cohesive interaction between the flanks that physically must occur.

What now becomes apparent, once we start to introduce interatomic considerations, is that when $x<0$, the boundary conditions hold at $y = s_e/2$ for the upper crack flank and $y = -s_e/2$ for the lower. That is, through the centers of atoms comprising the bottom surface of the upper half-space, the top of the lower. To be consistent then, we should view conditions ahead of the crack tip as applying at the same locations for their respective half-spaces. As a result, Eqs. (2.13) and (2.14) must have a cohesive law ahead of the crack with

an infinite stiffness for $\nu^+ = \nu^- = 0$ there, as required by the second of Eqs. (2.13) and (2.14). This situation is indicated schematically in Fig. 8*a* and *b*, wherein circles represent atoms and springs with stiffness k represent cohesive laws.

A more consistent introduction of cohesive laws for the mathematically sharp crack under symmetric loading takes, on the crack plane,

$$\sigma_y = k_e(\nu^+ - \nu^-), \quad \tau_{xy} = 0, \quad \text{for all } x \tag{2.15}$$

Then the same cohesive law acts throughout, consistent with the same material comprising the half-spaces both in front and in back of the crack tip (Fig. 8*c*).

An alternative crack-tip configuration sometimes implemented in the literature just inserts the cohesive law ahead of the tip while maintaining stress-free crack flanks. The conditions on the crack plane for this type of crack tip are:

$$\sigma_y = \tau_{xy} = 0, \quad \text{for } x < 0$$
$$\sigma_y = k_e(\nu^+ - \nu^-), \quad \tau_{xy} = 0, \quad \text{for } x > 0 \tag{2.16}$$

Now, in effect, the cohesive law in back of the crack tip has zero stiffness (Fig. 8*d*). For this choice to be physically justifiable, appropriate arguments from solid state physics need to be made. Presumably such arguments reflect a history of the crack flanks which, at one time, had them at significantly greater separations than for the mathematically sharp crack.

For Eqs. (2.13) and (2.14), with their effectively infinite stiffnesses, singularities result. This is shown asymptotically in Williams [20] for the traditional conditions, and in Sinclair [67] for Barenblatt's conditions.[10] Indeed, for Eqs. (2.14) a singularity is necessary if cancellation of singularities is to be effected as in Barenblatt [57]. For Eqs. (2.15) and (2.16), with their absence of infinite stiffnesses, no singularities result (Sinclair [67]). For Eqs. (2.15), no singularity is clearly the result to be expected, there being no discontinuity in either boundary directions or conditions.

Thus, the presence of effectively an infinite stiffness in a cohesive law is what is the underlying source of the singularity for the mathematically sharp crack under symmetric loading. The situation is akin to contact/impact in rigid body dynamics. There, rigid bodies with their infinite stiffnesses lead to infinite contact forces. Once deformation is admitted and finite stiffnesses introduced, finite contact forces result. Likewise with only finite stiffnesses in cohesive laws, finite rather than singular stresses result for the crack.

At this time, the use of cohesive/adhesive laws in boundary conditions in solid mechanics has seen quite widespread use. Sinclair [68] provides a recent bibliography: Most of the references therein cancel singularities after Barenblatt [57], but some introduce cohesive/ adhesive laws ahead of crack tips instead. An early example of the latter type of implementation is Cribb and Tomkins [69]. A fairly recent review of a number of contributions of this ilk is furnished in Needleman [70]. An implementation of Eqs. (2.15) when k_e is backed out from constitutive relations is summarized in Sinclair, Meda and Smallwood [71].

[10]Here, by Barenblatt's conditions we mean Eqs. (2.14): While Barenblatt [57] does not explicitly give these conditions, they are nonetheless implicit in the approach therein.

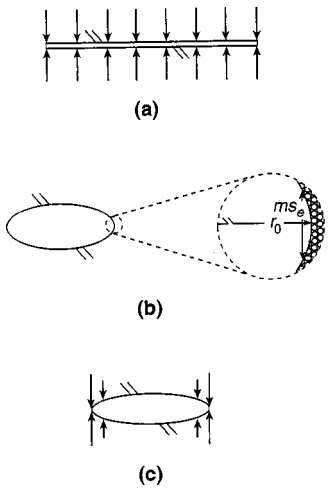

Fig. 9 Crack flank configurations when introducing cohesive stresses: *a*) mathematically sharp crack, *b*) stress-free crack, *c*) intervening crack

In Sinclair et al [71], cohesive laws are taken to act throughout the length of the mathematically sharp crack at the outset before any external loading is applied (Fig. 9*a*). That is, no assumption is made that cohesive stresses are confined to a small region near the crack tip, but rather the cohesive law itself interacts with the configuration to determine cohesive stress distributions. Not surprisingly, this not only leads to finite stresses but also to a stress concentration factor of unity for the mathematically sharp crack. This has to be the case when the cohesive law is made consistent with the surrounding continuum because then the continuum never knows the mathematically sharp crack is present. How is it, then, that the real stress concentration occurring at crack tips can be reflected by this type of modeling?

The answer lies in treating cracks that are not mathematically sharp. One way of doing this is to proceed as in Griffith [51] and form cracks via elliptical holes in elastic plates. Then two types of configuration can be distinguished. The first has stress-free crack surfaces (Fig. 9*b*). This occurs when the root radius r_0 of the elliptical hole is sufficiently large. Here, by sufficiently large is meant such that the first pair of atoms or molecules on opposite flanks at the tip are separated by a sufficient distance so that the cohesive law itself sets the surface tractions for this pair to zero. That is, this distance is a sufficient number of multiples m of the equilibrium separation s_e so that the law of Fig. 7 has $\sigma_c = 0$ effectively (see close-up in Fig. 9*b*). The second has cohesive stresses acting near its tip (Fig. 9*c*). This occurs when the root radius decreases from the minimum value required for stress-free flanks. Ultimately this configuration becomes the mathematically sharp crack as the root radius decreases still further.

Resulting stress concentration factors for stress-free cracks coincide with classical K_T (ie, as on the right-hand side of Eqs. (2.3) plus one for transverse tension alone). Thereafter, as root radii are decreased so that cohesive stress starts to act, K_T fall below classical values. Ultimately for a small but nonzero root radius, the crack closes and a K_T of unity results, the same as for the mathematically sharp crack.

Other erstwhile singular configurations can be rendered singularity-free by similar means. Viewed from a cohesive/adhesive stress perspective, it is possible to identify effectively infinite stiffnesses in almost all of the examples of stress singularities given in the Introduction. Hence their singular nature. When cohesive/adhesive laws without infinite stiffnesses are introduced, these examples are rid of stress singularities.

To explain further, traditional contact and clamped conditions are really simplifications of cohesive or adhesive conditions. When exchanged for the latter, only two principal types of boundary conditions remain in planar elasticity: cohesive/adhesive conditions and stress-free conditions. When these last two types of boundary conditions act on an in-plane geometry which entails a vertex angle ϕ of π or less, no power singularities are possible (Sinclair [67]). When effectively infinite stiffnesses in cohesive/adhesive laws are removed on lines of symmetry or antisymmetry, the examples in the Introduction all have $\phi \leqslant \pi$, hence no power singularities. Moreover, there are no log singularities for these two types of boundary conditions provided there are no step discontinuities in shear tractions when $\phi = \pi$. This last requirement, in particular, means that one cannot implement the shear counterpart of Fig. 8*d* for antisymmetric (Mode II) loading of a crack if one is to avoid log singularities. It also means any shear tractions in contact problems with sharp edges must go to zero continuously, even if very rapidly, outside of contact regions if one is to avoid log singularities. Further explanation is given in Sinclair [72].

While the introduction of cohesive/adhesive laws with finite stiffnesses and no shear jumps shows promise of ridding elasticity of most if not all stress singularities, the implementation of this approach in toto faces some stiff challenges. These principally stem from the determination of the appropriate cohesive/adhesive law. For example, consider the case of brittle fracture, arguably the simplest physical response once the limit of elastic behavior is reached. For real materials that behave in a brittle fashion, there is a question as to what ultimate stress governs fracture in the presence of now finite but highly concentrated stresses. It is not likely to be as high a strength as the material's theoretical ultimate stress, $\sigma_U \approx E/10$. Nor is it likely to be as low as the material's ultimate stress as determined using standard tension tests, $\sigma_u \approx E/1000$. In the short term, an estimate of the applicable intervening value for a limited range of sizes might be made via direct calibration with test results. In the long term, this question is likely to require modeling of the material's microstructure itself. In addition to such modeling issues confronting the full implementation of boundary conditions with cohesive/adhesive laws, companion analysis is now nonlinear, even in the elastic regime. And this analysis must be of sufficient refinement to accurately capture the local stresses involved, with their high gradients. For the present, therefore, we can expect to continue to face the longstanding challenges represented by singularity analysis and interpretation even for configurations that could be freed of singularities with cohesive/adhesive laws.

2.4 Removing singularities via boundary conditions: Enforcing inequality constraints

Alternative modifications to boundary conditions which can remove stress singularities may be found in additional local inequalities that are physically required. We begin by demonstrating the way in which this occurs for some *simple, frictionless, contact problems*.

The different types of frictionless contact entertained in this regard may be distinguished by whether or not they are conforming. Here, by ''conforming'' is meant contact which, from no load to full load, has the indentor and indented material share a common tangent as the contact region's boundary is approached from outside. An example is a roller on a relatively flat surface, as occurs in roller bearings. Initially, before any loading, the contact region for this configuration consists of a line through the contact point C (Fig. 10*a*). Subsequently, under loading, C splits into C and C' as the contact region spreads (Fig. 10*b*). Throughout, contact is conforming at C (or C') in the above sense. A further example is the closely conforming contact of a journal bearing which tends to produce a larger contact region under load (Fig. 10*c*). In contrast is a sharp-edged indentor or flat punch contacting a horizontal surface. This is an example of nonconforming contact at both C and C' (Fig. 10*d*).

In addition to assuming contact in the configurations of Fig. 10 is frictionless or perfectly lubricated, we further simplify the exposition by taking the indentors (shown vertically hatched) to be rigid. We also assume that they are long in the out-of-plane direction so that the 2D state of plane strain applies. Then traditional local boundary conditions at C in Fig. 10*b*, in terms of the r, θ coordinates of Fig. 11, take the form

$$\sigma_\theta = \tau_{r\theta} = 0 \quad \text{on} \quad \theta = \pi$$

$$u_\theta = u_0, \quad \tau_{r\theta} = 0, \quad \text{on} \quad \theta = 0 \tag{2.17}$$

for $r > 0$. The first of Eqs. (2.17) are the stress-free conditions external to the contact region. The second reflects *local* indentation by an amount $u_0 = u_0(r)$ without any friction within the contact region. The local fields for Eqs. (2.17) admit to being supplemented by their fully homogeneous counterparts, namely those for Eqs. (2.17) with $u_0 = 0$. Then we recover the classical boundary conditions for a crack (cf, Eqs. (2.13)), so that inverse-square-root stress singularities are possible.

To remove the possibility of stress singularities, we adjoin physically sensible constraints. These insist that within the contact region there can be no tensile contact stresses,[11] while without there can be no interpenetration or contact between the indentor and the indented material. Thus we require

$$\sigma_\theta \leqslant 0 \quad \text{on} \quad \theta = 0$$

$$u_\theta < R_0 - \sqrt{R_0^2 - r^2} \quad \text{on} \quad \theta = \pi \tag{2.18}$$

[11] Actually, adhesive stresses can supply tensile stresses within the contact region, but for most interfaces these stresses are negligible. Johnson [73], Section 5.5, has an interesting discussion of such effects.

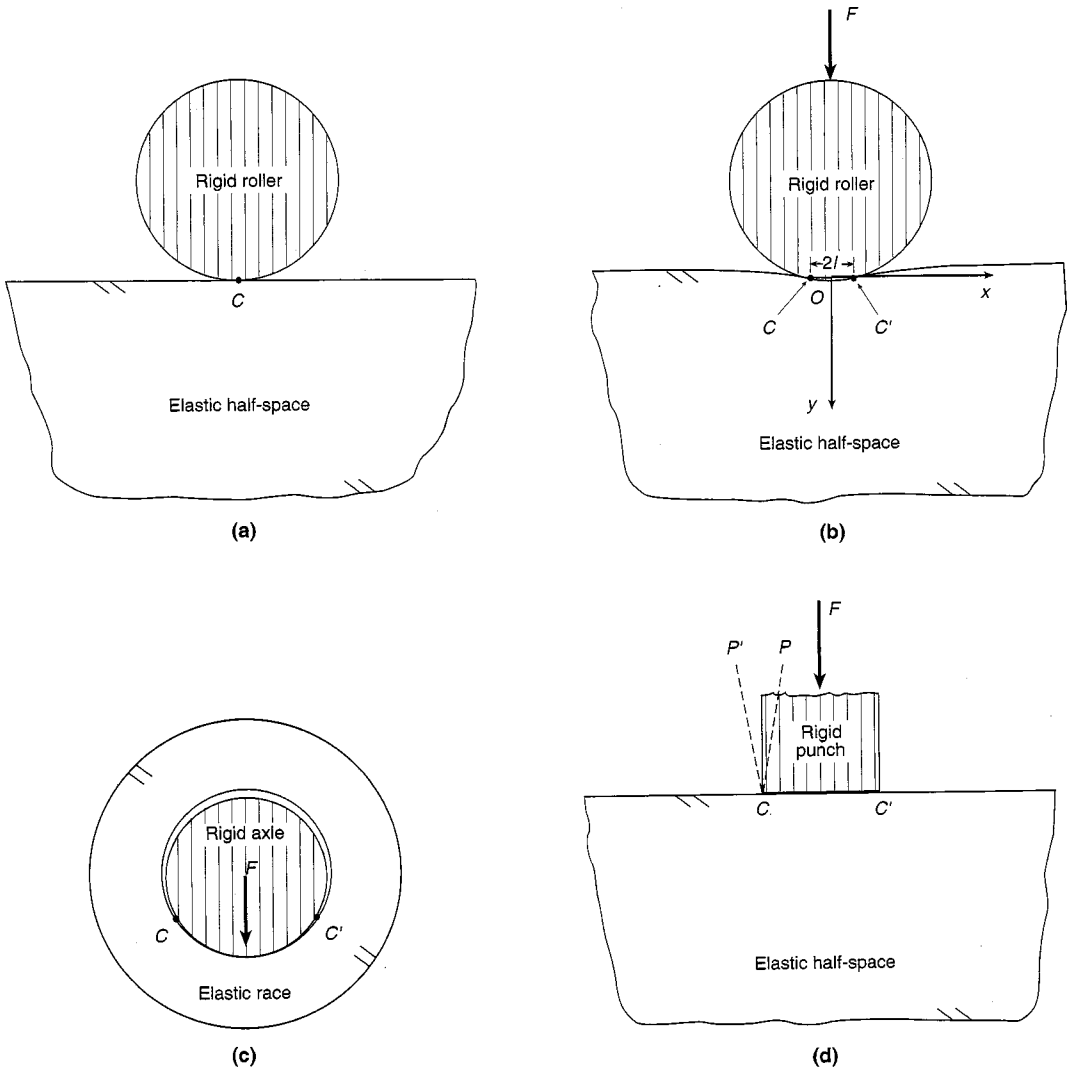

Fig. 10 Contact configurations: *a*) unloaded roller bearing, *b*) loaded roller bearing, *c*) journal bearing under load, *d*) piston ring pressing against a cylinder wall (deformation not indicated)

for $r>0$, where R_0 is the radius of the indenting roller. Given compliance with these added restrictions, singular response is no longer possible.

To see this, consider what happens otherwise. There are two cases.

i) Singular stresses participate with a positive stress intensity factor of $K_{\mathrm{I}}(K_{\mathrm{I}}>0)$.
ii) Singular stresses participate with a negative stress intensity factor of $-K_{\mathrm{I}}$.

Under i, the singular stress field must dominate all others as C is approached from within the contact region, so that the contact stresses must become tensile (indicated on $\theta=0$ in Fig. 11). This is in violation of the first of Eqs. (2.18). Under ii, the displacement of the indented material just outside C is vertically upwards and consequently interpenetrates the indentor (indicated on $\theta=\pi$ in Fig. 11). This is in violation of the second of Eqs. (2.18). Hence, the classical singular fields associated with a crack cannot participate in the conforming contact configuration of Fig. 10*b* if the inequality constraints of Eqs. (2.18) are enforced.

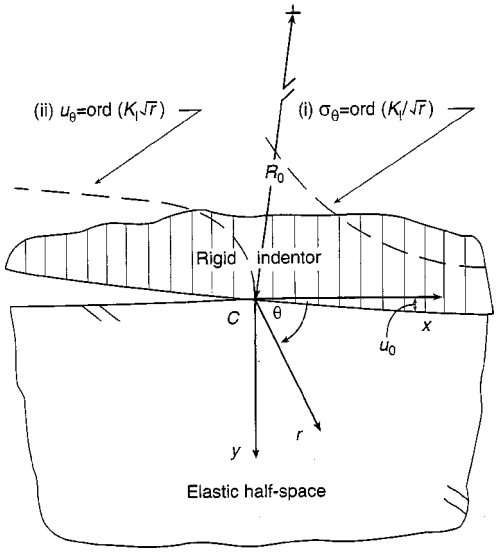

Fig. 11 Local contact configuration at C in Fig. 10*b*: coordinates and consequences of singularities

The question that now arises is can we, in actuality, enforce the inequality constraints of Eqs. (2.18) and so remove singularities? The fact that Eqs. (2.18) would seem to be physically sensible and therefore desirable does not necessarily mean they can be enforced within classical elasticity. After all, singularities in general are nonphysical so it would be physically sensible and desirable if we could simply legislate them out of elastic solutions. Unfortunately, such legislation typically leads to the posing of a problem that has no solution, the local regular elastic fields being incomplete without their singular counterparts.

For conforming contact, however, we have an additional degree of freedom of which we can take advantage. This is the extent of the contact region (ie, the length between C and C' that $2l$ denotes in Fig. 10*b*). By suitably adjusting this extent, the inverse-square-root stress singularity can be removed. Then, since there are no other singular fields within elasticity satisfying the local boundary conditions Eqs. (2.17), or their homogeneous counterparts, the configuration is rendered singularity free.

Implicitly, this adjustment of contact extent so as to remove stress singularities is what Hertz did when he solved contact problems of the genre of the roller of Fig. 10*a* and *b* (Hertz [74]). His solutions all feature contact stresses which are nonsingular and, indeed, go to zero at the edges of the contact region. For example, for the roller of Fig. 10*b*, the Hertzian contact stress is

$$\sigma_y = -\frac{2F}{\pi l^2}\sqrt{l^2-x^2} \quad \text{on} \quad y=0 \tag{2.19}$$

for $-l \leqslant x \leqslant l$, where F is the force per unit length in the out-of-plane direction, and x and y are now as in Fig. 10*b* with origin O in the middle of the contact region.

The same situation obtains for frictionless conforming contact by rigid indentors in general. Namely, that the extent of the contact region can be adjusted so that only compressive tractions occur within it and there is no interpenetration outside of it. Given compliance with these constraints, stresses are nonsingular. An example of more extensive conforming contact than that of the roller on the half-space under Hertzian assumptions is furnished in Steuermann [75]. Therein closed-form expressions for contact stresses show they behave as ord$(r^{1/2})$ as $r \to 0$ at the edges of the contact region, the same behavior as in Eqs. (2.19). As a further example, the closely conforming contact of Fig. 10*c* is treated in Persson [76], and demonstrates that stress singularities can also be removed in this instance.

The same situation does not obtain for nonconforming contact. Herein the sharp edges present can set the limits of the contact region so that the contact extent is not available to be adjusted to remove singular behavior. This is the case for the indentor of Fig. 10*d*. Such configurations require the introduction of appropriate cohesive/adhesive laws to render them singularity free (as in Section 2.3).

We now admit *two extensions* to the limited class of contact problems considered heretofore. First, we entertain the introduction of *friction effects*. To obtain a bound on these effects to complement that of frictionless conditions, we can assume that there is no slipping whatsoever. The resulting stick conditions within the contact region, in terms of the coordinates of Fig. 11, take the form

$$u_\theta = u_0, \quad u_r = 0, \quad \text{on} \quad \theta = 0 \tag{2.20}$$

for $r > 0$. In Eqs. (2.20), u_r is the radial displacement which is set to zero by virtue of the indented material completely sticking to the rigid indentor. Again the homogeneous counterpart of Eqs. (2.20), taken together with the stress-free condition on $\theta = \pi$ in Eqs. (2.17), admits the possibility of stress singularities. These are the same as for the adhering tire of the Introduction (P_3 of Table 2 and Fig. 2*b*) which has singularities of ord $(r^{-1/2}\cos(\eta \ln r))$ and ord $(r^{-1/2}\sin(\eta \ln r))$. Hence we can anticipate the same response as $r \to 0$ at C in Fig. 11. These two singularities occur in combination in *two distinct local fields* which can participate independently of each other (except for incompressible plane strain for which $\eta = 0$ and there is but one local singular field—see Eqs. (1.4)). Thus adjusting the *one* parameter we have available to us, the contact extent, is generally not sufficient to remove both of them. Accordingly, now it can be impossible to find elastic solutions in compliance with Eqs. (2.18), and singular stresses can occur. For example, returning to the Hertzian contact of the roller of Fig. 10*b* but now with stick conditions as in Eqs. (2.20), the normal contact stress becomes

$$\sigma_y = -\frac{2F}{\pi l^2}\left[\sqrt{l^2-x^2}\cos\left(\eta \ln\left(\frac{l-x}{l+x}\right)\right) + \frac{2\eta l x}{\sqrt{l^2-x^2}}\sin\left(\eta \ln\left(\frac{l-x}{l+x}\right)\right)\right] \tag{2.21}$$

on $y = 0$, for $-l < x < l$.[12] The shear contact stress is similarly singular.

To alleviate the singular response of direct conforming contact with no slip, one can allow some lateral displacement. This can be done by applying the load incrementally so that surface material outside the contact region is at least allowed to move laterally prior to coming into contact. Mossakovskii [78] describes the implementation of such a physically more realistic approach. Results are nonsingular and comply with the constraints of Eqs. (2.18). Indeed, for the normal contact stress, σ_y is as in Eqs. (2.21) but with $\eta = 0$, so that the Hertzian contact stress of Eqs. (2.19) is recovered. Similar results obtain for the axisymmetric counterpart (see Goodman [79] and Mossakovskii [80]).[13] For both configurations, though, in the limit as the edge of the contact region is approached from within, the ratio of the shear contact stress divided by the normal approaches infinity. This implies that an infinite coefficient of friction is needed for no slip once contact is made. This in turn suggests that we entertain the possibility of slip in the outer portions of the contact region itself.

[12] The derivation of Eq. (2.21) is straightforward using complex potential methods as in, eg, Gladwell [77], Chapter 4.

[13] Spence subsequently showed via dimensional analysis that the stress fields involved are self similar, thereby enabling direct implementation rather than incremental (Spence [81]).

For such slip under a rigid indentor up to the contact limit at C in Fig. 11, the boundary conditions take the form

$$u_\theta = u_0, \quad \tau_{r\theta} = f\sigma_\theta, \quad \text{on} \quad \theta = 0 \tag{2.22}$$

for $r>0$. In Eqs. (2.22), f has the magnitude of the coefficient of friction. The sign of f is taken to be such that $\tau_{r\theta}$ opposes any slipping displacement u_r. Consequently for compressive normal contact stresses, $\operatorname{sgn} f = -\operatorname{sgn} u_r$, where sgn is the signum function. The conditions of Eqs. (2.22) with the first of Eqs. (2.17) prescribe local boundary conditions for a slip-to-free transition: When taken abutting the displacement requirements in Eqs. (2.20) if $|\tau_{r\theta}| < |f\sigma_\theta|$, they prescribe local boundary conditions for a slip-to-stick transition. For both transition configurations, it is possible to show only a single singularity exists. Accordingly, by appropriately adjusting the positions of these two transitions, both singularities can be removed. To capture the physics better, the loading needs to continue to be applied incrementally (or effectively so via similarity arguments). Such an analysis may be found in Spence [82] and produces singularity-free stresses.

As a second extension to the class of contact problems considered, we admit *deformation of the indentor*. Results remain essentially the same. For conforming contact without friction, or with friction but allowing for slip, physically reasonable inequalities can be complied with by adjusting boundary region extents and configurations rendered free of singularities. Dundurs and Comninou [83] furnish asymptotic arguments that obeying such inequality constraints removes singular behavior, while there are a number of examples showing that one can actually adjust extents to do this (eg, Johnson [73]).

In sum, when sufficient degrees of freedom are available to enable compliance with the pertinent inequalities, stress singularities can be removed from conforming contact problems. The resulting nonsingular stresses may be loosely termed Hertzian, and have been found to be generally supported by experiments (Johnson [73], Chapter 4). In these circumstances, therefore, the stress analyst should make every effort to comply with the inequality conditions.

3 TRYING TO MAKE PHYSICAL SENSE OF PERSISTENT STRESS SINGULARITIES

3.1 Interpreting crack-tip singularities: The energy release rate hypotheses

We now turn to configurations in elasticity for which the foregoing strategies, while removing singular stresses, do so with an approach that is yet not mature. Principal amongst these in their practical importance are those involving cracks as treated within classical elasticity, so we initially focus on trying to interpret the crack-tip singularities.

Griffith was first to appreciate that it is futile to attempt to directly interpret the implications for fracture of singular crack-tip stresses. He also appreciated that, while singular, nonetheless these stresses are integrable; therefore they can be integrated to arrive at a bounded quantity which may be physically interpreted. In essence, the particular integrated quantity taken in Griffith [51] is the *energy release rate* accompanying crack extension G, and Griffith hypothesized that G controls brittle fracture at cracks.

The basic elements of the argument which establish the energy release rate for incipient crack propagation and define its role in a brittle fracture criterion may be described as follows. To fix ideas, reconsider the tensile crack of Fig. 3 but now with the surrounding material being strictly linear elastic all the way to fast fracture. Such a material is sometimes termed ''perfectly brittle.'' By symmetry in Fig. 3, tensile crack extension can be expected to occur along the x-axis where the maximum tensile stresses occur. The energy available to drive this extension comes from the strain energy of the material surrounding the crack tip: Unlike its contributing stress and strain fields, the strain energy is bounded by virtue of being an integral of these fields. If the rate such energy releases at the newly formed surfaces in the extension exceeds the rate at which it needs to be supplied to form them, brittle fracture is hypothesized to occur.

One way in which such an energy argument for crack extension can be implemented is as follows. First, compute the drop in strain energy accompanying a crack extension within some region surrounding the crack tip. Next, subtract the energy transported away as work terms across the boundary of this region not including the newly formed crack surfaces. Thus, the energy released on the crack extension is obtained. Dividing this energy by the extension length, and taking the limit as this length goes to zero, then gives the energy release rate for crack propagation.

Alternatively, one can simply compute the strain energy released as work terms on the boundary of the newly formed crack surfaces, then divide by the crack extension length and take the limit as it goes to zero to obtain the energy release rate. Both approaches, properly carried out, give the same result. Both are true energy balances in the sense of classical physics. Both have the strain energy as the potential energy source, since this is the ability of an elastic system to perform work by virtue of its deformed state. Given this equivalence, we choose to focus further discussion on the second approach here because it is relatively direct.[14]

In describing such an energy argument, we follow Irwin [84] because the analysis therein is elegant in its simplicity. Hence we consider a crack tip under symmetric loading which produces a small extension δa aligned with the original crack (Fig. 12). Prior to the extension, the tensile stress ahead of the crack tip σ_y and the crack opening displacement back of it v can be identified using an asymptotic analysis as in Williams [20]. Locally this results in

$$\sigma_y = \frac{K_{\mathrm{I}}}{\sqrt{2\pi x}} + O(x^{1/2}) \quad \text{as} \quad x \to 0 (x>0)$$

[14]It is unfortunate that the variational statement of equilibrium in elasticity is often termed the ''theorem of minimum potential energy'' and the functional involved in this theorem the ''potential energy.'' This has led some to confuse this functional with the true elastic potential energy, the strain energy. By serendipity, though, it is possible to make this mistake and define G as a derivative of this functional and still obtain the correct energy release rate (essentially this happens because there is no energy transported across parts of the boundary where displacements are held fixed).

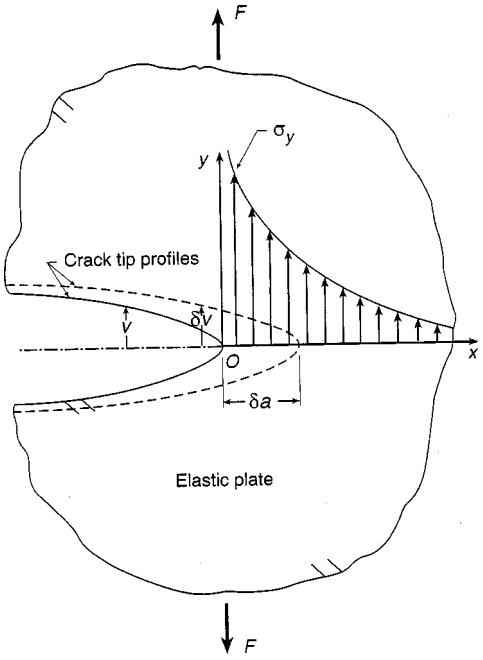

Fig. 12 Tensile stress ahead of a crack and displacements accompanying a small extension under symmetric (Mode I) loading

$$v=\frac{1+\kappa}{2\mu}K_{\mathrm{I}}\sqrt{\frac{-x}{2\pi}}+O(|x|^{3/2}) \quad \text{as} \quad x\to 0(x<0) \tag{3.1}$$

for $y=0$, wherein K_{I} continues as the symmetric, or Mode I, stress intensity factor. The displacement accompanying the extension δv therefore is

$$\delta v=\frac{1+\kappa}{2\mu}K_{\mathrm{I}}[1+O(\delta a)]\sqrt{\frac{\delta a-x}{2\pi}} +O((\delta a-x)^{3/2}) \quad \text{as} \quad x\to\delta a(x<\delta a) \tag{3.2}$$

on $y=0$. In Eqs. (3.2), the term in square brackets accounts for the perturbation in K_{I} resulting from the extension. Now the strain energy released on the extension must equal the work needed to heal it and restore the crack to its unextended state. For an infinitesimal element of the upper flank in the extension, this healing work is one half force times displacement, or $(1/2)(\sigma_y\,dx)(\delta v)$. Adding up all such contributions for both the upper and lower flanks of the crack extension gives the total work needed to heal it. Dividing by the extension length δa, then taking the limit as $\delta a\to 0$, gives the energy release *rate* for crack propagation G. That is,

$$G=\lim_{\delta a\to 0}\frac{1}{\delta a}\int_0^{\delta a}\sigma_y\ \ \delta v\ \ dx \tag{3.3}$$

To evaluate G, we introduce σ_y of Eq. (3.1) and δv of Eq. (3.2) into Eq. (3.3) to obtain

$$G=\frac{1+\kappa}{4\pi\mu}K_{\mathrm{I}}^2\lim_{\delta a\to 0}\left[\frac{1}{\delta a}\int_0^{\delta a}\sqrt{\frac{\delta a-x}{x}}\,dx+o(\delta a)\right] \tag{3.4}$$

The integral in Eq. (3.4) is readily performed by taking $x=\delta a\sin^2 t$, thereby giving

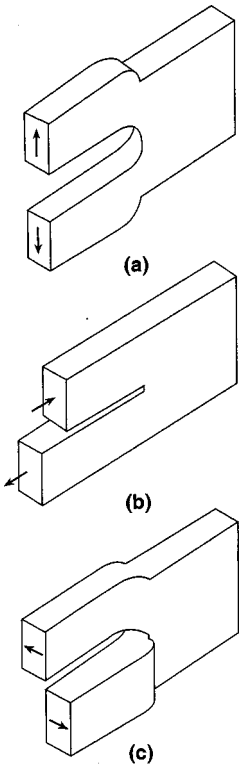

Fig. 13 Modes of deformation at a crack tip: *a*) Mode I, *b*) Mode II, *c*) Mode III

$$G_{\mathrm{I}}=\frac{1+\kappa}{8\mu}K_{\mathrm{I}}^2 \tag{3.5}$$

In Eq. (3.5) we have added the subscript I to G to distinguish it as being associated with Mode I or tensile crack extension (with deformation as sketched in Fig. 13*a*).

It is also possible to determine the energy release rate associated with Mode II or shear crack extension (Fig. 13*b*). The corresponding energy release rate G_{II} is

$$G_{\mathrm{II}}=\lim_{\delta a\to 0}\frac{1}{\delta a}\int_0^{\delta a}\tau_{xy}\ \ \delta u\ dx \tag{3.6}$$

Proceeding analogously to the derivation of Eq. (3.5) leads to

$$G_{\mathrm{II}}=\frac{1+\kappa}{8\mu}K_{\mathrm{II}}^2 \tag{3.7}$$

where K_{II} is the stress intensity factor in Mode II. There is a further mode of crack propagation associated with out-of-plane shear, Mode III (Fig. 13*c*). For this mode, a similar derivation gives

$$G_{\mathrm{III}}=\frac{K_{\mathrm{III}}^2}{2\mu} \tag{3.8}$$

where K_{III} is the stress intensity factor in Mode III.

Each of the foregoing modes of crack extension is associated with a different way of separating material to form new surfaces. Consequently, each must be assessed individually in a given application in order to enable meaningful comparisons with corresponding critical values. In practice,

brittle fracture typically occurs in tension rather than in shear. This means that under general loading, with both symmetric and antisymmetric contributions, crack extension may well not occur aligned with the originating crack (as in Fig. 12), but rather along a ray emanating from the crack tip which maximizes the energy release rate in Mode I. Even so, we still need to be able to distinguish amongst the different contributions to the total energy release rate so as to obtain the maximum G_{I} and determine the ray on which it acts for a given loading.

Two observations can be made on the foregoing results for energy release rates. First, only the singular stresses and their displacements contribute to these rates. Second, accepting the hypothesis that G_{I}, G_{II}, and G_{III} control brittle fracture in their various modes is completely equivalent to accepting the corresponding stress intensity factors, K_{I}, K_{II}, and K_{III}, in this role.

The literature has a number of other developments of the elastic energy argument for brittle fracture which are consistent with the preceding.[15] Several of these express the energy release rate with path-independent integrals which enclose the crack tip: in chronological order, Eshelby [86], Sanders [87], Cherepanov [36], and Rice [88]. The isolation of the contributions from different modes of crack propagation is a little more awkward to effect with these integrals. This may in part account for current practice preferring to express brittle fracture criteria in terms of stress intensity factors rather than energy release rates.

Originally, Griffith hypothesized that brittle fracture occurs when the energy release rate equals the surface energy of the solid being fractured. Later, Irwin [89] and Orowan [90] independently argued that the energy ''sink'' for fracture could also include some plastic dissipation, provided the extent of any accompanying yield region is limited to the immediate neighborhood of the crack tip. This extension of Griffith's original hypothesis realized the practical benefit of enabling the approach to be applied to metals. Aside from these hypotheses as to acceptable energy sinks for fracture, there is a further basic hypothesis underlying either approach. This has that the integral of something which is not physically appropriate—namely singular crack-tip stresses—can yet furnish something which is—namely the energy release rates accompanying crack extension. Thus, the energy arguments of classical fracture mechanics contain two hypotheses: one for the energy sources for fracture, the other for the energy sinks. Each one needs to be complied with for the approach to be successful. The extent to which they are, in fact, can be judged by the degree of agreement of the physical evidence with predictions based on the pair. We review some physical data with this issue in mind in Section 3.4.

3.2 Energy release rates for interface cracks

The ease with which the singular fields for a crack can be integrated to provide energy release rates suggests trying to extend this means of singularity interpretation to other configurations. Perhaps the most natural to consider in this way is the *interface crack* configuration wherein material on each side of the crack plane can have different elastic moduli (Fig. 14). Now, as noted in the Introduction, Williams [21] shows that the inverse-square-root singularity of a crack can have oscillatory multipliers. For example, in terms of the cylindrical polar coordinates of Fig. 14,

$$\sigma_\theta = O(r^{-1/2}\cos(\eta \ln r)) + O(r^{-1/2}\sin(\eta \ln r)) \quad \text{as} \quad r \to 0 \tag{3.9}$$

on $\theta = 0$, where η is as in Eq. (1.3). That these possible local singular stresses do in fact participate in the response of global configurations is confirmed by solutions to such problems, as in England [91]. Undertaking an analysis as earlier for companion energy release rates associated with crack extension along the interface then gives, for Mode I,

$$G_{\mathrm{I}} = c + \lim_{\delta a \to 0} [c' \cos(2\eta \ln \delta a) + c'' \sin(2\eta \ln \delta a)] \tag{3.10}$$

where c, c', and c'' are constants (generally $\neq 0$). Clearly the limit in Eq. (3.10) does not exist. A like result holds for G_{II}, and accordingly neither is a well-defined quantity. In combination, however, the terms that are undefined in G_{I} and G_{II} can be shown to cancel, so that a total energy release rate does exist. Nonetheless, the inability to distinguish between modes is unsatisfactory for the reasons indicated earlier. Moreover, the situation is not improved if crack extension in directions other than along the interface is entertained. Accordingly, the generally more nonphysical singular stresses of interface cracks would seem to require special attention in order to effect satisfactory physical interpretations.

This need has occasioned a series of models for the interface crack to be put forward since Williams [21]: the contact zone model of Comninou [92], the crack-opening-angle model of Sinclair [93], the intervening-layer models of At-

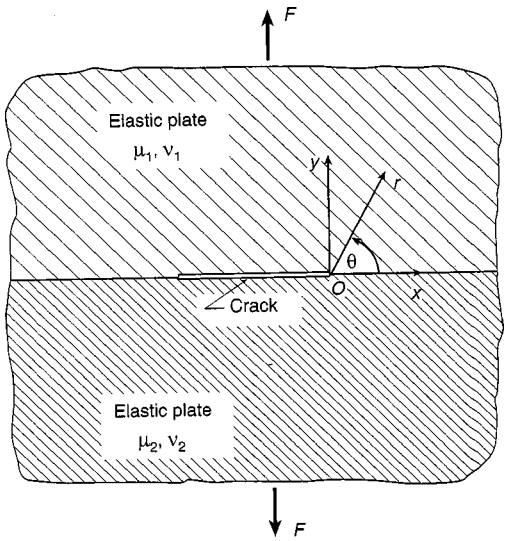

Fig. 14 An interface crack configuration

[15] There are also some articles which are not consistent and may be shown to be in error—see Keating and Sinclair [85] for a review.

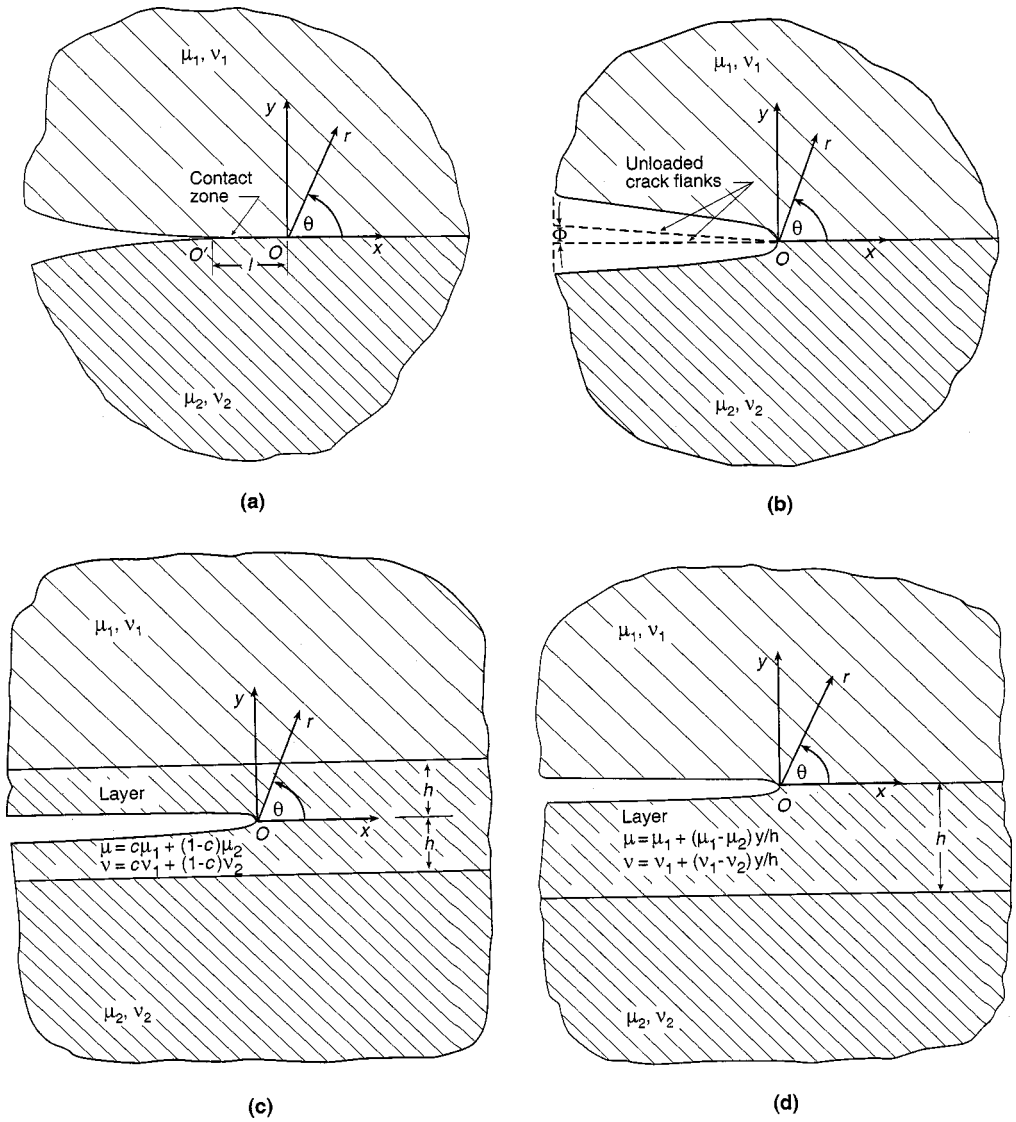

Fig. 15 Crack-tip models for the interface crack: *a*) contact zone model, *b*) crack opening angle model, *c*) intervening layer model with constant moduli, *d*) intervening layer model with continuously varying moduli

kinson [94], and the perturbed moduli model of He and Hutchinson [95] and Suo and Hutchinson [96]. We review these models next.

There is a further unsatisfactory aspect of elastic solutions for interface cracks based on the model of Williams [21]. As pointed out in England [91] and Malyshev and Salganik [97], the crack-flank displacements also oscillate and in so doing interpenetrate one another. This interference between the crack flanks lead Malyshev and Salganik to suggest introducing a contact zone for the crack flanks immediately contiguous to the crack tip. Such a *contact zone model* was first pursued in Comninou [92], and subsequently has seen quite extensive investigation—see references in Comninou [98]. The basic elements of such a model are as follows.

In terms of the cylindrical polar coordinates of Fig. 15*a*, three types of conditions near the original crack tip at O are prescribed in the contact zone model for the interface crack: the matching conditions for perfect bonding ahead of O,

$$\sigma_\theta\big|_{\theta=0^+} = \sigma_\theta\big|_{\theta=0^-}, \quad \tau_{r\theta}\big|_{\theta=0^+} = \tau_{r\theta}\big|_{\theta=0^-}$$
$$u_r\big|_{\theta=0^+} = u_r\big|_{\theta=0^-}, \quad u_\theta\big|_{\theta=0^+} = u_\theta\big|_{\theta=0^-} \tag{3.11}$$

for $r>0$; the frictionless contact conditions behind O,

$$\sigma_\theta\big|_{\theta=\pi} = \sigma_\theta\big|_{\theta=-\pi}, \quad u_\theta\big|_{\theta=\pi} = u_\theta\big|_{\theta=-\pi}$$
$$\tau_{r\theta}=0 \quad \text{on} \quad \theta=\pm\pi \tag{3.12}$$

for $0<r<l$, where l is the extent of the contact zone; and the stress-free conditions once contact ceases at O',

$$\sigma_\theta=\tau_{r\theta}=0 \quad \text{on} \quad \theta=\pm\pi \tag{3.13}$$

for $r>l$. Equations (3.11)–(3.13), when taken together with the planar elastic field equations for the respective materials and boundary conditions describing loading remote from the

crack, can constitute a complete problem statement in elasticity. In addition, though, we would like to adjoin a constraint which prohibits interpenetration once contact ceases—a primary motivation for the model in the first place—as well as a constraint which only admits compressive stresses within the contact zone. Can we do this? The answer is yes for two reasons. First, we can adjust the extent of the contact region l so as to remove the one singular field possible at O', thereby ensuring no interpenetration: This is the same adjustment as used to the same end in frictionless conforming contact in Section 2.4. Second, the local fields at O (elucidated in the Appendix of Comninou [92]) can feature a compressive inverse-square-root singularity in the normal stress within the contact zone (viz, in σ_θ on $\theta=\pi$ in Fig. 15*a*). Once present, this singular stress means that, no matter how hard we pull the overall configuration apart with remote tensile loading, the finite biaxial tensile stresses so induced at O can never completely negate the infinite compressive normal stress there. Hence there can always exist a region, albeit possibly a small one, in which contact stresses are compressive.

The question that now arises is when is such a local singular stress field excited in global problems? Somewhat surprisingly, Comninou [92] shows that the closing of the crack tips present in the contact zone models can occur in global configurations when the loading over the crack flanks is predominantly in the opening mode (as in Fig. 14). In Comninou [92], when an interface crack is under uniform tensile loading at infinity, fields for the contact zone model are determined which have compressive stresses within the contact zone. These fields are also free of any interference between the crack flanks. Furthermore, the solution obtained once the contact zone model is adopted may be shown to be unique (see Comninou [98]). Looking ahead of the crack tip in the model (O in Fig. 15*a*), we find the shear stress alone to be singular (see the Appendix in Comninou [92]). This has to be the case since a normal singular stress there, if tensile, would separate the crack flanks in the contact zone, while if compressive, would cause them to overlap one another. The associated energy release rates for crack propagation along the interface are (Comninou [98])

$$G_{\mathrm{I}}=0, \quad G_{\mathrm{II}}=\frac{\hat{\mu}_1\hat{\mu}_2}{4\mu_1\mu_2(\hat{\mu}_1+\hat{\mu}_2)}K_{\mathrm{II}}^2$$

$$\hat{\mu}_1=\mu_1+\kappa_1\mu_2, \quad \hat{\mu}_2=\mu_2+\kappa_2\mu_1 \tag{3.14}$$

The Mode I energy release rate is zero by virtue of there being no singular normal stress on the bonded interface in the contact zone model.

In an attempt to complement the contact zone model with one which does permit crack propagation along the interface in an opening mode accompanied by a positive energy release rate, the following simple tactic is suggested in Sinclair [93]. While the singular character of a crack can be increased by the introduction of an abrupt material discontinuity on the crack plane, it can be reduced by opening the angle subtended at the crack tip prior to loading (Fig. 15*b*). The two effects can be adjusted so as to offset one another and recover the nonoscillatory inverse-square-root singularity of a crack in a single material. This *crack-opening-angle model* shares with the contact zone model the matching conditions for a perfectly bonded interface ahead of the crack tip, namely Eqs. (3.11), and has stress-free conditions on the crack flanks which are taken to subtend an angle of Φ in the unloaded state. That is, in terms of the cylindrical polar coordinates of Fig. 15*b*,

$$\sigma_\theta=0, \quad \tau_{r\theta}=0, \quad \text{on} \quad \theta=\pi-\Phi,-\pi \tag{3.15}$$

for $r>0$. For given material moduli, the value of Φ that removes the oscillatory multiplier of the stress singularity at O may be found in Sinclair [93]. For this angle, the crack flanks open without interference under tensile loading as indicated in Fig. 15*b*.

The approach may be viewed as the dual of the contact zone model. In the contact zone model, contact of the crack flanks is anticipated and boundary conditions thereon updated to reflect this event. In the crack-opening-angle model, crack opening is anticipated and the crack flanks angled apart to promote this event. For a specific applied tensile load, assuming crack opening via the crack-opening-angle model can be shown to lead to a unique solution (the proof follows along the lines of Knowles and Pucik [99]). Both the normal and shear stress on the bonded interface in such a solution are singular (provided $\Phi\neq 0$). Companion energy release rates are given by

$$\begin{Bmatrix} G_{\mathrm{I}} \\ G_{\mathrm{II}} \end{Bmatrix} = \begin{Bmatrix} c \\ c' \end{Bmatrix} \frac{[\mu_1^2(1+\kappa_2)^2+\mu_2^2(1+\kappa_1)^2]}{\mu_1\mu_2(\hat{\mu}_1+\hat{\mu}_2)}K^2 \tag{3.16}$$

where $\hat{\mu}_1$ and $\hat{\mu}_2$ are as in Eqs. (3.14), c and c' are now dimensionless constants whose values depend on elastic moduli, and K is the one stress intensity factor present in the model.

For a given interface crack configuration with predominantly tensile loading as in Fig. 14, both the contact zone model and the crack-opening-angle model can be applied. Once a decision is made as to which model to use, the solution for that model is unique and free of interference between crack flanks. So which one should we use? The answer is not obvious, but quite possibly neither. This is because, in choosing one or the other, the *modeler* is making the decision as to the relative contributions of Mode I and Mode II to crack propagation along the interface. In effect this decision has that, for a broad spectrum of remote loadings having a significant tensile component, the ratio of G_{I} to G_{II} is to be in one or the other of the but two fixed proportions prescribed by Eqs. (3.14) and (3.16). If it happens that this a priori selection is physically appropriate, the use of the model chosen may be justifiable. If not, then not. In general, the *model* should make the decision as to the relative participation of Modes I and II, and this decision should be sensitive to the specific loading being applied.

Atkinson [94] furnishes a pair of alternative models for the interface crack tip. These each have the attribute of letting loading interact with the model itself to set relative mode participation. They both feature an interface layer which contains a stress-free crack. In the first (Fig. 15*c*), the

intervening layer is taken to be homogeneous with elastic moduli which are intermediate to the parent moduli ($0 \leqslant c \leqslant 1$ in Fig. 15*c*). In the second (Fig. 15*d*), the intervening layer is taken to have varying moduli which effect a continuous transition from those for one of the parent materials to the other (a linear variation is shown by way of simple example). For both of these *intervening-layer models*, the inverse-square-root singularities of a crack in a single material are recovered together with their associated energy release rates, Eqs. (3.5) and (3.7). Therefore, response as to mode of crack propagation is essentially the same as for a crack in a single material. That is, in accordance with one of the following scenarios.

i) If any tensile Mode I fields are excited by the applied loading, no interference or contact occurs between crack flanks and Mode I propagation along the interface is possible. Mode II contributions to propagation may also be present under these circumstances.

ii) If any compressive Mode I fields are excited, interpenetration of the crack flanks is predicted and must be alleviated by admitting contact between them. Crack propagation along the interface can only occur in Mode II under these circumstances.

iii) If Mode I fields are not excited at all, Mode II is obviously the only possibility for propagation along the interface. Such propagation may occur with or without contact between the crack flanks, depending on the participation of other regular crack-tip fields.

Consequently here, under tension, there would not appear to be any reason for the modeler to fix the relative participation of modes prior to applying actual loading.

For the models of Atkinson [94] to be physically appropriate, the heights of the layers ($2h$ and h in Figs. 15*c* and *d*) need to be physically reasoned. On the atomic/molecular level, one can envisage a small region in which the cohesive laws acting within material 1 switch to adhesive laws between materials 1 and 2, then to cohesive laws within material 2. The height of this transition region can be expected to be of the order of several atomic/molecular diameters. Constitutive laws can therefore also be expected to vary over a similar size scale. Thus the incorporation of intervening layers into the global analysis of crack configurations is not without significant analytical challenges.

Nonetheless, the intervening-layer models of Atkinson [94] are conceptually valuable and support the mode of crack propagation being dependent on applied loading in much the same way as for the crack in a homogeneous plate. It follows that these models do not in general support the use of either the contact zone model or the crack-opening-angle model. Rather they lend support adopting the strategy for treating interface cracks first put forward in He and Hutchinson [95], and subsequently amplified in Suo and Hutchinson [96]. This strategy simply sets η of Eqs. (1.3), (3.9), and (3.10) to zero by suitably adjusting material moduli. Such a *perturbed moduli model* has no oscillatory character and accompanying crack-flank interference, and has decoupled energy release rates, G_{I} and G_{II}, as in Eqs. (3.5) and (3.7).

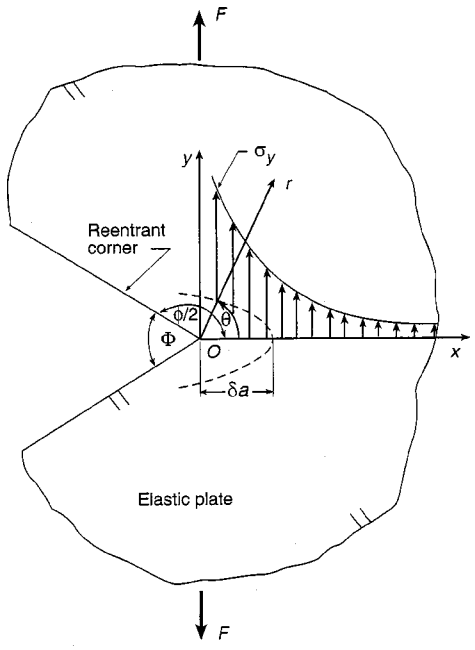

Fig. 16 Tensile stress ahead of a reentrant corner and displacements accompanying a small extension under symmetric loading

Further support for the perturbed moduli model stems from the fact that, generally, η is small ($|\eta| < 7/40$, see Eq. (1.3)). Hence setting it to zero does not change the absolute value of the singularity exponent much ($<6\%$), nor does it necessitate dramatic changes in elastic moduli. Indeed, for plane strain, it is always possible to maintain the actual ratio of shear moduli sought in an application and get η to be zero by adjusting a Poisson's ratio while still maintaining it within the physical range of zero to one half. More precisely in this regard, one can proceed as follows. Without loss of generality, number the materials so that $\mu_1 \leqslant \mu_2$. Then replace the actual κ_1 by $\hat{\kappa}_1$ where

$$\hat{\kappa}_1 = (\kappa_2 - 1)\frac{\mu_1}{\mu_2} + 1 \tag{3.17}$$

This replacement value by itself ensures $\eta = 0$ for plane strain. For plane stress, though, some modifications to the true ratio of the shear moduli are needed to render $\eta = 0$ when one shear modulus differs from the other by more than a factor of three. Even so, the strategy would seem to be the most effective way of treating interface cracks within classical elasticity at this time.

3.3 Interpreting other singularities: The *K*-controlled annulus hypothesis

In attempting to interpret other singular configurations, it is natural at the outset to try and extend energy release rate arguments. As a demonstration, we consider the sharp reentrant corner under symmetric loading (Fig. 16).

The stresses directly ahead of the corner are dominated by the singular field there. Thus, in terms of the rectangular Cartesian coordinates of Fig. 16,

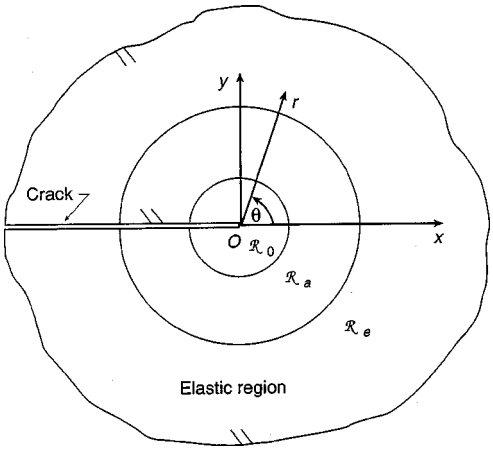

Fig. 17 *K*-controlled annulus at a crack tip

$$\sigma_y = \frac{K_{2\gamma}}{\sqrt{2\pi}\, x^{\gamma}} + o(1) \quad \text{as} \quad x \to 0 (x \geqslant 0) \tag{3.18}$$

on $y=0$, wherein γ is the singularity exponent and $K_{2\gamma}$ its associated stress intensity factor. In the event that the corner angle Φ tends to zero and the corner becomes a crack with $\gamma = 1/2$, we recover the first of Eqs. (3.1). Other values of the singularity exponent for other corners can be determined using Williams [20]. These values show that $\gamma < 1/2$ for $\Phi > 0$ (eg, for $\Phi = 90°$, $\gamma = 0.46$).

Now we entertain a small crack-like extension of length δa. We take this extension to be in the form of a mathematically sharp small crack when undeformed so that no material is removed. Its deformed shape is indicated in Fig. 16 and the companion displacement assumes the same expression as previously, namely as in Eq. (3.2). Furthermore, using the same energy argument as in Section 3.1 results in the same expression for the energy release rate, namely Eq. (3.3). On introducing Eqs. (3.18) and Eq. (3.2) into Eq. (3.3), and making the change of variable as for (3.4), we obtain

$$G_{\mathrm{I}} = \frac{1+\kappa}{4\pi\mu} K_{2\gamma} B(1-\gamma, 3/2) \lim_{\delta a \to 0} K_{\mathrm{I}} \delta a^{1/2-\gamma} \tag{3.19}$$

where B is the beta function. What becomes apparent in Eq. (3.19) is that the crack is a somewhat fortunate "corner" since it is the only one which has a finite G_{I} (because $\gamma = 1/2$ and $K_{\mathrm{I}} \neq 0$ as $\delta a \to 0$). All other corners have zero G_{I} (because $\gamma < 1/2$ and K_{I} is bounded as $\delta a \to 0$). This conclusion can also be reached using any of the valid path-independent integrals for the energy release rate mentioned in Section 3.1. Accordingly, we cannot use an energy release rate interpretation for reentrant corners with $\Phi > 0$. Moreover, energy release rate arguments break down in a similar way for a wide variety of other singular configurations. Needed, therefore, is an alternative interpretation.

One alternative interpretation argues for a *K*-controlled annulus. The essential elements of such an argument are given in Irwin [100]; a more extensive discussion is given in Rice [101] in the context of extending the applicability of linear elastic fields for cracks to instances in which small scale yielding is admitted. These elements are as follows.

In the immediate vicinity of a crack tip there exists a region wherein the *K* fields are just not physically appropriate by virtue of the singularity they contain. To keep the development simple, enclose this region within a circle centered on the crack tip ($\mathfrak{R}_0$ in Fig. 17). If the radius of this region in small enough, immediately outside it stresses for the *K* fields dominate those for all other elastic fields. As one moves further away, the stresses of the *K* fields become of comparable magnitude to the others present. Under these circumstances, the region exterior to $\mathfrak{R}_0$ may be subdivided into an annular region $\mathfrak{R}_a$ in which the *K* fields are valid and dominant, and a still further removed exterior region $\mathfrak{R}_e$ in which the *K* fields, while valid, have comparable stresses to the regular fields (Fig. 17). Within the annulus $\mathfrak{R}_a$, then, the *K* fields can be regarded as prescribing physically appropriate traction boundary conditions for the innermost crack-tip region $\mathfrak{R}_0$. In this sense, *K* can be expected to control what happens at the crack tip. If the material is perfectly brittle, this means *K* controls brittle fracture at the crack tip. If the material is ductile but any yielding is confined to within $\mathfrak{R}_0$, *K* may be still be viewed as controlling fracture at the crack tip.

Before examining the implications of a *K*-controlled annulus interpretation further, some additional clarification of the notion of the *K* stress fields dominating the other regular stresses present in the annulus is helpful. At the outset, one might be tempted to adopt the obvious but stringent criterion that the tractions from *K* fields dominate those from regular fields at *all* points on a circular arc within the annulus. Unfortunately, this is typically not possible. To explain further, the stress components that can act as tractions on a circular arc within $\mathfrak{R}_a$ are σ_r and $\tau_{r\theta}$ (Fig. 17). If the crack is under symmetric loading, the K_{I} stress field has $\sigma_r = 0$ at $\theta = \pm\pi$ (see, eg, Tada et al [55], p. 1.4b). Thus, the magnitude of the associated traction cannot dominate that of any regular field with $\sigma_r \neq 0$ at $\theta = \pm\pi$, and there are a number of such regular fields for Mode I cracks (these stem from polynomial solutions). Alternatively, if the crack is under antisymmetric loading, the K_{II} stress field has $\sigma_r = \tau_{r\theta} = 0$ at $\theta = \pm 2\sin^{-1}1/\sqrt{3}$ (ibid). Again there are regular fields whose tractions are not dominated. Accordingly, while σ_r and $\tau_{r\theta}$ may act as controlling tractions within $\mathfrak{R}_a$, the criterion for them to do so needs to be based on something other than their own values point by point throughout $\mathfrak{R}_a$.

To develop an alternative criterion, we take the principal physical phenomenon we are trying to capture with our *K*-controlled annulus interpretation for a crack to be brittle fracture on radial rays emanating from the crack tip. Physically, brittle fracture is predominantly caused by tensile stresses. It follows that we can expect the hoop stress on radial rays σ_θ to control this event. Of course, within $\mathfrak{R}_0$ this stress component goes to infinity in traditional elastic treatments. However, within $\mathfrak{R}_a$ it does not. Hence, in principle we can check if the maximum σ_θ for the *K* fields in $\mathfrak{R}_a$ is an

order of magnitude greater than the maximum σ_θ from any regular fields. If this is the case, it would seem reasonable to view the K fields as dominant.

The foregoing is but one fairly simple possibility for assessing the dominance of K fields in the annulus; others exist. For Mode I configurations, the resulting K-controlled annulus interpretation is the same as accepting the energy release rate G_I as controlling fracture. For mixed-mode situations, it is essentially equivalent to the fracture criterion proposed in Erdogan and Sih [102] and supported by some experimental evidence therein. Thus while this choice is not unique, it does not appear unreasonable and it does help focus ensuing discussion. Moreover, it is not expected that other reasonable alternatives would significantly alter the conclusions drawn from this discussion.

One attribute of the K-controlled annulus interpretation that we have adopted is that it can be applied to singularities other than just those at a crack. Reconsider our earlier example of a reentrant corner under symmetric tensile loading (Fig. 16). Even for a corner subtending an angle of 90°, the singularity is almost as strong as for a crack. Hence, if the K-controlled annulus argument is successful for a crack, it can reasonably be expected to be capable of extension to reentrant corners subtending angles up to 90° and subjected to tensile loading. For other singularities which are yet weaker, the dominance of the associated stresses is confined to a smaller neighborhood of the singular point, but so too may be the region wherein stresses are not physically appropriate. Consequently, it would not seem unreasonable to entertain the possibility of a K-controlled annulus for these situations as well.[16]

While successful in extending the range of singular configurations that can be interpreted over that with just energy release rate arguments, there are some shortcomings in the K-controlled annulus approach for these other singularities. We demonstrate this next with some examples.

Returning to the special case of the 90° reentrant corner, typically mixed-mode loading can be expected in practice. That is, loading which is neither purely symmetric nor purely antisymmetric about the bisector of the corner angle. Under these circumstances, there are two *different types* of stress singularities that can be present (as for F in Fig. 2*d* and P_5 of Table 2). Thus, in terms of the cylindrical polar coordinates of Fig. 16,

$$\sigma_\theta = \frac{K_s}{\sqrt{2\pi}r^{0.46}} + \frac{K_a}{\sqrt{2\pi}r^{0.09}} \quad \text{as} \quad r \to 0 \tag{3.20}$$

on $\theta = 0$. In Eq. (3.20), K_s and K_a are the generalized stress intensity factors associated with symmetric and antisymmetric loading, respectively. Given the different orders of the stress singularities associated with K_s and K_a in Eq. (3.20), it is not clear that they share a common annulus. Further, even if they do, we cannot always tell if one of the two fields is dominant with respect to the other, or how to combine their effects. This is so even if we continue to base our decisions in this regard on σ_θ in the annulus despite σ_θ now having distinctly different dependencies on r. The reason is that, if K_a happens to be bigger than K_s, we cannot tell which has the larger σ_θ without a knowledge of the radius of the arc whereon we are making the comparison. However, because we do not know the true physical stress field, we are not really able to specify the location of the annulus with this arc. So here a K-controlled annulus interpretation does not readily permit predictions of what happens under mixed-mode loading.

A further example of a potential shortcoming in the K-controlled annulus approach is that of the epoxy-steel butt joint (as for P_7 of Table 2 and Fig. 2*e*). Herein there is but one stress intensity factor for both the normal stress and the shear on the interface. Hence, any fracture on the interface is constrained by traditional elastic modeling to occur with a fixed ratio of tensile contribution to shear, irrespective of the composition of the far-field loading. This sort of unrealistic limitation makes it unlikely that this single K can be reliably used to predict brittle fracture for widely differing loads.

On the other hand, for a single type of configuration, one may be able to use stress intensity factors to *rank* different adhesives' strengths. When the adhesives share a common Poisson's ratio and the adherend is relatively rigid, there is a common singularity exponent and the value of K at fracture can be expected to reflect the relative strength of the adhesives for the particular test configuration used. For other adhesive-adherend interfaces wherein the singularity exponents are not identical but are close to one another, it may be possible to perturb elastic moduli so that the singularity exponents become the same, and then rank adhesive strengths for the specific configuration of concern. However, when singularity exponents differ to the point that it is not judged to be reasonable to coalesce them via moduli modifications, comparisons of adhesive strengths can be expected to be less consistent.

To explain further, suppose that, for a butt joint under tension with a single adherend, glue 1 has a singularity exponent γ_1 and a stress intensity factor at brittle fracture along the interface of K_1, while glue 2 has a singularity exponent γ_2 and a stress intensity factor at fracture of K_2. Thus, if $\sigma_f^{①}$ and $\sigma_f^{②}$ are the normal stresses on the interface at fracture for glue 1 and 2, respectively,

$$\sigma_f^{①} = \frac{K_1}{\sqrt{2\pi}r^{\gamma_1}} + o(1), \quad \sigma_f^{②} = \frac{K_2}{\sqrt{2\pi}r^{\gamma_2}} + o(1), \quad \text{as} \quad r \to 0 \tag{3.21}$$

where r is now the distance from where the interface meets the outside of the specimen (P_7 in Fig. 2*e*). Two different situations can now be envisaged. First, we have the situation where we can name the two glues so that

$$\gamma_1 > \gamma_2 \quad \text{and} \quad K_1 > K_2 \tag{3.22}$$

Then the local stresses are uniformly higher for glue 1 and it is reasonable to conclude that glue 1 is probably stronger than glue 2 for the given butt joint in tension, and quite

[16] K-controlled annulus interpretations have also been advanced for the interface crack (Rice [103]). They particularly merit being considered when the perturbed moduli approach is not applicable. Such can be the case in anisotropic configurations; Hutchinson and Suo [104] reviews such instances.

possibly so for like butt joints. Second, we have the situation wherein, regardless of how we name the two glues, we have a jumbled result as in

$$\gamma_1 > \gamma_2 \quad \text{but} \quad K_1 < K_2 \tag{3.23}$$

or vice versa. Then the local stresses vary as to which glue has higher values and it is difficult to decide which is the *locally* stronger glue just for the given butt joint, let alone more generally. As with the earlier reentrant corner example, we would need to know the actual location of a common K-controlled annulus to make a judgment, assuming a common annulus exists.

As a final example of a shortcoming in the K-controlled annulus approach, we consider a relatively rigid chisel indenting a block (as for P_9 of Table 2 and Fig. 2g). The singularity coefficient, or generalized K, in this instance depends upon the angle of the chisel tip and the elastic moduli of the block. However, it is independent of the load applied to the chisel. Accordingly, even if a K-controlled annulus existed for such a configuration, the K involved could not be used to estimate loads to fracture.

These examples illustrate the sort of difficulties that can be encountered in employing the more generally applicable interpretation of a K-controlled annular region to stress singularities. They underscore that care needs to be exercised in order to appreciate the limitations of the approach and use it consistently.

The hypothetical nature of K-controlled annulus arguments also bears comment. The basic hypothesis has that, as one moves away from a singularity, the singular stresses become physically applicable while they still dominate the other stresses present. So what is ''physically applicable?'' Certainly the singular fields would seem to have to comply with all three of the underlying and unpoliced assumptions of linear elasticity to be assured of attaining this quality. This is not difficult to check in specific instances. For example, for the Griffith crack (Fig. 4 with $b \to 0$), compliance with the assumptions of elasticity on the crack plane ahead of the crack tip is tantamount to insisting that the stresses there are at or below yield levels. Using coordinates as in Fig. 3, the normal stress on this plane is (see, eg, Tada et al [55], pp 1.20, 5.1),

$$\frac{\sigma_y}{\sigma_0} = \frac{x+a}{\sqrt{x(x+2a)}} \quad \text{on} \quad y=0 \tag{3.24}$$

for $x > 0$. Determining the location x_Y when this stress equals the yield stress gives

$$\frac{x_Y}{a} = \left[1 - \left(\frac{\sigma_0}{\sigma_Y}\right)^2\right]^{-1/2} - 1 \tag{3.25}$$

The corresponding contribution of the K field, the singular stress σ_y^s, is then given by (ibid, pp 1.3, 5.1)

$$\frac{\sigma_y^s}{\sigma_Y} = \frac{\sigma_0}{\sigma_Y}\sqrt{\frac{a}{2x_Y}} \tag{3.26}$$

Provided far-field loading is maintained below 50% of the yield stress, Eqs. (3.25) and (3.26) have the K field as contributing 90% or more of the normal stress at x_Y. Consequently, here we can readily find a location at which the K field dominates while complying with the assumptions within elasticity theory. Similarly, other configurations can and should be checked for such compliance.

Unfortunately, while complying with the underlying assumptions of elasticity may be a necessary requirement for the K fields to be physically applicable, it is generally not a sufficient one. This is because the physical discrepancy between the singular stresses and reality that must occur near a singular point may result in the singular stresses continuing to deviate significantly from the true physical stresses even when they are in accord with all three linearizing assumptions. We demonstrate how this type of deviation can occur in the simpler context of beam theory next.

To this end, we reconsider the earlier cantilever beam example taken from Frisch-Fay [34] (Section 1.4). This example compares tip deflections from nonlinear and linear beam theory, and demonstrates that linear theory is seriously in error. At the other end of the beam where it is built in, though, both theories give the same ''deflection,'' namely zero. Moreover, we can identify a length of the beam, starting where it is built in, within which it is reasonable to regard linear theory as being in compliance with the assumption that recovers it from nonlinear theory. This assumption has

$$\left[1 + \left(\frac{dv}{dx}\right)^2\right]^{3/2} \approx 1 \tag{3.27}$$

where v is now the beam deflection and x the coordinate along the beam's length. Suppose now we adopt the view that anything up to a 10% difference between the right-hand and left-hand sides of Eq. (3.27) can be regarded as the two sides being in fair agreement. It follows that linear theory is in fair agreement with its underlying assumption if

$$\frac{dv}{dx} \leqslant \frac{1}{4} \tag{3.28}$$

Solving the linear beam problem, with x measured from the built-in end and for the specifications of Frisch-Fay [34], we find Eq. (3.28) is met for $0 \leqslant x \leqslant 64$ mm (2 1/2 inches). Thus, in this range linear beam theory can be regarded as conforming with its underlying assumption. However, also in this range, linear beam theory has the bending moment as varying from 11.3 to 11.0 N-m (100 to 97.5 lbf-in). In fact, nonlinear beam theory gives the bending moment as varying from 5.0 to 4.7 N-m (44 to 41.5 lbf-in). This is a discrepancy of more than a factor of two. What is happening here is that the physically inaccurate predictions of linear theory for $x > 64$ mm are continuing to pollute predictions when $x < 64$ mm, even though linear theory is in fair agreement with its underlying assumption in this range.

The same sort of pollution is a possibility for singular stress fields. Not to say that it has to happen, just that it might. Accordingly, we simply cannot know whether a K-controlled annulus really exists without knowing what the true physical stress field is, something we typically do not know. Consequently we need to resort to indirect means to

infer the existence or otherwise of a K-controlled annulus. Arguably the best of these is to examine the physical accord with predictions made via K. We look to examine some physical evidence in this light next.

3.4 How well do K interpretations work?

As remarked in Section 3.1, the two interpretations of stress singularities discussed here are mutually consistent inasmuch as both identify stress intensity factors as the parameters controlling brittle fracture. The energy release rate hypothesis does this for cracks; the K-controlled annulus for cracks and other singularities. Too, both interpretations share an integration of singular stresses. The energy release rate approach does this directly as in Eqs. (3.3) and (3.6); the K-controlled annulus indirectly by, in effect, considering control on the boundary of a region including the singularity. Henceforth, therefore, we refer to both as simply K interpretations.[17]

By far the greatest practical application of K interpretations is to configurations entailing cracks. The attendant technology is termed linear elastic fracture mechanics (LEFM). Currently, LEFM plays a central role in attempts to try and ensure the structural reliability of components in the presence of cracks. Accordingly we focus our assessment of how well K interpretations work on their performance within LEFM.

Linear elastic fracture mechanics leads the field of solid mechanics when it comes to explicitly recognizing the presence of singularities and attempting to interpret them in a physically meaningful way. In implementing this activity, it has made considerable progress in the last 50 years. At this time, the analytical tools for determining stress intensity factors are well in hand. For most configurations, sufficiently accurate determinations of stress intensity factors for practical purposes can be made either by drawing directly on compendia of K's (Tada et al [55], Rooke and Cartwright [105], Sih [106], and Murakami et al [107–109]), or by applying suitably-adapted numerical methods that have been developed. On the testing side, procedures have been well thought out so as to limit plasticity effects and, thereby, enhance the applicability of LEFM. For fracture under monotonic loading, the design of these procedures was led by Srawley and Brown [110]. In essence, [110] takes advantage of the constraint inhibiting plastic flow that is produced by increasing thickness. This constraining effect enables restriction of an estimate of the yield region extent to being within about 2 percent % of the crack length. This in turn allows application of the approach to metals, and [110] is now the basis of a standard for the determination of plane-strain *fracture toughness* for metallic materials, K_{Ic}. That is, the test procedure to be followed to ensure limited plasticity when obtaining K_{Ic}, the critical value of K_{I} at which fracture commences for a given metallic material. This standard of the American Society for Testing and Materials, ASTM E399, has further evolved since Srawley and Brown [110] to the point that it is difficult to imagine any further significant refinements.[18] Present-day testing practice that applies this standard is also typically reliable.

Table 3. Scatter in K_{Ic} testing

Specimen type	Intralaboratory	Interlaboratory
Bend	±7%	±11%
Compact tension	±4%	± 7%
C-shaped	±5%	±10%

Evidence of the reproducibility achieved by testing laboratories in applying ASTM E399 is available in the results found from round-robin testing programs described in Heyer and McCabe [112], McCabe [113], and Underwood and Kendall [114] for bend specimens, compact tension specimens, and C-shaped specimens, respectively. All told, 17 different laboratories took part in these programs. From these test results, scatter can be estimated in K_{Ic} determination.

In undertaking this assessment, we use results for a single specimen type with a fixed nominal size and comprised of the same material. As a measure of scatter we take the 95% confidence limits of the normal distribution divided by the mean and expressed as a percentage. That is, $\pm 100\,(1.96 s_{K_{\mathrm{Ic}}}/\overline{K}_{\mathrm{Ic}})$, $s_{K_{\mathrm{Ic}}}$ being the sample standard deviation in K_{Ic}, and $\overline{K}_{\mathrm{Ic}}$ being the mean value of K_{Ic}. We compute these scatter measures using only results which have no reported violations of ASTM E399 whatsoever. That is, results that are free of any designation indicating concerns regarding compliance with the standard in Tables 3, 2, and 3 of Heyer and McCabe [112], McCabe [113], and Underwood and Kendall [114], respectively. We then average the scatter measures so found for the different materials tested with a given specimen type to obtain an overall representative measure of scatter for that particular type of specimen. Results are presented in Table 3. Given the considerable demands placed on testing by ASTM E399, the reproducibility of K_{Ic} evident in this table is a tribute to the effort and care expended by the various laboratories taking part.

In all, the implementation of a K interpretation for crack-tip singularities is a credit to the fracture mechanics community. Hence, in considering how well such K interpretations work, the practice of them can generally be regarded as being well done and reliable.

As, arguably, the most basic means of assessing how well the K interpretation of LEFM works we can check the degree to which fracture toughness is truly a material property. That is, a property for a given material which remains *constant* for different configurations which are acceptable within the limits of applicability of the theory. One way of doing this is to consider values of K_{Ic} for the same material found by different laboratories over the years.

In undertaking this survey we draw upon compendia of sources of such data assembled in Hudson and Seward [115-117]. Materials selected for inclusion in the survey are those with greater numbers of different sources furnishing results so as to gauge the presence of any variability better. To this

[17]It is also possible to regard Barenblatt's approach as an "interpretation" of singular stress fields, although it removes them. Viewed in this way, it too identifies K as the parameter controlling fracture.

[18]A recent version of this standard may be found in ASTM [111].

Table 4. Variability in K_{Ic}

Material	Sample size	Variability
Steels		
4340:T1	14	±50%
4340:T2	32	±62%
4340:T3	39	±41%
4340:T4	29	±41%
Aluminum alloys		
6061-T651	11	±25%
7075-T6	35	±51%
7079-T6	13	±44%
Titanium alloys		
Ti-6A1-4V:P1	23	±39%
Ti-6A1-4V:P2	29	±62%
Ti-6A1-4V:P3	21	±49%
Ti-6A1-4V:P4	39	±61%
Ti-6A1-4V:P5	17	±43%

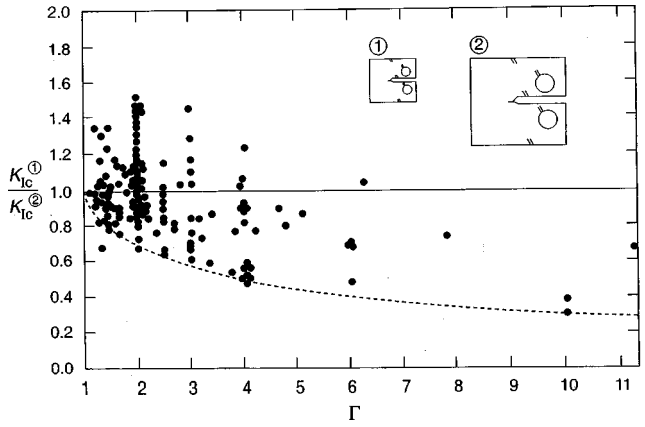

Fig. 18 Size dependence of fracture toughness

end, the following materials are chosen: four 4340 steels distinguished by tempering temperatures (T1–T4), three aluminum alloys, and five Ti-6A1-4V titanium alloys separated by processing (P1–P5). Details of the different tempering temperatures and processing may be found in Hoysan and Sinclair [118]. Values of K_{Ic} are included only if contributors claimed them to be in compliance with ASTM E399. Results are summarized in Table 4.

Results in Table 4 are drawn from over 50 different laboratories. When these testing laboratories repeated tests of the same material made with the same sized specimens of the same kind, just the average value is kept in the survey. On the other hand, if one laboratory tested different materials, or the same material but with different types of specimens, then companion fracture toughness results from that laboratory are viewed as being independent and included as multiple values. The total number of independent measurements of K_{Ic} for a given material is designated the sample size in Table 4. Also in Table 4, variability for a single material is represented as previously (ie, $\pm 100\ (1.96 s_{K_{Ic}}/\overline{K_{Ic}})$).

Evident in Table 4 is that there is considerable variation in fracture toughness values. On average over all materials considered, the variability is ±47%, or a factor of 2.8 between the lowest value and the highest. By way of comparison, the yield strength of the same materials varies on average by ±11%, or a factor of 1.2 between the lowest and the highest.

Clearly, one needs to exercise care in obtaining a representative toughness for a particular material and using it to predict fracture in an attempt to guard against this event. If the material is one in Table 4, then taking the low end of the spread should probably furnish a conservative estimate (corresponding actual numerical values can be found in [118]). If the material is not one in Table 4, and no information is readily available as to its distribution of K_{Ic}, then dividing an isolated value by a factor of three should probably furnish a conservative estimate.

The foregoing raises the issue of the identity of the source of the substantial variations in fracture toughness reported in Table 4, especially since these variations are significantly larger than the scatter indicated in Table 3. Current practice for measuring fracture toughness applies predominantly bending loads to cracks in test pieces; for example, three-point-bend, compact, disk-shaped compact, and arc-shaped specimens.[19] Furthermore, test pieces are quite geometrically similar, with cracks penetrating about half the widths of specimens and being about equal in extent to their thicknesses (see [111]). Therefore, loading type and geometric proportions can be expected to cause little of the fracture toughness variations reported in Table 4. In contrast, absolute size is not completely dictated in ASTM E399. Thus size effects are possible sources of discrepancy in a material's fracture toughness. We consider this possibility further next.

To assess whether size has any effect on fracture toughness, we need results from tests performed on a single material using a single type of specimen with size alone being altered. Sinclair and Chambers [119] collects data of this genre—specifics of the restrictions enforced to try to ensure testing varied solely as to size scale are described therein.

Focusing on plane-strain brittle response (yield region, if any, of extent less than about 2% of the crack length), Fig. 18 presents results from 43 different papers which together contain over 800 distinct tests. In the figure, $K_{Ic}^{①}$ is the fracture toughness determined via the smaller specimen, $K_{Ic}^{②}$ via the larger, with Γ being the scale factor between the two (the inserted compact specimens with a $\Gamma \approx 2$ are merely intended to be illustrative). While designated as K_{Ic} to reflect being in the plane-strain brittle regime, only about 30% of the fracture toughness values used in Fig. 4 are claimed by their contributors to be valid in the sense of complying with ASTM E399. For some, being nonmetals, such compliance is not appropriate. For others, it is hard to tell completely. However, all were checked for compliance with the central restriction of ASTM E399, namely limited yielding. Further, separating those claimed as in accord with the standard from the remainder did not reveal any major differences between the two sets of results in terms of the ratios $K_{Ic}^{①}/K_{Ic}^{②}$ for different Γ.

For fracture toughness to be size independent, the ratio $K_{Ic}^{①}/K_{Ic}^{②}$ should be unity for all scale factors Γ (the solid line in Fig. 18). Evident in Fig. 18 are clear demonstrations of

[19]While the compact specimen was formerly referred to as the compact tension specimen, this designation was simply to reflect the means by which loading is applied, namely by pulling. The peak nominal stress ahead of the crack is largely (≈90%) due to bending rather than tension.

fracture toughness being *size dependent*. Given that the range of variation of $K_{\mathrm{Ic}}^{①}/K_{\mathrm{Ic}}^{②}$ spans more than a factor of four, such size dependence could be a source of at least some of the variability found in fracture toughness.

One should not be that surprised that, even when fracture is appropriately brittle in nature, the fracture toughness of a given material can vary by about a factor of three, quite possibly due to fracture toughness being size dependent. Fracture toughness' role as a material constant controlling brittle fracture is the outcome of the hypothesis (or hypotheses) that led to the K interpretation for singularities. Being hypothetical, this role may or may not be fulfilled in practice. The physical evidence, in fact, shows that the hypotheses underlying LEFM are not complied with, or at least, not closely so.

Nonetheless, LEFM can take credit for predicting trends in the fracture of cracked components. By way of example, we reconsider the data in Fig. 18. For the specimens involved in generating this data, the stress intensity factors can in general be expressed by

$$K_1=\sigma_0\sqrt{\pi a}f(a/w) \tag{3.29}$$

where σ_0 is an applied stress, a continues as crack length, and $f(a/w)$ is a function of geometry with w being some other dimension of the specimen, such as the overall width at the crack plane. At fracture, therefore, for two completely scaled specimens,

$$K_{\mathrm{Ic}}^{①}=\sigma_f^{①}\sqrt{\pi a}f(a/w),\quad K_{\mathrm{Ic}}^{②}=\sigma_f^{②}\sqrt{\pi\Gamma a}f(\Gamma a/\Gamma w) \tag{3.30}$$

wherein the subscript f is now put on the applied stresses to denote values at fracture. If fracture toughness is size independent, Eqs. (3.30) have

$$K_{\mathrm{Ic}}^{①}/K_{\mathrm{Ic}}^{②}=1,\ \ \sigma_f^{①}/\sigma_f^{②}=\sqrt{\Gamma} \tag{3.31}$$

That is, the strength or stress at fracture decreases with increasing size. If, on the other hand, the strength is size independent, Eqs. (3.30) have

$$\sigma_f^{②}/\sigma_f^{②}=1,\ \ K_{\mathrm{Ic}}^{①}/K_{\mathrm{Ic}}^{②}=1/\sqrt{\Gamma} \tag{3.32}$$

The dashed line in Fig. 18 plots $K_{\mathrm{Ic}}^{1}/K_{\mathrm{Ic}}^{2}$ of Eqs. (3.32). Evident in Fig. 18 is that nearly all the data lie above this dashed line. This means that nearly all the data comply with the *trend* predicted by fracture mechanics of decreasing strength of cracked components with increasing size. Unfortunately, all the data do not agree well with the *precise reduction* predicted by fracture mechanics, that of Eqs. (3.31). Typically, this is the case for other predictions of fracture mechanics: Qualitatively they are correct, yet quantitatively there is room for considerable improvement.[20]

3.5 How well do other "interpretations" work?

Given the potential for greater predictive capability, it is natural at this point to seek alternatives to K interpretations of singular stresses. To this end, one could consider dispensing with any 2D or 3D stress analysis and predicting failure by merely comparing *nominal net-section stress* ahead of singularities with some suitable measure of material strength. Certainly this is a procedure which appeals in its ease of implementation. However, what Fig. 18 demonstrates is that such an approach does not agree well with the physical data. This is because it predicts strength size independence. That is, it predicts Eqs. (3.32) and the dashed line in Fig. 18. This prediction is almost an outlier of the physically measured responses. In contrast, at least fracture predictions based on a K interpretation capture the trend in the data. This superior predictive performance can be attributed, in part, to the fact that at least a K interpretation recognizes the presence of a stress concentration, albeit with a somewhat nonphysical measure. Nominal net-section stress does not. Since, in reality, fracture can be expected to be significantly influenced by stress concentrations, this recognition realizes a significant real advantage for K interpretations over ones made with nominal net-section stress. That said, there is no reason to preclude the use of a fracture criterion based on nominal net-section stress in an adjunct role. Indeed, if K ever failed to predict brittle fracture when the nominal net-section stress exceeded the ultimate stress of a brittle material, a nominal net-section stress criterion should be enforced.

What about other alternatives that do attempt to recognize the influence of stress concentrations in singular configurations? Over the years, a number of these have been wittingly or otherwise suggested, and they continue to be used today. All, in essence, draw on field quantities near but not at the singularity of concern to infer failure right at the singular point. As a result they may be termed *nearby fracture criteria*.

In implementing nearby fracture criteria, two choices need to be made: what to monitor as governing fracture, and where to monitor it. With respect to the first option, several possibilities have been entertained in the literature over the years. Among these are measures reflecting stresses and strains at the singularity. Stresses are usually used in elastic analyses and typically in complex configurations (eg, for failure in composites as in Chamis [121]; and for biomedical applications as in Valliappan, Kjellberg, and Svensson [122]). Strains are normally preferred when significant plastic flow accompanies fracture (eg, Belie and Reddy [123], Kim and Hsu [124], and Chen [125]). Other quantities employed are the crack opening displacement of Wells [126] and the crack opening angle of Andersson [127], the former having gained sufficient acceptance to have a British Standard [128] and an ASTM Test Procedure [129] to govern its measurement.[21] While the majority of these quantities selected in the role of governing fracture are for plastic response, given that elastic precedes plastic it is fair to examine them all with respect to performance in the elastic regime.

All of the nearby fracture criteria concomitant with the

[20]The focus here of the assessment of K interpretations is on monotonic loading rather than cyclic. This is because this is the simpler situation and accordingly where one could expect K interpretations to perform best. Some evidence that this is in fact so may be found in Sinclair and Pieri [120].

[21]Crack opening displacement was independently introduced in Cottrell [130] to effect a somewhat different objective, that of classifying brittle fracture—see Burdekin [131] for a review of its role in fracture mechanics.

above measures must make their comparisons at locations which are *removed* from the actual singular point. This is because the elastic stresses and strains at a singularity are infinite while, for the case of the tensile crack, the displacement and opening angle at the tip are fixed independent of load level (being zero and π, respectively).

Indeed, this quality of being removed, even if only by a short distance, is a principal motivation for selecting the foregoing quantities in the first place, namely having a quantity which is responsive to loading yet ''measurable.'' Such measurement can be effected either via FEA or some other analytical method for nearby stresses and strains, or even by direct physical means for crack opening displacement and angle. Nevertheless, the decision to withdraw from the actual singular point of concern should not imply a retreat from the original objective of predicting failure at the singular point. It is therefore a logic requirement of proposers/users of nearby fracture criteria to clearly identify what is their corresponding fracture criterion *at the singularity*. Despite inferences in various papers to the contrary, the complexity of the configuration being considered does not obviate one from this responsibility.

Turning to a consideration of possible companion fracture criteria at the singularity, it is almost embarrassingly obvious to make the following comments at the outset, but necessary nonetheless given suggestions made in the literature. It is an exercise in futility to attempt to use nearby quantities to infer elastic stresses and strains at the singularity because they are unbounded there. Thus their true infinite values are useless for comparison with any corresponding finite limiting ones. The fact that *estimates* of stress and strain at a singularity can be finite reflects the limitations of the procedure used to do the estimation, not physics. One simply cannot rely upon errors in analysis to make a nonphysical field in a model physically appropriate. Ultimately, with a sufficiently accurate analysis, a large enough value of stress or strain at the singular point must result so as to exceed any finite corresponding limit imposed, irrespective of load level. Such comparisons are therefore meaningless. Moreover, the situation is not improved in any real sense by introducing plastic flow (recall the discussion in Section 2.1).

Given the need for a bounded quantity at the singularity, and one which reflects load levels, there would not seem to be any significantly different alternative to K. In fact, K is the explicit choice made in the elastic regime by criteria based upon crack opening displacement or angle. It follows that nearby fracture criteria cannot be expected to realize any real improvement in predictive capability over that offered by K interpretations.

Indeed, nearby fracture criteria can typically be expected to be even less reliable. The reason for this is that attempting to determine K from nearby quantities can be, in itself, an unreliable undertaking. A demonstration of this possibility is given in Sinclair [132]. Therein, two artificial applications are constructed which each have known closed-form solutions. Thereafter, nearby stress, strain, and crack opening displacement and angle are used to infer K, with all specifics of corresponding estimation procedures being set a priori. All four estimate $K \neq 0$ when $K = 0$ in the first application, and all four find $K = 0$ when $K \neq 0$ in the second. Such dramatically erroneous determinations can be attributed to the mischievous intent of the author of this article. Nevertheless, they do indicate the potential of further discrepancies being introduced by the use of nearby fracture criteria.

At this time then, K interpretations of elastic singularities represent the best available. Properly implemented, they can provide qualitative predictions to guide in designing for structural integrity. Quantitatively, they may provide satisfactory predictions, but they cannot be relied upon to do so in general. Hence, ultimately, one can expect that most designs based on K interpretations are going to require specific and rigorous testing.

4 ANALYZING STRESS SINGULARITIES

4.1 Asymptotic identification: Classical analysis

Asymptotic characterization of elastic singularities can aid the stress analyst in two ways. In the first instance, it can alert the analyst to the possibility of singular stresses—''possibility'' because whether or not local singular stress fields in fact participate in a particular global configuration usually depends on the actual far-field loading in that global configuration. If this possibility is realized, it is essential for it to be appreciated if any useful information whatsoever is to be gleaned from such a physically limited model. At present, the best use of such a stress analysis is via a K interpretation. This requires a definition of an appropriate K, which in turn requires the identification of the local singular field present. This is the second way in which asymptotic characterization can be of assistance.

Several methods are available for analytically undertaking the asymptotic analysis of stress singularities in elasticity. One is the use of potentials together with separation of variables. This approach appeals in its directness. It was first used in Knein [28] to identify the singularity in a single elastic configuration. Since, it has seen use in Williams [20,133] and Kitover [134] to establish the eigenvalue equations governing singularity exponents for a wide range of configurations. These equations are solved in Williams [20,133] so as to explicitly identify possible stress singularities.

Alternatively, complex variables may be introduced to yield an approach which is compact in its representations. This method of analysis was first employed in Huth [135] to treat the same class of problems as in Williams [20], then shown in Williams [136] to lead to the same results as the earlier separation of variables.

These two methods were applied to elastic configurations having locally homogeneous boundary conditions. When local boundary conditions are inhomogeneous, transform methods are natural to consider. Brahtz [27] does this for an angular plate comprised of a single elastic material, while Bogy [137], following Tranter [138], uses the Mellin transform for a bimaterial plate, and the Mellin transform has seen extensive use since. It is, though, quite possible to explore the effects of inhomogeneous conditions using the

original separation-of-variables method or complex variables. Essentially, all three methods enable the same identification of possible stress singularities to be made. The choice of which one to use is really a matter of personal preference for the analyst undertaking the asymptotics: We choose separation of variables here and describe its basic elements next.

By way of a simple illustration, we reconsider the elastic plate with a stress-free reentrant corner, or notch, and subjected to tensile loading (Fig. 16). The symmetry of the configuration enables attention to be confined to the upper half of the plate which, in terms of the polar coordinates r and θ of Fig. 16, is contained in $0<\theta<\phi/2$. Here ϕ is the entire angle subtended at the corner within the plate ($0<\phi \leqslant 2\pi$). What we seek is the local character of the stresses σ_r, σ_θ, and $\tau_{r\theta}$, and displacements u_r and u_θ in the corner of the plate (viz, as $r\to 0$). These fields are to satisfy the equations of elasticity together with the following traditional boundary conditions: the stress-free conditions on the plate edge,

$$\sigma_\theta=\tau_{r\theta}=0 \quad \text{on} \quad \theta=\phi/2 \tag{4.1}$$

for $0<r<\infty$; and the symmetry conditions ahead of the notch,

$$u_\theta=0, \quad \tau_{r\theta}=0, \quad \text{on} \quad \theta=0 \tag{4.2}$$

for $0<r<\infty$.

To construct appropriate forms for the solutions to the field equations of elasticity for complying with the conditions Eqs. (4.1) and (4.2), we follow Williams [20] and let the stresses be generated by an Airy stress function χ in accordance with

$$\sigma_r=\frac{1}{r}\frac{\partial\chi}{\partial r}+\frac{1}{r^2}\frac{\partial^2\chi}{\partial\theta^2}$$

$$\sigma_\theta=\frac{\partial^2\chi}{\partial r^2}, \quad \tau_{r\theta}=-\frac{\partial}{\partial r}\left(\frac{1}{r}\frac{\partial\chi}{\partial\theta}\right). \tag{4.3}$$

Such stresses satisfy the equilibrium requirements: Provided χ is biharmonic, they are also compatible so that companion displacements exist. These may be determined with the aid of an auxiliary harmonic function which is given in Section 2.45, Coker and Filon [139] (see also Williams [20]).

The determination of a biharmonic χ for Eqs. (4.3) can be further reduced to the determination of two harmonic functions Ψ and $\hat{\Psi}$, since χ admits to being represented by

$$\chi=\Psi+r^2\hat{\Psi} \tag{4.4}$$

Separation of variables directly furnishes a candidate Ψ as

$$\Psi=r^{\lambda+1}[c_1\cos(\lambda+1)\theta+c_2\sin(\lambda+1)\theta] \tag{4.5}$$

wherein λ, c_1, and c_2 are constants (the choice of $\lambda+1$ as an exponent rather than just λ follows Williams [20], and results in somewhat simpler equations for λ later). In selecting $\hat{\Psi}$, it is essential that the resulting χ involve a single power of r. This is so that each of the boundary conditions in Eqs. (4.1) and (4.2) holding for $0<r<\infty$ leads to but one condition on the constants in Ψ and $\hat{\Psi}$. Then we have a chance of complying with these boundary conditions by virtue of having four constants—two each for Ψ and $\hat{\Psi}$—for four equations. Accordingly we take

$$\hat{\Psi}=r^{\lambda-1}[c_3\cos(\lambda-1)\theta+c_4\sin(\lambda-1)\theta] \tag{4.6}$$

where c_3 and c_4 are the further constants. Hence, substituting Eqs. (4.5) and (4.6) into Eq. (4.4) realizes a χ with four constants sharing a common $r^{\lambda+1}$ multiplier. Processing this Airy stress function, using Eqs. (4.3) and the Coker and Filon relations, furnishes corresponding stresses and displacements. Thus we have, as our *basic separable fields*,

$$\begin{aligned}
\sigma_r&=-\lambda r^{\lambda-1}[c_1\cos(\lambda+1)\theta+c_2\sin(\lambda+1)\theta\\
&\quad+(\lambda-3)(c_3\cos(\lambda-1)\theta+c_4\sin(\lambda-1)\theta)]\\
\sigma_\theta&=\lambda r^{\lambda-1}[c_1\cos(\lambda+1)\theta+c_2\sin(\lambda+1)\theta\\
&\quad+(\lambda+1)(c_3\cos(\lambda-1)\theta+c_4\sin(\lambda-1)\theta)]\\
\tau_{r\theta}&=\lambda r^{\lambda-1}[c_1\sin(\lambda+1)\theta-c_2\cos(\lambda+1)\theta\\
&\quad+(\lambda-1)(c_3\sin(\lambda-1)\theta-c_4\cos(\lambda-1)\theta)]\\
u_r&=\frac{-r^\lambda}{2\mu}[c_1\cos(\lambda+1)\theta+c_2\sin(\lambda+1)\theta\\
&\quad+(\lambda-\kappa)(c_3\cos(\lambda-1)\theta+c_4\sin(\lambda-1)\theta)]\\
u_\theta&=\frac{r^\lambda}{2\mu}[c_1\sin(\lambda+1)\theta-c_2\cos(\lambda+1)\theta\\
&\quad+(\lambda+\kappa)(c_3\sin(\lambda-1)\theta-c_4\cos(\lambda-1)\theta)]
\end{aligned} \tag{4.7}$$

In Eqs. (4.7), c_1 and c_2 of Eq. (4.5) have been exchanged for $c_1/(\lambda+1)$ and $c_2/(\lambda+1)$ so as to slightly simplify expressions, and μ continues as the shear modulus, κ as the function of Poisson's ratio given in Eq. (1.3) et seq.

Now applying the symmetry conditions Eqs. (4.2) gives

$$c_2=c_4=0 \tag{4.8}$$

Applying the outstanding stress-free conditions Eqs. (4.1) to the remaining terms then yields the 2×2 system of equations

$$r^{\lambda-1}\boldsymbol{A}\boldsymbol{c}=\boldsymbol{0}$$

$$\boldsymbol{A}=\begin{pmatrix}\lambda\cos(\lambda+1)\phi/2 & \lambda(\lambda+1)\cos(\lambda-1)\phi/2\\ \lambda\sin(\lambda+1)\phi/2 & \lambda(\lambda-1)\sin(\lambda-1)\phi/2\end{pmatrix}$$

$$\boldsymbol{c}=\begin{pmatrix}c_1\\ c_3\end{pmatrix} \tag{4.9}$$

for $0<r<\infty$. For this homogeneous system of equations to have a nontrivial solution, the determinant of the coefficient matrix must be zero. That is

$$D=0 \tag{4.10}$$

where D is the determinant of $\boldsymbol{A}$. Hence we obtain the *eigenvalue equation* for our example as

$$\lambda^2(\sin\lambda\phi+\lambda\sin\phi)=0 \tag{4.11}$$

The eigenvalue Eq. (4.11) is for the eigenvalues, or characteristic values, of the boundary value problem described in Eqs. (4.1), (4.2), and surrounding text.

Given the r-dependence of the stresses in Eqs. (4.7), if we focus on *integrable singular stresses* we can confine our search for roots of Eq. (4.11) to the range

$$0<\lambda\leqslant 1 \tag{4.12}$$

Within this range, a root for each of two special cases is immediate:

$$\lambda=1/2 \quad \text{for} \quad \phi=2\pi$$
$$\lambda=1 \quad \text{for} \quad \phi=\pi \tag{4.13}$$

The first of these gives the familiar inverse-square-root singularity of a tensile crack or a flat lubricated rigid punch on a half-space (see Table 2, points P_2 and P_3). For $\pi<\phi<2\pi$, there is one real root for λ satisfying Eq. (4.11): For $0<\phi<\pi$, there are no real roots. Actual values of λ for ϕ in the first of these ranges need to be found numerically. Results so obtained can be fairly readily fitted to within 0.5% by

$$\lambda=0.5+2.425\hat{\phi}^3+6.3\,\hat{\phi}^5$$
$$\hat{\phi}=1-\frac{\phi}{2\pi}, \quad \pi\leqslant\phi\leqslant 2\pi \tag{4.14}$$

The fit of (4.14) recovers the λ's of Eqs. (4.13) and connects the two for other ϕ.

For any $\phi>\pi$, the associated singular *eigenfunction* can be assembled as follows. First, substitute the corresponding eigenvalue, λ from Eqs. (4.14), into the fields of Eqs. (4.7). Next, set $c_2=c_4=0$ therein in accordance with Eqs. (4.8). Last, determine the relationship between c_1 and c_3 from Eqs. (4.1) when λ equals the eigenvalue, and substitute this relationship into the fields. By way of example, for the special case of a crack ($\phi=\pi$), these steps give $\lambda=1/2$ and $c_3=2c_1$. Then, on exchanging c_1 for $K_{\mathrm{I}}/2\sqrt{2\pi}$ so as to recover the stress intensity factor, the stresses from Eqs. (4.7) are:

$$\begin{Bmatrix}\sigma_r\\ \sigma_\theta\end{Bmatrix}=\frac{K_{\mathrm{I}}}{4\sqrt{2\pi r}}\left[\begin{Bmatrix}5\\3\end{Bmatrix}\cos\frac{\theta}{2}\begin{Bmatrix}-\\+\end{Bmatrix}\cos\frac{3\theta}{2}\right]$$
$$\tau_{r\theta}=\frac{K_{\mathrm{I}}}{4\sqrt{2\pi r}}\left[\sin\frac{\theta}{2}+\sin\frac{3\theta}{2}\right] \tag{4.15}$$

Displacements follow similarly from Eqs. (4.7). The stress field of Eqs. (4.15) is one form of the now classical, Mode I, singular eigenfunction for crack-tip stresses, originally identified in Williams [140] and Irwin [84].

Another form of stress singularity can be directly identified via the same approach. This type of singularity stems from complex roots to the eigenvalue equation, a possibility appreciated in Williams [20,133], and further amplified in Williams [21]. For our illustrative example, the eigenvalue Eq. (4.11) is simply comprised of algebraic and trigonometric functions of λ. For other configurations, this essentially remains the case. Thus, since these functions are symmetric in the complex domain, complex eigenvalues occur as complex conjugates. That is, as

$$\lambda=\xi\pm i\,\eta \tag{4.16}$$

with $0<\xi\leqslant 1$ as the counterpart of Eq. (4.12). For such complex eigenvalues, the definition of equality in the complex domain assures that the real and imaginary parts of associated *eigenfunctions* are each individually eigenfunctions in themselves. For example, the c_1 contribution to σ_r of Eqs. (4.7), when λ is as in Eq. (4.16), becomes the two expressions

$$\begin{aligned}\sigma_r=&-c_1r^{\xi-1}[\cos(\xi+1)\theta\cosh\eta\theta(\xi\cos(\eta\ln r)\\&-\eta\sin(\eta\ln r))+\sin(\xi+1)\theta\sinh\eta\theta(\xi\sin(\eta\ln r)\\&+\eta\cos(\eta\ln r))]\end{aligned}$$

$$\begin{aligned}\sigma_r=&-c_1'r^{\xi-1}[\cos(\xi+1)\theta\cosh\eta\theta(\xi\sin(\eta\ln r)\\&+\eta\cos(\eta\ln r))-\sin(\xi+1)\theta\sinh\eta\theta(\xi\cos(\eta\ln r)\\&-\eta\sin(\eta\ln r))]\end{aligned} \tag{4.17}$$

where c_1' is generally a distinct constant from c_1. Evident in Eqs. (4.17) is the oscillatory nature that accompanies complex eigenvalues.

Returning to our illustrative example, the determination of eigenvalues of the form Eq. (4.16) proceeds routinely on separating the eigenvalue Eq. (4.11) into real and imaginary parts. For $\pi<\phi<2\pi$, given $0<\xi\leqslant 1$, graphical arguments can then be used to establish that there are no complex roots. There are complex eigenvalues when $\xi>1$, though these do not give rise to singular stresses. There do exist other configurations, though, for which complex eigenvalues do give rise to singular stresses. Examples include the interface crack and the adhering rigid indentor (as for points P_2 and P_3 in Table 2 and Fig. 2*a* and *b*).

The foregoing analysis can be applied to other boundary conditions for in-plane loading, as well as to out-of-plane shear, bending within classical theory, and to composite versions of all of these configurations. However, there are some further stress singularities and different types of boundary conditions for which it is not immediately applicable. We look to its adaptation to accommodate these situations next.

4.2 Asymptotic identification: Further developments

An additional form of stress singularity results from entertaining logarithmic character. To investigate this possibility, we need to augment the fields of Eqs. (4.7) with ones containing $\ln r$. To this end, observe that Eqs. (4.7) satisfy the plane field equations of elasticity for any λ. In fact, these fields are continuously differentiable functions of λ. Hence, because their r-dependence is of the form $r^{\lambda-1}=e^{(\lambda-1)\ln r}$,

they can be differentiated with respect to λ to generate the sought-after fields containing $\ln r$. This is the approach adopted in Dempsey and Sinclair [29]. For the basic fields of Eqs. (4.7) it leads to, as our *auxiliary fields*,

$$\begin{aligned}
\sigma_r &= -r^{\lambda-1}[(1+\lambda\ln r)(c_1\cos(\lambda+1)\theta+c_2\sin(\lambda+1)\theta)\\
&\quad+(2\lambda-3+\lambda(\lambda-3)\ln r)(c_3\cos(\lambda-1)\theta\\
&\quad+c_4\sin(\lambda-1)\theta)-\lambda\theta(c_1\sin(\lambda+1)\theta-c_2\cos(\lambda+1)\theta\\
&\quad+(\lambda-3)(c_3\sin(\lambda-1)\theta-c_4\cos(\lambda-1)\theta))]\\
\sigma_\theta &= r^{\lambda-1}[(1+\lambda\ln r)(c_1\cos(\lambda+1)\theta+c_2\sin(\lambda+1)\theta)\\
&\quad+(2\lambda+1+\lambda(\lambda+1)\ln r)(c_3\cos(\lambda-1)\theta\\
&\quad+c_4\sin(\lambda-1)\theta)-\lambda\theta(c_1\sin(\lambda+1)\theta-c_2\cos(\lambda+1)\theta\\
&\quad+(\lambda+1)(c_3\sin(\lambda-1)\theta-c_4\cos(\lambda-1)\theta))]\\
\tau_{r\theta} &= r^{\lambda-1}[(1+\lambda\ln r)(c_1\sin(\lambda+1)\theta-c_2\cos(\lambda+1)\theta)\\
&\quad+(2\lambda-1+\lambda(\lambda-1)\ln r)(c_3\sin(\lambda-1)\theta\\
&\quad-c_4\cos(\lambda-1)\theta)+\lambda\theta(c_1\cos(\lambda+1)\theta+c_2\sin(\lambda+1)\\
&\quad\times\theta+(\lambda-1)(c_3\cos(\lambda-1)\theta+c_4\sin(\lambda-1)\theta))]
\end{aligned} \tag{4.18}$$

$$\begin{aligned}
u_r &= \frac{-r^\lambda}{2\mu}[(c_1\cos(\lambda+1)\theta+c_2\sin(\lambda+1)\theta)\ln r\\
&\quad+(1+(\lambda-\kappa)\ln r)(c_3\cos(\lambda-1)\theta+c_4\sin(\lambda-1)\theta)\\
&\quad-\theta(c_1\sin(\lambda+1)\theta-c_2\cos(\lambda+1)\theta\\
&\quad+(\lambda-\kappa)(c_3\sin(\lambda-1)\theta-c_4\cos(\lambda-1)\theta))]\\
u_\theta &= \frac{r^\lambda}{2\mu}[(c_1\sin(\lambda+1)\theta-c_2\cos(\lambda+1)\theta)\ln r\\
&\quad+(1+(\lambda+\kappa)\ln r)(c_3\sin(\lambda-1)\theta-c_4\cos(\lambda-1)\theta)\\
&\quad+\theta(c_1\cos(\lambda+1)\theta+c_2\sin(\lambda+1)\theta\\
&\quad+(\lambda+\kappa)(c_3\cos(\lambda-1)\theta+c_4\sin(\lambda-1)\theta))]
\end{aligned}$$

Together, the stresses and displacements of Eqs. (4.18) continue to satisfy the field equations of elasticity because these equations are independent of λ (that such is the case may be verified by direct substitution). What now becomes apparent is that the stresses of Eqs. (4.18) can also be singular when $\lambda=1$, the upper limit admitted in Eqs. (4.12), since then they can go to infinity as $\ln r$ when $r\to 0$. For $\lambda>1$, though, they remain bounded when $r\to 0$.[22]

The fields found via λ-differentiation can be supplemented by the originating fields of Eqs. (4.7). When combined in this way, the constants need no longer be the same so we now distinguish the constants in Eqs. (4.7) as $\boldsymbol{c}'$. Introducing the combination into the boundary conditions in our example, the earlier system Eq. (4.9) now involves different functions of r, with

$$r^{\lambda-1}\ln r\boldsymbol{A}\boldsymbol{c}+r^{\lambda-1}\left[\frac{\partial\boldsymbol{A}}{\partial\lambda}\boldsymbol{c}+\boldsymbol{A}\boldsymbol{c}'\right]=\boldsymbol{0} \tag{4.19}$$

for $0<r<\infty$. In Eq. (4.19), $\partial\boldsymbol{A}/\partial\lambda$ is the matrix with elements obtained by differentiating all corresponding elements of $\boldsymbol{A}$ of Eqs. (4.9) with respect to λ. For our example, Eq. (4.19) is a 2×2 system. In general, it can be an $n_A\times n_A$ system, n_A being the order of $\boldsymbol{A}$. In either case, the first term in Eq. (4.19) recovers our original determinant condition, Eq. (4.10), for a nontrivial $\boldsymbol{c}$. The second term requires some analysis to establish the necessary conditions for maintaining a nontrivial $\boldsymbol{c}$—essentially these conditions result from ensuring a consistent or solvable system for $\boldsymbol{c}'$.

Under Eq. (4.10), $D=0$ and the rank of $\boldsymbol{A}$ must be less than its order n_A. If the rank of $\boldsymbol{A}$ is n_A-1, then necessary conditions for a nontrivial $\boldsymbol{c}$ are

$$D=\frac{\partial D}{\partial\lambda}=0 \tag{4.20}$$

That is, the eigenvalue is a repeated root. Equations (4.20) are effectively the conditions that are noted to hold for a pure logarithmic singularity ($\lambda=1$) with inhomogeneous boundary conditions in Bogy [141]: sans $D=0$, Eqs. (4.20) for $\lambda=1$ are stated as the condition for a pure log singularity under homogeneous boundary conditions in Bogy and Wang [142]. Equations (4.20) are shown to be necessary for $\boldsymbol{c}\neq\boldsymbol{0}$ for $0<\lambda\leq 1$ under homogeneous boundary conditions, and when the rank $r_A=n_A-1$, in Dempsey and Sinclair [29].

If, instead, the rank r_A is further reduced to n_A-2, n_A-3,.., the conditions in Eqs. (4.20) are not enough. Under these circumstances, necessary conditions for a nontrivial $\boldsymbol{c}$ are

$$D=\frac{\partial D}{\partial\lambda}=\frac{\partial^2 D}{\partial\lambda^2}=\cdot\cdot\frac{\partial^{n_A-r_A}D}{\partial\lambda^{n_A-r_A}}=0 \tag{4.21}$$

This result is established in Appendix 1, [29], for either pure logarithmic singularities ($\lambda=1$), or logarithmic intensification of power singularities ($\lambda<1$, see Eqs. (4.18)): It includes the previous result Eqs. (4.20). We note, however, that $\boldsymbol{c}\neq\boldsymbol{0}$ and the existence of local fields of the form of Eqs. (4.18) does not necessarily mean local logarithmic terms. It is possible for a nontrivial $\boldsymbol{c}$ to exist yet the coefficient of $\ln r$ terms be zero. This occurs for $\lambda=1, c_1=c_2=c_3=0$, and $c_4\neq 0$—see Eqs. (4.18).

Returning to our illustrative example, there are no repeated roots to Eq. (4.11) within the range of Eq. (4.12). Therefore, there is no logarithmic character in the singular stresses because Eqs. (4.20) are necessary condition for the same. On the other hand, if instead of confining attention to symmetric loading in our reentrant corner example we had admitted antisymmetric as well, we would have had a repeated root for the case of a crack (viz, for $\phi=2\pi$ and $\lambda=1/2$ with a multiplicity of 2). Accordingly Eqs. (4.20) would have been satisfied. Nonetheless, there is no logarithmic intensification of the singularity in this instance. This is because the rank of the now 4×4 coefficient matrix drops to two for $\lambda=1/2$, and Eqs. (4.20) are not sufficient under such circumstances. Furthermore, Eqs. (4.21) are not satisfied so

[22]One might be inclined to try to employ the classical Michell solution for auxiliary fields since it does contain log terms. However, in its usual form (eg, Art 43, Timoshenko and Goodier [16]), this solution does not contain all the terms in Eqs. (4.18).

that no logarithmic intensification results. There are, though, other instances in which Eqs. (4.21) are satisfied and logarithmic singular character is possible: Quite a number of these are identified in Part II of this review.

In summary, then, the *singular stresses that are possible with homogeneous boundary conditions* follow as below, in what might reasonably be regarded as order of decreasing singular character. For any stress component σ, as $r\to 0$,

$$\begin{aligned}
&\sigma = O(r^{\xi-1}\cos(\eta \ln r)) + O(r^{\xi-1}\sin(\eta \ln r))\\
&\quad \text{when } D=0 \text{ for complex } \lambda = \xi + i\eta\ (0<\xi<1)\\
&\sigma = O(r^{\lambda-1}\ln r) + O(r^{\lambda-1}) \text{ when } D=0,\ \frac{\partial^n D}{\partial \lambda^n}=0\\
&\quad \text{for } n=1,..,n_A-r_A \text{ and real } \lambda\ (0<\lambda<1)\\
&\sigma = O(r^{\lambda-1}) \text{ when } D=0 \text{ for real } \lambda\ (0<\lambda<1)\\
&\sigma = O(\ln r) \text{ when } D=0,\ \frac{\partial^n D}{\partial \lambda^n}=0,\\
&\quad \text{for } n=1,..,n_A-r_A \text{ and } \lambda=1,\\
&\quad \text{with } c_1^2+c_2^2+c_3^2\neq 0\\
&\quad \text{in the auxiliary stress field of Eqs. (4.18)}\\
&\sigma = O(\cos(\eta \ln r)) + O(\sin(\eta \ln r))\\
&\quad \text{when } D=0 \text{ for complex } \lambda = 1+i\eta
\end{aligned} \tag{4.22}$$

Herein, D is the determinant of the coefficient matrix $\boldsymbol{A}$ resulting from applying boundary conditions, n_A is the order of this matrix, and r_A its rank when λ is an eigenvalue. For the single material plate in extension, at most $n_A=4$. For bimaterial plates, both boundary and interface conditions are involved in assembling $\boldsymbol{A}$: Then typically $n_A=8$. And so on.

In the last of Eqs. (4.22) we have included, as a type of ''singularity,'' stresses which in fact are bounded for $r=0$. These same stresses, though, are undefined for $r\to 0$. Consequently, to a degree, they share with actual singular stresses the futility of trying to use them directly in stress-strength comparisons at $r=0$.

In addition to the types of singularity in Eqs. (4.22), it is theoretically possible to have a combination of the first two types in Eqs. (4.22) when λ is a complex root of the appropriate multiplicity, n_A-r_A. The actual occurrence of this last sort of singularity with homogeneous boundary conditions is yet to be noted in the literature. It is also theoretically possible to have log-squared singularities. Again, the actual occurrence of this last sort of singularity with homogeneous boundary conditions is yet to be noted in the literature. It can occur, however, with inhomogeneous boundary conditions.

For inhomogeneous boundary conditions, any response can include that for the corresponding homogeneous conditions. Further, stress singularities typically stem from the homogeneous boundary conditions, especially if we require any applied inhomogeneous conditions to be sufficiently continuous. Even so, for some inhomogeneous boundary conditions, logarithmic singularities can be induced. We illustrate how to treat this sort of response by reconsidering our symmetric notch example.

Suppose in this example, the stress-free conditions of Eqs. (4.1) are replaced with conditions applying a uniform shear traction q. That is, with

$$\sigma_\theta = 0, \quad \tau_{r\theta} = q, \quad \text{on } \theta = \phi/2 \tag{4.23}$$

for $0<r<\infty$. Now introducing into Eqs. (4.23) the symmetric part of the basic stress field, Eqs. (4.7) with Eqs. (4.8), yields the 2×2 system

$$r^{\lambda-1}\ \boldsymbol{A}\boldsymbol{c} = \boldsymbol{q} \tag{4.24}$$

for $0<r<\infty$. Here $\boldsymbol{A}$ and $\boldsymbol{c}$ are as in Eqs. (4.9), and the vector $\boldsymbol{q}$ is given by $\boldsymbol{q}=(0,q)$. For Eqs. (4.24) to hold for all r, we set $\lambda=1$. Then solving for $\boldsymbol{c}$ yields $c_1 = q\csc\phi$ and $c_3 = -(q/2)\cot\phi$. Hence, for example, the shear stress is

$$\tau_{r\theta} = q\,\frac{\sin 2\theta}{\sin\phi} \tag{4.25}$$

for $0\leqslant\theta\leqslant\phi/2$. Clearly $\tau_{r\theta}$ of Eqs. (4.25) complies with the shear boundary condition in Eqs. (4.23). However, what is also clear is that there is a problem with the solution if the vertex angle is such that $\sin\phi=0$. That is, if $\phi=\pi,\ 2\pi$. Then $\tau_{r\theta}$ is *everywhere infinite* throughout the plate. Furthermore, the other stresses and even the displacements in this solution are everywhere infinite. This sort of ''singularity'' is no longer trying to reflect a physical stress concentration at the plate vertex. Rather, it represents a total breakdown in the solution procedure adopted, something which must be rectified before any physical interpretation is attempted.

The reason for the breakdown is that the fields used to arrive at Eqs. (4.25) are incomplete. To overcome this shortcoming we follow Dempsey [143] and supplement them with those of Eqs. (4.18) with Eqs. (4.8) applied. If we continue to use $\boldsymbol{c}'$ to distinguish the constants in the original stress field, our system for solution becomes

$$r^{\lambda-1}\ln r\ \ \boldsymbol{A}\boldsymbol{c} + r^{\lambda-1}\left(\frac{\partial \boldsymbol{A}}{\partial\lambda}\boldsymbol{c} + \boldsymbol{A}\boldsymbol{c}'\right) = \boldsymbol{q} \tag{4.26}$$

for $0<r<\infty$. We set $\lambda=1$ again so that the second term on the left-hand side of Eq. (4.26) becomes independent of r like the right-hand side. Now, though, we still have a system which depends on r by virtue of the $\ln r$ term. The vector coefficient of this $\ln r$ term must therefore be zero. For the problem vertex angles, $\phi=\pi$ and 2π, this can be arranged. This is because the determinant of $\boldsymbol{A}$ is zero for these angles when $\lambda=1$ (see Eqs. (4.9)): Indeed, in some sense it is the determinant of $\boldsymbol{A}$ being zero that causes the problem with these angles in the first place by prohibiting a solution to Eq. (4.24). Consequently, we merely need to make $\boldsymbol{c}$ a solution of $\boldsymbol{A}\boldsymbol{c}=\boldsymbol{0}$ for $D=0$. Then it in concert with $\boldsymbol{c}'$ enables a solution of Eq. (4.26). For example, for $\phi=\pi$, a solution is $c_1 = 2c_3 = -4c_3' = -2q/\pi, c_1' = 0$. The corresponding shear stress becomes

$$\tau_{r\theta} = \frac{-2q}{\pi}[(1+\ln r)\sin 2\theta + \theta\cos 2\theta] \tag{4.27}$$

for $0\leqslant\theta\leqslant\pi/2$. Clearly $\tau_{r\theta}$ of Eq. (4.27) complies with the shear boundary condition in Eqs. (4.23). Clearly, also, $\tau_{r\theta}$ of Eq. (4.27) is logarithmically singular at the plate vertex.

Given symmetry for our plate of vertex angle π, it realizes a half-space with a jump in surface shear traction from $-q$ to q. Accordingly, the log singularity present is akin to that at P_8 of Table 2 and Fig. 2*f*. This sort of singularity is admissible in elasticity and does reflect the physical stress concentration that occurs at a step discontinuity in shear traction.

While the analysis leading to Eq. (4.27) and like expressions for the other stresses does solve the plate loaded by a uniform shear when $\phi=\pi$, it does not provide a reasonable transition from stresses like that of Eq. (4.25) as ϕ passes through π. In fact, from Eq. (4.25) it would appear that, for ϕ near but not equal to π, $\tau_{r\theta}$ can be made arbitrarily large.

To furnish a more sensible transition, Ting [144] supplements the solution of Eq. (4.25) with its homogeneous counterpart (ie, the stresses for $q=0$). This leaves compliance with Eqs. (4.23) unaltered. By suitably adjusting the participation of these additional stresses, a reasonable transition from $\tau_{r\theta}$ of Eq. (4.25) through $\tau_{r\theta}$ of Eq. (4.27) can be effected as ϕ passes through π. Such transitions are obtained for the other stresses and for further configurations in Ting [144]. Since they recover results found via Eqs. (4.18), the approach in Ting [144] can be used just by itself.

Either via Dempsey [143] plus Ting [144], or just by Ting [144], a number of configurations that would otherwise have breakdowns in their analysis can be treated. Typically, this leads to logarithmic stress singularities when constant tractions are applied; ''typically'' because occasionally systems like Eq. (4.24) with $D=0$ are still consistent because the augmented matrix also drops in rank. Analogous results hold for linear displacements.[23]

Observe that, for these log singularities with *inhomogeneous* boundary conditions, the requirements in the last of Eqs. (4.22) do not apply. All that is required is $D=0$ when $\lambda=1$. Indeed, if D has a repeated root at $\lambda=1$, further fields other than just those of Eqs. (4.18) are typically needed. These fields stem from further differentiation with respect to λ. As noted in Dempsey and Sinclair [29], this leads to $\ln^2 r$ terms. For the auxiliary field of Eqs. (4.18), it gives the *further auxiliary stress field*

$$\begin{aligned}
\sigma_r=&-r^{\lambda-1}[(\lambda\ln^2 r+2\ln r-\lambda\theta^2)(\hat{c}_1\cos(\lambda+1)\theta\\
&+\hat{c}_2\sin(\lambda+1)\theta+(\lambda-3)(\hat{c}_3\cos(\lambda-1)\theta\\
&+\hat{c}_4\sin(\lambda-1)\theta))-2\theta(1+\lambda\ln r)(\hat{c}_1\sin(\lambda+1)\theta\\
&-\hat{c}_2\cos(\lambda+1)\theta+(\lambda-3)(\hat{c}_3\sin(\lambda-1)\theta\\
&-\hat{c}_4\cos(\lambda-1)\theta))+2(1+\lambda\ln r)(\hat{c}_3\cos(\lambda-1)\theta\\
&+\hat{c}_4\sin(\lambda-1)\theta)-2\lambda\theta(\hat{c}_3\sin(\lambda-1)\theta\\
&-\hat{c}_4\cos(\lambda-1)\theta)]\\
\sigma_\theta=&r^{\lambda-1}[(\lambda\ln^2 r+2\ln r-\lambda\theta^2)(\hat{c}_1\cos(\lambda+1)\theta\\
&+\hat{c}_2\sin(\lambda+1)\theta+(\lambda+1)(\hat{c}_3\cos(\lambda-1)\theta\\
&+\hat{c}_4\sin(\lambda-1)\theta))-2\theta(1+\lambda\ln r)(\hat{c}_1\sin(\lambda+1)\theta\\
&-\hat{c}_2\cos(\lambda+1)\theta+(\lambda+1)(\hat{c}_3\sin(\lambda-1)\theta\\
&-\hat{c}_4\cos(\lambda-1)\theta))+2(1+\lambda\ln r)(\hat{c}_3\cos(\lambda-1)\theta\\
&+\hat{c}_4\sin(\lambda-1)\theta)-2\lambda\theta(\hat{c}_3\sin(\lambda-1)\theta\\
&-\hat{c}_4\cos(\lambda-1)\theta)]\qquad(4.28)\\
\tau_{r\theta}=&r^{\lambda-1}[(\lambda\ln^2 r+2\ln r-\lambda\theta^2)(\hat{c}_1\sin(\lambda+1)\theta\\
&-\hat{c}_2\cos(\lambda+1)\theta+(\lambda-1)(\hat{c}_3\sin(\lambda-1)\theta\\
&-\hat{c}_4\cos(\lambda-1)\theta))+2\theta(1+\lambda\ln r)(\hat{c}_1\cos(\lambda+1)\theta\\
&+\hat{c}_2\sin(\lambda+1)\theta+(\lambda-1)(\hat{c}_3\cos(\lambda-1)\theta\\
&+\hat{c}_4\sin(\lambda-1)\theta))+2(1+\lambda\ln r)(\hat{c}_3\sin(\lambda-1)\theta\\
&-\hat{c}_4\cos(\lambda-1)\theta)+2\lambda\theta(\hat{c}_3\cos(\lambda-1)\theta\\
&+\hat{c}_4\sin(\lambda-1)\theta)]
\end{aligned}$$

wherein $\hat{c}_i$ and $i=1, 2, 3, 4$, are further constants. Similarly, expressions can be obtained for displacements. With Eqs. (4.28), log-squared stress singularities may be possible. ''May'' because there are constants for this additional stress field which remove all $\ln^2 r$ terms when $\lambda=1$, yet do not remove the field in its entirety. These constants are $\hat{c}_1=\hat{c}_2=\hat{c}_3=0$, $\hat{c}_4\neq 0$ in Eqs. (4.28).

In summary, then, the *singular stresses that can be possible with uniform tractions/linear displacements applied* follow as below, in order of decreasing singular character.[24] For any stress component σ, as $r\to 0$,

$$\begin{aligned}
&\sigma=\mathrm{ord}(\ln^2 r)+\mathrm{ord}(\ln r)\ \text{ when }\ D=0,\quad \frac{\partial^n D}{\partial\lambda^n}=0,\\
&\quad\text{for }\ n=1,..,n_A-r_A,\quad \hat{c}_1^2+\hat{c}_2^2+\hat{c}_3^2\neq 0\\
&\quad\text{in the further auxiliary field of (4.28)}\\
&\sigma=\mathrm{ord}(\ln r)\ \text{ when }\ D=0,\quad \frac{\partial^n D}{\partial\lambda^n}=0,\\
&\quad\text{for }\ n=1,..,n_A-r_A,\quad \hat{c}_1=\hat{c}_2=\hat{c}_3=0\qquad(4.29)\\
&\quad\text{in the auxiliary field of Eqs. (4.28)}\\
&\sigma=\mathrm{ord}(\ln r)\ \text{ when }\ D=0,\quad \frac{\partial^n D}{\partial\lambda^n}\neq 0,\\
&\quad\text{for }\ n=n_A-r_A,\quad c_1^2+c_2^2+c_3^2\neq 0\\
&\quad\text{in the auxiliary stress field of Eqs. (4.18)}\\
&\quad\text{provided throughout (4.29)}\\
&\lambda=1,\quad r_A\neq r_{A'}\qquad(4.30)
\end{aligned}$$

where $r_{A'}$ is the rank of the augmented matrix formed by $\boldsymbol{A}$ and the forcing vector attending the inhomogeneous boundary conditions. The conditions in Eqs. (4.29) and (4.30) can be inferred from Dempsey and Sinclair [29] and Dempsey

[23]There are other singular configurations wherein supplementary fields like Eqs. (4.18) are needed to make the analysis complete. These involve concentrated loads. See Ting [145] for a review.

[24]Some singularities possible with other inhomogeneous boundary conditions for plates in extension are discussed in Part II. In large part, these are self evident. Singularities can also be induced with other inhomogeneous boundary conditions for plates under bending: These are also discussed in Part II.

[143]. When Eqs. (4.29) and (4.30), or their analogues for other configurations, are satisfied, log singularities do result. Examples are given in Part II of this review. When these singularities occur, their participation is controlled by the local applied loading rather than far-field conditions. When such local loading is nonzero, they must occur. Hence, the use of the ord notation in Eqs. (4.29). As noted earlier, these singularities can occur in concert with the singularities for corresponding homogeneous boundary conditions.

There is an additional type of boundary condition which requires further consideration. These are conditions which, while homogeneous in themselves, promote equations which are not homogeneous in their r-dependence when the fields of Eqs. (4.7) are introduced into them. For example, suppose normal cohesive stresses are applied ahead of the notch in our reentrant corner configuration of Fig. 16. Thus,

$$\sigma_\theta = k_e u_\theta \quad \text{on} \quad \theta = 0 \tag{4.31}$$

for $0<r<\infty$ is exchanged for the first of Eqs. (4.2), where k_e continues as the cohesive law stiffness. Substituting Eqs. (4.7) into Eqs. (4.31) then gives

$$\lambda r^{\lambda-1}[c_1+(\lambda+1)\,c_3]+\frac{k_e r^\lambda}{2\mu}[c_2+(\lambda+\kappa)\,c_4]=0 \tag{4.32}$$

for $0<r<\infty$. Since (4.32) holds for all r and now involves two distinct powers of r, it is effectively two boundary conditions. Taken together with the stress-free conditions of Eqs. (4.1) and the zero-shear condition of Eqs. (4.2), Eq. (4.32) realizes five equations in the but four unknowns, c_1-c_4. These equations cannot be made consistent for any $\lambda\neq 0$. Therefore, no nontrivial solution exists which is simply of the form of Eqs. (4.7).

To overcome this difficulty, we form fields as series by replacing λ of Eqs. (4.7) by $\lambda_n=\lambda+n$, with corresponding constants obtained on extending c_i $(i=1,2,3,4)$ to c_{i+n}, then summing on n. This series approach is the one adopted in Sinclair [146] to handle heat conduction problems with convective cooling: It is also the one used in Ting [147] to handle elastic plates with curved boundaries. With series for the fields, the cohesive condition of Eq. (4.31) becomes

$$\sigma_\theta\Big|_{\lambda_0=\lambda}+\sum_{n=1}^{\infty}\left[\sigma_\theta\Big|_{\lambda_n=\lambda+n}-k_e u_\theta\Big|_{\lambda_n=\lambda+n-1}\right]=0 \tag{4.33}$$

for $0<r<\infty$. The order of the terms in Eq. (4.33) is

$$O(r^{\lambda-1})+\sum_{n=1}^{\infty}O(r^{\lambda+n-1})=0 \quad \text{as} \quad r\to 0 \tag{4.34}$$

The lowest order terms in Eq. (4.34) are $O(r^{\lambda-1})$: Setting to zero the determinant of the coefficient matrix for these terms enables one to determine an eigenvalue λ, and corresponding eigenfunction constants c_i $(i=1-4)$. For this eigenvalue, the next terms are $O(r^\lambda)$ and serve to relate c_5-c_8 to c_1-c_4, and the terms thereafter relate c_9-c_{12} to c_5-c_8, whence c_1-c_4, and so forth (see Sinclair [67] for details). Thus, each complete eigenfunction itself becomes a series (which can be shown to converge for $r<1$). There is one such series for each eigenvalue. Hence, for a series of eigenvalues, we have a series of series for eigenfunctions.

The preceding means of constructing asymptotic fields has, as a direct consequence, that the part of the cohesive law that is active in determining eigenvalues is the stress (see Eqs. (4.7), (4.33), and (4.34)). That is, cohesive laws have exactly the same effect on singular character as setting the stress contained within them to zero. Similar outcomes hold for other boundary conditions which, on a first analysis, give rise to equations that are inhomogeneous in r. An example is the out-of-plane bending of plates within the context of sixth-order theory.

The foregoing summarizes some of the analytical tools that can be fairly readily applied to asymptotic singular analysis within classical elasticity. As mentioned earlier, alternatives exist. Faced with a specific problem, the stress analyst could entertain using any of these approaches to check for the possibility of singular stresses. It is probably easier, though, to try to draw on the literature for a pertinent analysis. To assist in this activity, there already exist some reviews: for cracks, those in Atkinson [148] and Hwang, Yu, and Yang [149]; for some bimaterial plates, that in Murakami [150]. For other configurations, hopefully Part II of the present review can help. In the event that no such analysis can readily be found, one could perform the necessary asymptotics oneself. Ultimately, this may be necessary for interpretation. However, it may be more efficient at the outset to carry out a global analysis. This is because, while it is not likely it is nonetheless possible that any associated stress singularities do not actually participate in the problem at hand if it involves local homogeneous boundary conditions.[25] Under these circumstances, singularities do not have to be asymptotically identified, and just a global analysis suffices. We turn our attention to this activity next.

4.3 Numerical analysis: Detection of singularities

In order to detect the actual presence of a stress singularity in a configuration being numerically analyzed, we need to design a sequence of successively refined analyses which can reasonably be relied on to produce diverging maximum stresses, thereby revealing the singularity. The most challenging singularities to unearth in this way can be expected to be the weakest, namely log singularities. Hence, we focus attention on this type of singularity initially.

To develop a scheme for detecting logarithmic divergence, we follow Sinclair [151] and consider an analogy with the numerical summation of series. For a series with individual members s_n, we form the partial sum $S_{\hat{n}}$ in accordance with

$$S_{\hat{n}}=\sum_{n=1}^{\hat{n}} s_n \tag{4.35}$$

[25] "Not likely" because usually the eigenfunctions remaining once the singular one is removed have zero stresses at the singular point, and are therefore unable to represent nonzero stresses there.

For such partial sums, it is sometimes implied in texts on numerical analysis that convergence can be examined by considering the sequence

$$S_{\hat{n}}, S_{2\hat{n}}, S_{3\hat{n}}, \ldots \tag{4.36}$$

With this sequence, the series sum is deemed to have converged if successive differences between sums decrease in magnitude with the last difference being less than some prescribed tolerance e. That is, the convergence criteria for the sequence of Eq. (4.36) are

$$|S_{2\hat{n}} - S_{\hat{n}}| > |S_{3\hat{n}} - S_{2\hat{n}}|, \quad |S_{3\hat{n}} - S_{2\hat{n}}| < e \tag{4.37}$$

Alternatively, a more stringent test for convergence is based upon a sequence in which the number of members in partial sums is successively doubled. Then the convergence criteria become

$$|S_{2\hat{n}} - S_{\hat{n}}| > |S_{4\hat{n}} - S_{2\hat{n}}|, \quad |S_{4\hat{n}} - S_{2\hat{n}}| < e \tag{4.38}$$

Now consider the application of the foregoing criteria to the particular instance of summing a harmonic progression, namely,

$$S_{\hat{n}} = \sum_{n=1}^{\hat{n}} \frac{1}{n} \tag{4.39}$$

Using an area estimate for Eq. (4.39) gives

$$S_{\hat{n}} \approx \int_{1/2}^{\hat{n}+1/2} \frac{dn}{n} = \ln(2\hat{n}+1) \tag{4.40}$$

While Eq. (4.40) is just an approximation, it does disclose the logarithmic divergence of the sum in Eq. (4.39). Consequently, Eq. (4.39) represents a good series to test the convergence criteria of Eq. (4.37) and Eqs. (4.38) to see if they can detect divergence.

Using Eq. (4.40) and the first sequence of partial sums in Eq. (4.36), we have, for $\hat{n}$ large,

$$\begin{aligned} &S_{\hat{n}} \approx \ln\hat{n} + \ln 2 \\ &S_{2\hat{n}} \approx \ln\hat{n} + 2\ln 2, \quad S_{2\hat{n}} - S_{\hat{n}} \approx \ln 2 - \ln 1 = 0.69 \\ &S_{3\hat{n}} \approx \ln\hat{n} + \ln 2 + \ln 3, \quad S_{3\hat{n}} - S_{2\hat{n}} \approx \ln 3 - \ln 2 = 0.41 \end{aligned} \tag{4.41}$$

Continuing, successive differences equal the difference between the natural logarithms of two successive integers. As a result, the convergence criteria of Eqs. (4.37) can be met, since differences are decreasing in magnitude and eventually can be made smaller than any prescribed e. The first convergence criteria of Eqs. (4.37) therefore *fail* to detect that the series is diverging.

On the other hand, the sequence with doubling has

$$\begin{aligned} &S_{2\hat{n}} \approx \ln\hat{n} + 2\ln 2, \quad S_{2\hat{n}} - S_{\hat{n}} \approx \ln 2 \\ &S_{4\hat{n}} \approx \ln\hat{n} + 3\ln 2, \quad S_{4\hat{n}} - S_{2\hat{n}} \approx \ln 2 \end{aligned} \tag{4.42}$$

Thus, the first convergence criterion of Eqs. (4.38) is not complied with, revealing the lack of convergence of this logarithmically divergent series. The second convergence criteria of Eqs. (4.38) therefore *pass* with respect to divergence detection. This suggests adopting the analogue of Eqs. (4.38) when undertaking numerical stress analysis.

Table 5. Numerical divergence in the presence of stress singularities

Configuration —analysis	No. of intervals or elements	$\frac{\sigma_{max}}{\sigma_{nom}}$	Percentage change
Periodic crack	32	4.49	—
under tension	64	6.22	39
—integral equation	128	8.71	55
Reentrant corner	48	2.75	—
under tension	192	3.99	45
—FEA with three	768	5.63	60
node triangles	3072	7.83	80
Epoxy-steel butt	10	1.22	—
joint under tension	40	1.49	22
—FEA with four	160	1.94	37
node quadrilaterals	640	2.51	47
	2560	3.23	59
Surface step shear	16	1.12	—
—FEA with four	64	1.35	21
node quadrilaterals	256	1.59	21

Accordingly, we successively systematically halve discretization intervals for a sequence of at least three analyses and examine whether the magnitude of differences in maximum stress values is decreasing. Initially, we favor uniform discretization throughout as a means of readily ensuring systematic refinement. We next demonstrate this approach on a set of four sample configurations, each having a different stress singularity present: The last three of these analyses are taken from Sinclair [151].

The first configuration analyzed features a crack subjected to remote tensile loading (as in Fig. 14 but with $\mu_1 = \mu_2$, $\nu_1 = \nu_2$, and F replaced by a uniform traction σ_0). So as to limit the extent of discretization, we in fact take a periodic array of such cracks sharing a common crack plane. The cracks all have length $2a$ and a center-to-center separation from their nearest neighbor of $4a$. An exact solution for such a configuration is given in Westergaard [152] and shows the presence of inverse-square-root singularities in the normal stresses ahead of the cracks. To analyze the configuration, we use an integral equation derived via periodic Flamant line loads. In the numerical analysis of this integral equation, we discretize the unknown as a piecewise constant on a set of intervals of equal length. Given an appreciation of the possible singular character of this unknown, numerical algorithms of superior efficiency can readily be devised. Here, though, we are proceeding as if we had *no such awareness* and asking the numerics themselves to reveal any singularity present. Results from applying our unsophisticated numerical analysis are presented in Table 5 for the maximum transverse normal stress ahead of a crack (σ_{max}), normalized by $\sigma_0(\sigma_{nom})$.

The second configuration treated entails a 90° reentrant corner under tension (as in Fig. 16 with $\phi = 3\pi/2$). The specific finite elastic plate chosen results from taking a square, with uniform traction σ_0 applied to its upper and lower edges, and cutting out a 90° corner on one side so that the vertex of the corner is right at the center of the original square. For such a configuration, the strongest of the singularities for P_5 in Table 2 and Fig. 2*d* can be anticipated

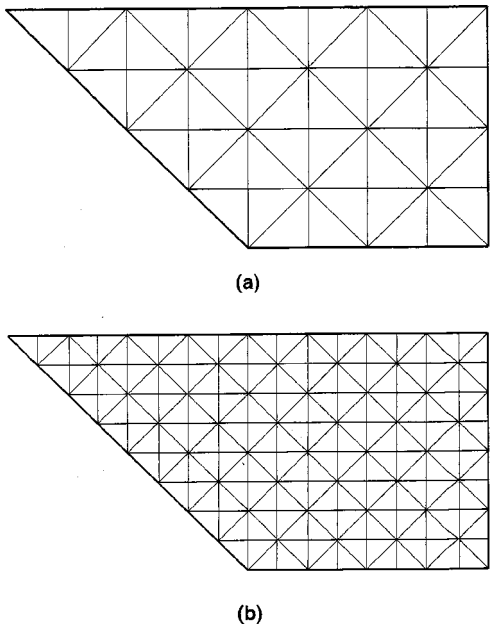

Fig. 19 Finite element grids for reentrant corner under tension: *a*) initial grid with 48 elements, *b*) first refinement with 192 elements

because this is the singularity associated with transverse tensile loading. That is, we expect stresses of $O(r^{-0.46})$ as $r \to 0$, where r here is the distance from the corner. Turning to the analysis of the configuration, symmetry enables attention to be confined to the upper half of the plate. For this upper half, we continue to proceed as if we had no appreciation of the possibility of a stress singularity and simply employ the finite element method with uniform grids comprised of three node triangles. The first grid has 48 such elements (Fig. 19*a*), the second is formed by halving element sides to result in 192 elements (Fig. 19*b*), and subsequent grids are formed by further halving element sides. Results are included in Table 5, wherein σ_{max} is the transverse normal stress directly ahead of the corner and σ_{nom} is σ_0.

The third configuration considered is that of an epoxy-steel butt joint under tension (as in Fig. 2*e*). The steel is taken to be rigid and only the epoxy analyzed. The aspect ratio of the epoxy layer is set as 10:1. The Poisson's ratio of the epoxy is taken to be approximately 3/8 so that stresses of $O(r^{-1/3})$ as $r \to 0$ can be expected, r here being the distance from points where the epoxy-steel interface meets the outside surface of the specimen (as for P_7 of Table 2 and Fig. 2*e*). Finite element analysis is again unsophisticated and uses a sequence of uniform meshes, with the elements comprising the meshes now being four node quadrilaterals. Results are included in Table 5, wherein σ_{max} is the maximum normal stress on the interface where it terminates at the outer surface, and σ_{nom} is the nominal stress at such a location.

The fourth and final configuration treated concerns an abrupt application of a shear traction to the edge of an elastic plate (as in Fig. 2*f*). The jump in the shear stress has magnitude τ_0. The singularity anticipated is logarithmic (as at P_8 in Table 2 and Fig. 2*f*). Finite element analysis is performed on a sequence of uniform grids comprised of four node quadrilaterals. Results are included in Table 5 with σ_{max} being the peak principal stress at the point of application of the shear step and σ_{nom} being τ_0.

To examine convergence in Table 5, we take the difference in $\sigma_{max}/\sigma_{nom}$ for successive analyses normalized by the ratio's value for the *first* analysis and expressed as a percentage. This process leads to the results under the column headed ''percentage change'' in Table 5. For these percentage changes, *no decrease* with successively refined analysis reveals divergence and the presence of a singularity (cf the first of Eqs. (4.38)).

For the first two configurations treated, the percentage change increases in a similar and pronounced way: This is to be expected since they have very similar singularities. For the third, with its somewhat weaker singularity, the increases are less marked but nonetheless clearly evident. In fact, for these first three, stress increases with grid refinement approach that expected from the singularity present. That is, stresses increasing by a factor of 2^{γ} where γ is 1/2, 0.46, and 1/3, respectively. For the last with its logarithmic singularity, the percentage changes remain constant, thus still indicating this singularity's presence even if only with a weak signal. Hence singularities are numerically unearthed for all four of our sample configurations.

The results in Table 5 support the use of systematic halving of discretization lengths to reveal the presence of singularities. However, they are merely a set of numerical experiments for which the approach works—for other configurations/results it may not. For example, the magnitudes of the singular shear stress on the interface in the epoxy-steel butt joint, as found on the same sequence of meshes as used for the normal stress there, are as follows.

$$\begin{aligned} &\tau_{max}/\sigma_0: \quad 0.29, \quad 0.40, \quad 0.50, \quad 0.61, \quad 0.74 \\ &\%\ \text{change:} \quad -, \quad 38, \quad 34, \quad 38, \quad 45 \end{aligned} \tag{4.43}$$

The results in Eq. (4.43) are consistent with a numerical analysis which is converging on the first three grids, even if only slowly so. The later grids, though, start to diverge, revealing the singularity present. What is happening here is that, in addition to a $O(r^{-1/3})$ singularity, the shear on the interface can have other regular contributions as $r \to 0$. The participation of these regular terms here hides the singularity from the coarser grids. Ultimately it has to show though. Nonetheless, the possibility of regular fields concealing singular ones to a degree underscores the value of an a priori appreciation of potential singular stresses, since such knowledge tends to make one check a more extensive set of analyses for their actual realization. Such an appreciation may also enable the region of grid refinement to be confined to that in the neighborhood of the potential singularity, thereby reducing computational effort.

4.4 Numerical analysis: Resolution of singular fields

Once a stress singularity's presence has been detected, it is necessary to *quantify* its participation if one is to effect a K interpretation. At this point, asymptotic identification of the nature of the singularity is no longer optional, but instead essential in order to properly define a stress intensity factor.

With a definition of K in hand, one can proceed with numerical assessment using either a boundary integral equation approach or a finite element analysis.

A good review of the early research on the application of finite element methods to singular elasticity problems is given in Gallagher [153]. This paper was part of a first symposium on numerical methods in fracture mechanics (Luxmoore and Owen [154]). Developments since, for both boundary integrals and finite elements, are reflected in subsequent symposia [155–158]. In what follows, we concentrate on finite element analysis since it enjoys more widespread use today.

There are two issues facing the stress analyst when attempting the numerical analysis of a singular problem. First, to resolve the singular fields themselves sufficiently accurately numerically. Second, to extract from the numerics the associated stress intensity factor without diminishing this level of accuracy. In this section we focus on the first activity.

With respect to resolution, a number of finite element methods have been developed. These may be loosely categorized as belonging to one of the following three classes: methods which add special elements, methods which use local grid gradation, and methods which use superposition procedures. Special elements attempt to improve resolution by introducing appropriately singular representations into the elements immediately contiguous to the singular point. Grid gradation attempts the same goal by suitably increasing the number of regular elements in the vicinity of the singular point. And superposition procedures attempt it by superimposing analytical singular fields throughout the entire region of interest, then letting the regular fields in standard elements effectively correct boundary values so that they comply with the prescribed conditions sought. In terms of implementation, special elements typically take the least amount of effort on the part of the stress analyst. This is especially so when the singular fields are introduced simply by moving the mid-side nodes of isoparametric elements. This technique is developed for cracks in Henshell and Shaw [159] and Barsoum [160]. The approach is generalized to apply to other singularities in Wait [161].[26] Given the relative ease of implementation, if such techniques can provide sufficient resolution in return for reasonable levels of computation, they would seem to be the method of choice at this time.

Before describing an assessment of the resolution of this particular method, it is appropriate to outline the elements of an *evaluation protocol* that needs to be adhered to in order for an appraisal of any numerical method to be meaningful.

i) The method needs to be completely prescribed with respect to how it is to be implemented *prior* to any testing. Under these circumstances, there is no mixing of the calibrating of any adjustable parameters in the method with true testing of the same.

ii) The problems employed must have no ambiguity as to what are their correct answers so that there is no ambiguity as to the errors incurred in their numerical analysis. This is probably best achieved via *test problems* with known and analytical solutions. Alternatively, if two or more independent analyses of the same problem employing different numerical methods have converged to exactly the same answer to more than the number of significant figures being used in the appraisal, the problem can reasonably be viewed as a *benchmark* one and used.

iii) An extensive set of such problems should be analyzed, with each member of the set being markedly *different* from all the others. Ideally, the set should be representative of all the decidedly distinct types of problem on which application of the subject numerical method is envisaged. Then it is reasonable to infer performance in general practice from the numerical experiments.

iv) The evaluation should include a check on *convergence*. In the case of FEA, this should be undertaken on a sequence of grids, with each grid being formed from its predecessor by refinement which is systematic, or nearly so. In this way one can obtain an estimate of the computational level likely to be required should further accuracy be needed.

Any evaluation that falls significantly short of complying with the above should be viewed as preliminary, and possibly encouraging further appraisal, but nevertheless seriously limited in its ability to justify the general use of the numerical method under consideration. Preliminary evaluations are to be expected by the initial developers of novel numerical procedures: Their contributions principally lie in conceiving the new approach in the first place, then explaining and demonstrating its use. However, subsequent evaluations and comparisons with other methods should, in essence, comply with the foregoing protocol.

Returning to the evaluation of special elements formed by displacing mid-side nodes, the originating papers are preliminary in this regard. Henshell and Shaw [159] treats some six problems that, as reported anyway, are not strictly benchmark problems in accordance with the protocol. Setting aside this limitation, for only three of the problems is the same grid used—the other three, therefore, can be viewed as calibrating the respective meshes used to a degree. For the three with the common grid, one problem in some sense calibrates the approach while the other two are quite similar. Hence, in effect, there is one trial problem in Henshell and Shaw [159]. For this trial problem, stress intensity factors are apparently determined to within about 1–2% using a modest amount of computational effort. Henshell and Shaw also do a convergence check on one of their problems: This exhibits divergence in computing K between a coarse and a medium grid, but convergence from the medium to a fine. Barsoum [160] analyzes only one 2D elastic configuration which again is not established as a benchmark problem within the paper. The paper uses several different meshes (which together do not constitute a convergence check), and suggests that quarter-point elements formed from six node triangles have superior accuracy to corresponding elements formed from eight node quadrilaterals. Barsoum also considers a thermoelastic and a

[26]Further references on the use of such elements may be found in Lim, Johnston, and Choi [162].

3D application. In sum, the main thrust of Henshell and Shaw [159] and Barsoum [160] is the development of quarter-point elements for the FEA of cracks, and demonstrations of its potential. This is well done in the two papers: Thorough testing of the approach, on the other hand, is not attempted.

Meda and Sinclair [163] provides an appraisal of the approach which adheres to the previous protocol in large part. Therein, a series of crack problems are analyzed using the quarter-point elements of [159,160]. The problems seek to simulate some of the variety of physical effects encountered in applications. The first configuration considered to this end involves a periodic array of cracks, all of length $2a$ with center-to-center separations of $2B$, and under far-field transverse tension. By considering different spacings ($a/B=1/4$, 1/2, and 3/4), crack interaction effects can be studied. The second configuration represents a round compact tension specimen: Herein, loading is predominantly in bending instead of tension. The third configuration simulates crack opening loading: This is basically the same configuration as the second except that loading is displacement controlled. The fourth configuration reflects crack arrest by placing the crack tip in close proximity to a stiffener. The fifth and final configuration is a slanted crack under remote tension: This is a mixed-mode situation. Together, the five configurations realize a total of seven different problems.

All of the problems are test problems in that they have known closed-form solutions. For the first problems with the different crack spacings, these solutions can be taken directly from Westergaard [152]. Notice, though, that Westergaard's treatment applies a uniform transverse tension at infinity. Since FEA requires that we treat a plate of finite height, the solution in [152] must be evaluated at the height chosen and the stresses found used to apply tractions there. While such tractions are nearly the same as those for simple tension when the height is greater than the crack spacing, they do differ a little. The inclusion of such differences is essential if one is to formulate a problem with a true exact solution using [152]. For problems entailing the next three configurations, exact solutions are constructed by the superposition of finite sets of eigenfunctions (identified using Williams [20]). The resulting sums maintain stress-free crack flanks and symmetry conditions ahead of the crack. They do not replicate the boundary conditions elsewhere that perhaps one would most naturally apply, but do reflect the character of the loading sought. In any event, whatever conditions they do realize on the remainder of the boundary are taken to be, in fact, the exact conditions thereon. Thus, these sums themselves are the exact solutions to the problems so posed. The last problem solution is obtained by combining the solution for a crack under uniform tension at infinity (see, eg, Tada et al [55], pp 1.20, 5.1), with the corresponding solution for uniform shear of Irwin [164]. As for the first problems, these solutions must be evaluated at finite stations in order to make a precise statement of the problem.

For the analysis of this series of test problems, two quarter-point elements are available: one obtained from eight node quadrilaterals, the other from six node triangles. Triangular elements are chosen over quadrilateral since the singular fields are then present within the element on all radial rays originating at its vertex, rather than just along its edges as is the case for quadrilateral elements. To be consistent, six node triangles are used as host elements. The local arrangement of the quarter-point elements follows ANSYS recommendations (Chapter 3, [32]). It features a fan of congruent isosceles triangles spreading out from the crack tip (Fig. 20). Each triangle subtends an angle of $\pi/6$ at the tip and has an altitude which is about one eighth of the crack length a The remainder of the mesh is generated automatically using the command AMESH (Chapter 9, [32]), since this is a convenient means of doing so, and one likely to be employed in practice. This procedure is adhered to for all problems to generate their baseline grids. These grids are taken as such in the first instance because they are essentially the grids recommended by ANSYS [32]. Furthermore, in practice, like grids should probably result in no more than an order of magnitude greater number of degrees of freedom, and accordingly be computationally tractable (the maximum number of degrees of freedom for the baseline grids used being 2533).

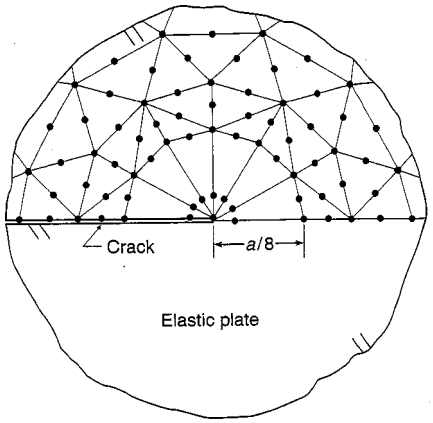

Fig. 20 Local arrangement of quarter-point elements at a crack tip (following ANSYS recommendations)

To examine convergence, baseline grids are coarsened and refined by approximately quadrupling and quartering element areas, respectively. The grid refinement is not systematic, though it is nearly so. This is because of the continued use of the convenient automatic mesh generator, AMESH, which is not completely systematic in its element configurations. It is also because of the different types of elements involved: That is, because the number of quarter-point elements remains constant while the number of host elements changes. Around the crack tip, though, the arrangement of Fig. 20 is preserved with element altitudes being doubled and halved, so that locally grid refinement may be viewed as being systematic. These pairs of additional grids are also used in the FEA of all seven test problems.

In evaluating the resolution of the finite element analysis in Meda and Sinclair [163], we focus on the stress intensity factors computed via it since these are the key results from a practical perspective. However, in making this choice, we are

Table 6. Resolution of *K* fields using quarter-point elements

Test problem description	Number of elements used in coarse, medium and fine grids	Absolute percentage error in K
Periodic crack	174	1
under tension:	620	0
$a/B=1/4, 1/2, 3/4$	1959	0
Round compact	97	1
tension specimen	328	0
	1207	0
Specimen with	97	37
crack opening	328	4
loading	1207	5
Crack arrest	97	4
at a stiffener	328	2
	1207	1
Mode I for	216	5
slanted crack	488	3
under tension	2000	1
Mode II	216	21
	488	10
	2000	4

unfortunately combining an appraisal of singular field resolution with one of *K* extraction capability. Provided the latter is consistently reasonably accurate, we should still be able to infer the effective levels of singular field resolution obtained (we examine the issue of *K* extraction in the next section).

With respect to the accuracy sought, we view 0–1% error as excellent, $1^{+}-5\%$ as good, $5^{+}-10\%$ as satisfactory, and greater than 10% as unsatisfactory. In justification thereof, given the likely level of agreement between physical response and predictions made via *K*, we can expect an excellent analysis, and even just a good analysis, to leave this agreement largely unaltered, while a satisfactory analysis probably would not impair it significantly.

The number of elements actually used and the corresponding errors in stress intensity factors are summarized in Table 6 (the same errors are obtained for all three separations in the periodic crack problem). On the baseline (medium) grid, the average absolute error is 2.4%, with four results of excellent accuracy, three with good, and one just satisfactory. With the exception of the problem with crack opening loading where results have yet to converge in going from the medium to the fine mesh, all results are converging.

A further evaluation of the resolution of quarter-point elements which largely adheres to the protocol given here may be found in Cooper et al [165]. This features more displacement controlled/Mode II loadings, the two situations which would appear to promote the greatest errors for the approach (Table 6). All told, 34 test problems are constructed in [165], with 18 being Mode I, 16 Mode II, and half for each mode having prescribed displacements. They are analyzed using the same elements and mesh generation scheme as in Meda and Sinclair [163] (ie, following ANSYS [32] recommendations coupled with easy-to-implement automatic mesh generation). This results in a baseline grid of 276 elements, and coarse and fine grids of 57 and 916 elements, respectively. For the baseline grid, the average absolute error in *K* for all 34 test problems is 1.6%, while the maximum is 5.9%. In terms of the previous rating scale, accuracy is excellent in 18 problems, good in 8, and satisfactory in 1. In 33 of the 34 problems, values of *K* computed are converging throughout the three-grid sequence employed. In the other problem, *K* values are diverging from the coarse to the medium mesh, but converging from the medium to the fine. Based on the number of elements used, the average convergence rate is about halfway between linear and quadratic.

In sum, therefore, the quarter-point elements of Henshell and Shaw [159] and Barsoum [160], when arranged around a crack tip in accordance with the recommendations of ANSYS [32], would seem to offer good levels of resolution of the singular fields involved in return for quite modest levels of computation. In general, then, the shifting of mid-side nodes on isoparametric elements would appear likely to provide a means of numerically analyzing singular fields with more than adequate accuracy, and doing so fairly readily.

4.5 Numerical analysis: Extraction of *K*'s

With respect to extraction, a variety of procedures have been suggested over the years. Probably the most obvious first approach is to attempt to take advantage of an appreciation of the asymptotic character of a singularity to fit local stresses or displacements and, thereby, estimate stress intensity factors. An early development of such *local fitting methods* is Chan, Tuba, and Wilson [166]. Alternatively, for cracks, one can obtain *K* by computing energy release rates (as in (3.5), (3.8), and (3.9)). Several distinct implementations of this approach have been put forward. The most widely practiced is via the *J* integral of Rice [88]. Others include the stiffness derivative technique of Parks [167], and the virtual crack extension method of Rybicki and Kanninen [168]. The virtual crack extension method uses local results to estimate *G*, hence *K*: accordingly it qualifies as a local fitting method. The *J* integral, on the other hand, is a *path-independent integral* and consequently does not have to draw on local fields. Parks [167], in an Appendix, shows that the stiffness derivative technique is an area-analogue of the *J* integral, so it also does not need to rely on local fields. This is a positive attribute since fields close to any singularity can be expected to be the least accurately determined via numerical analysis. A further set of procedures for extracting *K* which share this attribute are based on specially developed path-independent integrals. These integrals are constructed by an adroit invoking of Betti's reciprocal theorem: This leads to integrands that are akin to those in Somigliana integrals.[27] The method of construction has its origin in Stern [169]. The integrals that result are devoid of the direct physical interpretation of *J*, but are computationally more adaptable. For cracks, as a consequence, they can readily distinguish between different modes, as in Stern, Becker, and Dunham [170]. They can also be adapted to the fixed-free corner, as in Stern and Soni [171], and the interface crack, as in Hong and Stern [172]. Others have since taken advantage of the ideas underlying the construction of such path-

[27]A statement of Betti's reciprocal theorem may be found in Art 121, Love [12]: Somigliana integrals Art 169, ibid.

Table 7. Comparison of some *K*-extraction methods using Pang and Leggat [180]

Trial problems involved	Measures of apparent absolute error	*J* via stiffness derivative	Crack-flank displacement fit	Virtual crack extension	Stress fit ahead of crack
No. 1 with 8 grids	Average error (%)	0.5	1.2	2.3	3.8
	Accuracy distribution	8e	5e, 3g	8g	6g, 2s
Nos. 2–8	Average error (%)	2.8	3.0	—	4.7
	Accuracy distribution	6e, 10g 3s	4e, 12g 3s	—	1e, 11g 6s, 1u

Key: e...excellent (0–1%), g...good (1^+–5%), s...satisfactory (5^+–10%), u...unsatisfactory (>10%)

independent integrals to develop them for further singular configurations. Examples include the stress-free reentrant corner in Carpenter [173] and in Sinclair et al [174], the butt joint in Okajima and Sinclair [175], and the bimaterial reentrant corner in Carpenter and Byers [176]. The path-independent line integral of Okajima and Sinclair [175] can also be found in Banks-Sills [177], together with an equivalent area integral.

At the outset in evaluating these competing techniques, local fitting methods appeal in their ease of implementation and adaptability to different singularities. However, once corresponding path-independent integrals have been developed and made available as algorithms within standard codes, implementation typically requires little if any extra effort on the part of the stress analyst. Further, using Stern's approach, path-independent integrals are quite adaptable. So the initial advantages of local fitting methods can be expected to be of no great consequence in practice as the development of path-independent integrals continues. There is, though, an inherent deficiency in local fitting methods that is of concern in practice.

This deficiency stems from the fact that local fitting methods fit quantities near but not at the singularity. They must avoid the singular point because stresses there are unbounded and therefore not fitting, while displacements are zero leaving nothing to fit. Given such necessary backing off from the singular point, other regular fields can participate in any fit. This participation cannot generally be either completely accounted for by any local fitting method, or completely eliminated. As a result, local fitting methods have the potential to be unreliable in their accuracy. That is not to say they cannot furnish accurate, or even occasionally extremely accurate, estimates of K: Just that they can also provide unsatisfactory estimates.

One might think that all that is required to overcome such deficiencies is to develop a better local fitting method. Logically, though, this cannot be done in any complete sense. To explain further, any fit must match a *finite* number of quantities. Hence, since singular configurations can have an *infinite* number of regular eigenfunctions participate in addition to their singular ones, there always exists the possibility of some being left unaccounted. Indeed, the existence of such unfitted eigenfunctions at a crack tip is what is exploited in Sinclair [132] to cause the complete inaccuracy of several local fitting methods (ie, to have them estimate $K=0$ when $K\neq 0$, and vice versa).[28] Moreover, the approach therein can be adapted to ensure the downfall of any local fitting method once the specifics of how it is to be implemented have been decided. However, these types of demonstration are for contrived test problems, so that there is an open issue as to the degree such difficulties are actually encountered. To address this issue, we draw on evaluations in the literature.

The originators of local fitting methods as a means of extracting K from numerical analyses—here Chan et al [166] and Rybicki and Kanninen [168]—understandably perform preliminary evaluations that showcase potential applications rather than establish accuracy levels for a diverse range of true test or benchmark problems. Further, they do not employ their methods in conjunction with quarter-point elements, the selected approach for resolving singular fields. The same can be said of the originators of path-independent integrals as a means of K extraction—here Parks [167] and Stern et al [170].[29] Turning to evaluations that do use quarter-point elements, two limited assessments are available in Banks-Sills and Sherman [178], Pang [179], and Pang and Leggat [180].

In Banks-Sills and Sherman [178], three planar crack problems are analyzed, two being quite similar to each other. These problems are not true test problems, nor are they qualified in [178] as benchmarks in the sense defined earlier in the evaluation protocol. However, they could be accepted in the latter role with a less stringent definition than that adopted here. The best crack-flank displacement fitting procedure considered results in an apparent average error of 0.9%, with excellent accuracy for two problems, good on the other one. The path-independent integral used, the J integral as evaluated either directly or by the stiffness derivative technique, results in an apparent average error of about 0.2% with excellent accuracy on all three problems. This limited evaluation, therefore, would seem to indicate that path-independent integrals are more accurate than local fitting methods.

In Pang [179] and Pang and Leggat [180], an extensive set of crack problems is analyzed. The set entails five quite distinct configurations, eight different geometries, and twenty-seven different analyses/stress intensity factors. None

[28]Essentially, this is the same characteristic of local crack-tip fields as employed to produce the erroneous results for nearby fracture criteria that are described in Section 3.5.

[29]Rice [88] introduces the J integral to a different end and accordingly does not attempt any evaluation of it as a numerical tool.

Table 8. Evaluation of two *K*-extraction methods

Test problems involved	Absolute error measures for baseline grid	*H* via direct integration	Crack-flank displacement fit
7 (with 8 *K*'s), from Meda & Sinclair [163]	Average error (%)	2.4	10.6
	Accuracy distribution	4e, 3g 1s	4e, 1g 1s, 2u
34, from Cooper et al [165]	Average error (%)	1.6	9.3
	Accuracy distribution	18e, 15g 1s	7e, 10g 7s, 10u

Key: e...excellent (0–1%), g...good ($1^+-5\%$), s...satisfactory ($5^+-10\%$), u...unsatisfactory ($>10\%$)

are strictly qualified as true test or benchmark problems, though they could be viewed as the latter with a less stringent definition. Local fitting methods considered include displacement and stress fits, and virtual crack extension. Path-independent integrals considered include the *J* integral as calculated directly or via the stiffness derivative technique. Results for the best displacement and stress fits, as well as all those available from virtual crack extension and for the *J* integral computed via the stiffness derivative technique, are summarized in Table 7. The apparent order of decreasing accuracy is: *J* integral, displacement fit, virtual crack extension, and stress fit. When the *J* integral is computed directly, apparently the average absolute error is 1.4% with excellent accuracy in six instances, good in three: For the *J* integral computed via the stiffness derivative technique on the same set, apparently the average absolute error is 1.7% with excellent accuracy in three instances, good in six. Hence, if anything, this limited evaluation would indicate that direct calculation of *J* is slightly more accurate than via the stiffness derivative. Irrespective of the means of computation, path-independent integrals would definitely appear to be more accurate than local fitting methods in Pang and Leggat [180].

In the earlier cited papers, Meda and Sinclair [163] and Cooper et al [165], there are also contained assessments of *K* extraction methods. These assessments do basically adhere to the evaluation protocol. The two methods so evaluated are crack-flank displacement fitting and path-independent integrals developed à la Stern. For the first, its specifics are given in ANSYS [32]: Reasons for believing the particular approach prescribed therein is amongst the best of its genre available are given in Cooper et al [165]. For the second, the precise forms of the integrals used are given in Sinclair et al [174], wherein they are dubbed *H* integrals. Both approaches are applied to all the test problems for planar cracks that are set out in [163,165]. Implementation is in concert with the same arrangement of quarter-point elements as earlier. Results for the errors incurred on baseline grids are summarized in Table 8.

Evident in Table 8 is that the displacement fitting procedure on baseline grids typically leads to barely satisfactory estimates of *K*. What is more disconcerting is the scatter in performance. While this local fitting method produces estimates of excellent accuracy for a number of problems (11), it also furnishes unsatisfactory estimates on a comparable number (12). Half of the latter instances entail errors that are greater than 20%. Moreover, while performance can generally be improved by grid refinement, this is not always so: The displacement fitting procedure yields results which are not converging on going from a baseline grid to a yet finer grid on seven occasions. What is making its presence felt here is the inherent unreliability of local fitting methods.

The *H* integrals of Stern, on the other hand, almost uniformly provide good to excellent estimates of *K* on baseline grids. Moreover, the two instances of merely satisfactory accuracy converge to at least good on grid refinement. Actually, what is being displayed here is not the accuracy of *H* integrals in extracting *K*: They essentially do this exactly, as can be established by feeding the integrands in their algorithms exact values of the field quantities called for instead of finite element estimates. Thus, what is being shown is really the accuracy of the FEA determination of the fields in these singular test problems.[30] This accuracy is more than adequate provided fields in the quarter-point elements themselves, as well as those immediately contiguous to them, are avoided. This can readily be done by taking a path which lies outside these elements when computing an *H* integral: Where precisely does not matter as long as these inner elements are not on it.

In Meda and Sinclair [163], there is a further comparison of an *H* integral with *J*. Since *J* by itself cannot distinguish between different modes, the comparison does not include the mixed-mode test problem.[31] On a common subset of five test problems analyzed on the baseline grid, *J* averages 1.0% absolute error in *K*, while *H* averages 0.4%. Hence, if anything, this limited evaluation would indicate that *H* is slightly more accurate than *J*.

The foregoing discussion focuses on 2D analysis. To a degree, similar capabilities are available in three dimensions: see Banks-Sills [181] and Meda et al [182]

In all, therefore, path-independent integrals can be expected to be more reliable than local fitting methods as a means of extracting stress intensity factors. There are underlying reasons to think this might be so, and evaluations to date demonstrate that it is. Hence, path-independent integrals are to be preferred in practice. For cracks, the choice of a specific integral and the way in which it is computed is largely a matter of availability/convenience. For other singular configurations, it may well be that integrals developed along the lines of Stern and his coworkers are the only option for obtaining a corresponding path-independent integral.

When path-independent integrals are used in conjunction with isoparametric elements with mid-side nodes shifted to reflect the stress singularity present, more than adequate accuracy in the resolution and the extraction of stress intensity factors can be obtained in return for reasonable levels of both implementation and computation. Other approaches (see, eg, [154–158]), in concert with path-independent integrals, can

[30]It follows that our previous use of *K* to assess FEA resolution is not polluted by extraction error because *H* integrals are employed in this appraisal.

[31]The *J* integral can be supplemented by a further path-independent integral to enable the participation of different modes to be distinguished: see Ch 5, Cherepanov [62].

offer comparable and even superior accuracy for the same computation levels, but can take more effort on the part of the stress analyst.

5 CONCLUDING REMARKS

In classical elasticity, stress singularities can occur under point loads, line loads, and so on. They can also occur away from any such concentrated loading. Then typically they reflect, albeit crudely, physical stress concentrations. In this role, these singular stresses direct attention to *where* failure is likely to occur, but are useless in themselves for predicting *when* it occurs. It is this latter type of singularity that is of concern in attempting to ensure structural integrity. Accordingly, this type of singularity is the focus here, as well as in Part II of this review.

When stress singularities occur away from concentrated loads, they do so in concert with discontinuities. These discontinuities can be in boundary directions, or in boundary conditions, or in elastic moduli. While such discontinuities do not have to have associated stress singularities, often they do. *Discontinuity singularities* are thus far from rare in elasticity (Part II of this review amplifies their occurrence further).

At the outset in dealing with discontinuity singularities, it is essential that their *participation be recognized*. Otherwise one risks making stress-strength comparisons in their presence, an exercise in futility. Given recognition of a discontinuity singularity, the engineer has three options in seeking to ensure structural integrity.

i) To rely primarily on testing and forego analysis, other than perhaps nominal (1D) stress analysis.
ii) To proceed with classical stress analysis (2D or 3D), then try to interpret the stress singularity.
iii) To improve the modeling so that the singularity is replaced with physically sensible stresses that can be compared with strengths.

For the all-important first step of identifying the presence of a stress singularity in elasticity, two types of analysis are available: analytical asymptotics and numerical methods.

With respect to *asymptotics*, three principal approaches exist for 2D analysis: via the Airy stress function, via Kolossoff-Muskhelishvili complex potentials, and via the Mellin transform. These approaches are well developed at this time. Properly implemented, all three identify the same stress singularities: Hence, the choice of which to use is largely a matter of personal preference. In two dimensions, the various elastic stress singularities actually identified to date with these approaches may be summarized as follows. For any stress component σ, as the singular point is approached, elasticity can have:

$$\sigma = O(r^{-\gamma}\cos(\eta \ln r)) + O(r^{-\gamma}\sin(\eta \ln r))$$

$$\sigma = O(r^{-\gamma}\ln r) + O(r^{-\gamma})$$

$$\sigma = O(r^{-\gamma})$$

$$\sigma = \mathrm{ord}(\ln^2 r) + \mathrm{ord}(\ln r) \tag{5.1}$$

$$\sigma = \mathrm{ord}(\ln r)$$

$$\sigma = O(\ln r)$$

$$\sigma = O(\cos(\eta \ln r)) + O(\sin(\eta \ln r))$$

as $r \to 0$, wherein γ is the singularity exponent $(0 < \gamma < 1)$, and η is the imaginary part of the eigenvalue involved. In Eqs. (5.1), O is associated with locally homogeneous boundary conditions, ord with locally inhomogeneous (ord being defined in Section 1.2). Corresponding stress fields for plates in extension may be found in Section 4.1, Eqs. (4.7) and (4.17) ($\gamma = 1-\lambda, 1-\xi$, respectively), and in Section 4.2, Eqs. (4.18) and (4.28) ($\gamma = 1-\lambda$). Further corresponding stress fields for other configurations are given in Part II, together with specifics of the numerous configurations that engender such singularities.[32]

With respect to *numerical methods*, the presence of singularities can be *detected* by the divergence of peak stress values. Evidence of divergence requires a suitably refined sequence of discretizations. The sequence recommended here halves discretization intervals on a sequence of at least three analyses. With this approach in 2D FEA, element numbers quadruple with grid refinement. In 3D FEA, element numbers increase by a factor of eight. Even with such levels of computational effort, there is no guarantee that a singularity be detected. However, numerical experiments to date indicate that one is reasonably likely to unearth a singularity's presence with the approach.

Once a discontinuity singularity is known to be present, the singular fields active require special *interpretation* if they are to be used. The foremost such interpretation in elasticity takes the coefficient of the singularity, the stress intensity factor K, as the parameter controlling brittle fracture and failure in general. This remains the basic tenet of linear elastic fracture mechanics (LEFM) even today. While LEFM is concerned primarily with the stress singularities at cracks, it is possible to consider extension of its basic tenet to other singularities.

For the case of cracks within a single material, the practice of LEFM is quite accomplished at this time. In two dimensions in particular, finite element analysis is most capable when it comes to calculating stress intensity factors. The means favored here for resolving the crack-tip stresses is via quarter-point elements (Section 4.4), though certainly other possibilities are available. The most reliable means of extracting K from such an analysis would appear to be via path-independent integrals (Section 4.5). Companion testing is also well controlled and reproducible (Section 3.4). However, while predictions made by LEFM are typically trendwise correct, there are occasions when there is considerable room for improvement in their accuracy (Section 3.4), and extension to other singularities may well face yet greater difficulties in making accurate predictions (Sections 3.2 and 3.3). All told, there would appear to be a good case for at-

[32]The last stress of Eqs. (5.1) is not strictly singular, being bounded as $r \to 0$. However, it is undefined as $r \to 0$, and consequently shares some of the difficulties associated with stress singularities.

tempting to *improve the modeling* so that stress singularities are replaced with physically sensible stresses.

For *conforming contact problems* in elasticity, the removal of singularities is now well understood. This removal is accomplished by the policing of contact inequalities when there are sufficient degrees of freedom in a problem to effect such policing (Section 2.4). Commercial FEA codes are currently available to implement such analysis. Resulting finite stress fields continue to prove to be useful in engineering practice.

For *other singular configurations*, the removal of singularities is nowhere near as mature as it is for conforming contact. However, the real *source of such singularities* is emerging. These singularities do not really stem from the discontinuities present, nor from the field equations of elasticity (Section 2.1). Rather, they stem from a probably unwitting introduction of effectively infinite stiffnesses in cohesive laws. With this appreciation, it would appear to be possible to remove most if not all of the discontinuity singularities of elasticity by ensuring finite stiffnesses (Section 2.3). Such removals can be pursued with or without removing the original discontinuity, indicating the discontinuity's secondary role in the generation of stress singularities. They can also be undertaken without introducing plasticity or large strain effects, though such effects may merit inclusion as loading progresses. Implementation of this type of approach, however, faces some serious challenges. There are modeling issues, analytical tractability concerns, and interpretation questions. Nonetheless, research in this area holds the promise of significant improvements in the physical appropriateness of stress fields in classical elasticity in particular, and in solid mechanics in general.

ACKNOWLEDGMENTS

I am grateful for the numerous comments received from colleagues during the course of preparing this review: JL Beuth, Jr (Carnegie Mellon University), KL Johnson (Cambridge University, UK), G Meda (Corning, Inc), TP Pawlak (ANSYS, Inc), BS Smallwood (Chrysler Corporation), and PS Steif (Carnegie Mellon University). I am also grateful for the careful typing of the manuscript by M Gibb and R Kostyak, and the painstaking preparation of the drawings by K Young (all of Carnegie Mellon). In addition, I am grateful for the thoughtful input of reviewers, and the incorporation of resulting revisions by my wife, Della.

REFERENCES

[1] Thomson (Lord Kelvin) W (1848), Note on the integration of the equations of equilibrium of an elastic solid, *Camb. Dublin Math. J.* **3**, 87–89.
[2] Boussinesq J (1878), Equilibrium of an elastic isotropic half-space supporting different loads in the absence of gravity, *Acad. Sci., Paris, C. R.* **86**, 1260–1263 (in French).
[3] Cerruti V (1882), Studies of the equilibrium of isotropic elastic bodies, *Reale Academia dei Lincei, Serie* 3^a, *Memorie della Classe di Scienze Fisiche, Matematiche e Naturali* **13**, 81–122 (in Italian).
[4] Mindlin RD (1936), Force at a point in the interior of a semi-infinite solid, *Physics (N.Y.)* **7**, 195–202.
[5] Poulos HG, and Davis EH (1974), *Elastic Solutions for Soil and Rock Mechanics*, John Wiley and Sons, Inc, New York, NY.
[6] Michell JH (1900), Elementary distributions of plane stress, *Proc. London Math. Soc.* **32**, 35–61.
[7] Flamant M (1892), On the distribution of stresses in a two-dimensional solid under transverse loading, *Acad. Sci., Paris, C. R.* **114**, 1465–1468 (in French).
[8] Boussinesq J (1892), On the local disturbances which are produced under concentrated loads, uniformly distributed in the out-of-plane direction, and acting on the upper surface of a half-space, either horizontally or as a pair vertically, *Acad. Sci., Paris, C. R.* **114**, 1510–1516 (in French).
[9] Melan E (1932), The state of stress due to a concentrated load applied within a half-plane, *Z. Angew. Math. Mech.* **12**, 343–346 (in German).
[10] Kurshin LM (1959), Mixed plane boundary value problem of the theory of elasticity for a quadrant, *J. Appl. Math. Mech.* **23**, 1403–1408.
[11] Sternberg E, and Eubanks RA (1955), On the concept of concentrated loads and an extension of the uniqueness theorem in the linear theory of elasticity, *J. Ration. Mech. Anal.* **4**, 135–168.
[12] Love AEH (1944), *A Treatise on the Mathematical Theory of Elasticity, 4th Edition*, Dover Publ, New York NY.
[13] Turteltaub MJ, and Sternberg E (1968), On concentrated loads and Green's functions in elastostatics, *Arch. Ration. Mech. Anal.* **29**, 193–240.
[14] Chowdhury KL (1983), Solution of the problem of a concentrated torque on a semi-space by similarity transformations, *J. Elast.* **13**, 87–90.
[15] Chen T (1992), Some remarks on the solutions of a concentrated torque and double forces on an elastic half-space, *ASME J. Appl. Mech.* **59**, 690–692.
[16] Timoshenko SP, and Goodier JN (1970), *Theory of Elasticity, 3rd Edition*, McGraw-Hill Book Co, New York NY.
[17] Kolossoff G (1910), On an application of the theory of complex variables to the two-dimensional problem of elasticity theory, Dissertation, St Petersburg, Russia.
[18] Kolossoff G (1914), On some properties of the plane problem of elasticity theory, *Math. Phys.* **62**, 384–409 (in German).
[19] Inglis CE (1913), Stresses in a plate due to the presence of cracks and sharp corners, *Inst. Nav. Archit. Mar. Eng., Trans.* **55**, 219–241.
[20] Williams ML (1952), Stress singularities resulting from various boundary conditions in angular corners of plates in extension, *ASME J. Appl. Mech.* **19**, 526–528.
[21] Williams ML (1959), The stresses around a fault or crack in dissimilar media, *Bull. Seismol. Soc. Am.* **49**, 199–204.
[22] Sadowsky MA (1928), Two-dimensional problems of elasticity theory, *Z. Angew. Math. Mech.* **8**, 107–121 (in German).
[23] Abramov BM (1937), The problem of contact of an elastic infinite half-plane with an absolutely rigid rough foundation, *C. R. (Dokl.) Acad. Sci. URSS* **17**, 173–178.
[24] Zak AR (1964), Stresses in the vicinity of boundary discontinuities in bodies of revolution, *ASME J. Appl. Mech.* **31**, 150–152.
[25] Dempsey JP, and Sinclair GB (1981), On the singular behavior at the vertex of a bi-material wedge, *J. Elast.* **11**, 317–327.
[26] Thomson W, and Tait PG (1867), *A Treatise on Natural Philosophy*, Cambridge Univ Press, Cambridge, UK (this book is also available in two parts as *Principles of Mechanics and Dynamics*, Dover Pub Inc, New York NY).
[27] Brahtz JHA (1933), Stress distribution in a reentrant corner, *Trans. ASME Ser. E.* **55**, 31–37.
[28] Knein M (1926), On the theory of pressure testing, *Z. Angew. Math. Mech.* **6**, 414–416 (in German).
[29] Dempsey JP, and Sinclair GB (1979), On the stress singularities in the plane elasticity of the composite wedge, *J. Elast.* **9**, 373–391.
[30] Sneddon IN (1951), *Fourier Transforms*, McGraw-Hill Book Co, New York NY.
[31] ABAQUS personnel (1997), *ABAQUS Standard User's Manual*, Revision 5.7, Vol I, Hibbitt, Karlsson and Sorensen Inc, Pawtucket RI.
[32] ANSYS personnel (1995), *ANSYS User's Manual*, Revision 5.2, Vol I, ANSYS Inc, Canonsburg PA.
[33] Sinclair GB, and Epps BE (2002), On the logarithmic stress singularities induced by the use of displacement shape functions in boundary conditions in submodelling, *Commun. Numer. Methods Eng.* **18**, 121–130.
[34] Frisch-Fay R (1962), *Flexible Bars*, Butterworth Inc, Washington DC.
[35] Kondo M, and Sinclair GB (1985), A simple substructuring procedure for finite element analysis of stress concentrations, *Commun. Numer. Methods Eng.* **1**, 215–218.
[36] Cherepanov GP (1967), Crack propagation in continuous media, *J. Appl. Math. Mech.* **31**, 503–512.
[37] Hutchinson JW (1968), Singular behaviour at the end of a tensile crack in a hardening material, *J. Mech. Phys. Solids* **16**, 13–31.
[38] Rice JR, and Rosengren GF (1968), Plane strain deformation near a

crack tip in a power-law hardening material, *J. Mech. Phys. Solids* **16**, 1–12.
[39] Ramberg W, and Osgood WR (1943), Description of stress-strain curves by three parameters, Tech Note 902, Natl Advisory Committee on Aeronautics, Washington DC.
[40] Chao YT, and Yang S (1992), Singularities at the apex of a sharp V-notch in a linear strain hardening material, *Int. J. Fract.* **57**, 47–60.
[41] Rudge MRH, and Tiernan DM (1995), Interfacial stress singularities in a bimaterial wedge, *Int. J. Fract.* **74**, 63–75.
[42] Zhang N, and Joseph PF (1998), A nonlinear finite element eigenanalysis of singular plane stress fields in bimaterial wedges including complex eigenvalues, *Int. J. Fract.* **90**, 175–207.
[43] Wong FS, and Shield RT (1969), Large plane deformations of thin elastic sheets of neo-Hookean material, *Z. Angew. Math. Phys.* **20**, 176–199.
[44] Knowles JK, and Sternberg E (1973), An asymptotic finite-deformation analysis of the elastostatic field near the tip of a crack, *J. Elast.* **3**, 67–107.
[45] Knowles JK, and Sternberg E (1974), Finite-deformation analysis of the elastostatic field near the tip of a crack: Reconsideration and higher-order results, *J. Elast.* **4**, 201–233.
[46] Geubelle PH, and Knauss WG (1994), Finite strains at the tip of a crack in a sheet of hyperelastic material: I. Homogeneous case, *J. Elast.* **35**, 61–98.
[47] Geubelle PH, and Knauss WG (1994), Finite strains at the tip of a crack in a sheet of hyperelastic material: II. Special bimaterial cases, and III. General bimaterial case, *J. Elast.* **35**, 99–174.
[48] Knowles JK, and Sternberg E (1975), On the singularity induced by certain mixed boundary conditions in linearized and nonlinear elasticity, *Int. J. Solids Struct.* **11**, 1173–1201.
[49] Ru CQ (1997), Finite deformations at the vertex of a bi-material wedge, *Int. J. Fract.* **84**, 325–350.
[50] Duva JM (1990), The singularity strength at the apex of a wedge undergoing finite deformation, *ASME J. Appl. Mech.* **57**, 577–580.
[51] Griffith AA (1920), The phenomena of rupture and flow in solids, *Philos. Trans. R. Soc. London, Ser. A* **A221**, 163–198.
[52] Mansfield EH (1967), On the stresses near a crack in an elastic sheet, Tech Report 67030, Royal Aircraft Est, Cranfield UK.
[53] Truesdell C (1952), The mechanical foundations of elasticity and fluid dynamics, *J. Ration. Mech. Anal.* **1**, 125–300; (1953), **2**, 593–616.
[54] Zheltov YuP, and Khristianovitch SA (1955), On the mechanism of hydraulic fracture of an oil bearing stratum, *Izvestiya Akademiia Nauk SSSR, Otd. Tekhn. Nauk* **5**, 3–41 (in Russian).
[55] Tada H, Paris PC, and Irwin GR (1985), *The Stress Analysis of Cracks Handbook, 2nd Edition*, Paris Productions Inc, St Louis MO.
[56] Barenblatt GL (1959), On the equilibrium of cracks due to brittle fracture, *Dokl. Akad. Nauk SSSR* **127**, 47–50 (in Russian).
[57] Barenblatt GI (1962), The mathematical theory of equilibrium cracks in brittle fracture, *Adv. Appl. Mech.* **7**, 55–129.
[58] Willis JR (1967), A comparison of the fracture criteria of Griffith and Barenblatt, *J. Mech. Phys. Solids* **15**, 151–162.
[59] Goodier JN (1968), Mathematical theory of equilibrium cracks, *Fracture, An Advanced Treatise* H Liebowitz (ed), Vol II, Academic Press, New York NY, 1–66.
[60] Peierls R (1940), The size of a dislocation, *Proc. Phys. Soc. London* **52**, 34–37.
[61] Hirth JP, and Lothe L (1968), *Theory of Dislocations*, McGraw-Hill Book Co, New York NY.
[62] Cherepanov GP (1979), *Mechanics of Brittle Fracture*, McGraw-Hill Book Co, New York NY.
[63] Lennard-Jones JE (1931), Cohesion, *Proc. Phys. Soc. London* **43**, 461–482.
[64] Israelachvili JN (1992), *Intermolecular and Surface Forces, 2nd Edition*, Academic Press, San Diego CA.
[65] Lamé MG (1852), *Lectures on the Mathematical Theory of the Elasticity of Solid Bodies*, Bachelier Pub, Paris, France (in French).
[66] Sinclair GB, and Meda G (2001), On some anomalies in Lamé's solutions for elastic solids with holes, *ASME J. Appl. Mech.* **68**, 132–134.
[67] Sinclair GB (1996), On the influence of cohesive stress-separation laws on elastic stress singularities, *J. Elast.* **44**, 203–221.
[68] Sinclair GB (1999), A bibliography on the use of cohesive laws in solid mechanics, Report SM 99-8, Dept of Mech Eng, Carnegie Mellon Univ, Pittsburgh PA.
[69] Cribb JL, and Tomkins B (1967), On the nature of the stress at the tip of a perfectly brittle crack, *J. Mech. Phys. Solids* **15**, 135–140.
[70] Needleman A (1994), Computational modeling of material failure, *Proc of 12th US Nat Congress of Appl Mech*, Seattle WA, S34–S42.
[71] Sinclair GB, Meda G, and Smallwood BS (1995), On the physical stress field for the Griffith crack, *Proc of 15th Canadian Congress of Appl Mech*, Victoria, British Columbia, **1**, 210–211.
[72] Sinclair GB (2000), Ridding elastic configurations of stress singularities, *Proc of 20th Southeastern Conf of Theoretical and Appl Mech*, Callaway Gardens, GA, pp SM93.1–8.
[73] Johnson KL (1985), *Contact Mechanics*, Cambridge Univ Press, Cambridge, UK.
[74] Hertz H (1882), On the contact of elastic solids, *J. Reine Angew. Math.* **92**, 156–171 (in German: for an account in English, see Johnson [73], Ch 4).
[75] Steuermann E (1939), To Hertz's theory of local deformations in compressed elastic bodies, *C. R. (Dokl.) Acad. Sci. URSS* **25**, 359–361.
[76] Persson A (1964), On the stress distribution of cylindrical elastic bodies in contact, Dissertation, Chalmers Univ of Technology, Göteborg, Sweden.
[77] Gladwell GML (1980), *Contact Problems in the Classical Theory of Elasticity*, Sijthoff and Noordhoff Int Pub, Alphen aan den Rijn, The Netherlands.
[78] Mossakovskii VI (1954), The fundamental mixed problem of the theory of elasticity for a half-space with a circular line separating the boundary conditions, *Prikl. Mat. Mekh.* **18**, 187–196 (in Russian).
[79] Goodman LE (1962), Contact stress analysis of normally loaded rough spheres, *ASME J. Appl. Mech.* **29**, 515–522.
[80] Mossakovskii VI (1963), Compression of elastic bodies under conditions of adhesion (axisymmetric case), *J. Appl. Math. Mech.* **27**, 630–643.
[81] Spence DA (1968), Self similar solutions to adhesive contact problems with incremental loading, *Proc. R. Soc. London, Ser. A* **A305**, 55–80.
[82] Spence DA (1975), The Hertz contact problem with finite friction, *J. Elast.* **5**, 297–319.
[83] Dundurs J, and Comninou M (1979), Some consequences of the inequality conditions in contact and crack problems, *J. Elast.* **9**, 71–82.
[84] Irwin GR (1957), Analysis of stresses and strains near the end of a crack traversing a plate, *ASME J. Appl. Mech.* **24**, 361–364.
[85] Keating RF, and Sinclair GB (1995), On the fundamental energy argument of elastic fracture mechanics, *Int. J. Fract.* **74**, 43–61.
[86] Eshelby JD (1951), The force on an elastic singularity, *Philos. Trans. R. Soc. London, Ser. A* **A244**, 87–112.
[87] Sanders Jr JL (1960), On the Griffith-Irwin fracture theory, *ASME J. Appl. Mech.* **27**, 352–353.
[88] Rice JR (1968), A path independent integral and the approximate analysis of strain concentration by notches and cracks, *ASME J. Appl. Mech.* **35**, 379–386.
[89] Irwin GR (1948), Fracture dynamics, *Fracturing of Metals*, Am Soc for Metals, Cleveland OH, 147–166.
[90] Orowan E (1949), Fracture and strength of solids, *Reports on Progress in Physics* **12**, 185–232.
[91] England AH (1965), A crack between dissimilar media, *ASME J. Appl. Mech.* **32**, 400–402.
[92] Comninou M (1977), The interface crack, *ASME J. Appl. Mech.* **44**, 631–636.
[93] Sinclair GB (1980), On the stress singularity at an interface crack, *Int. J. Fract.* **16**, 111–119.
[94] Atkinson C (1977), On stress singularities and interfaces in linear elastic fracture mechanics, *Int. J. Fract.* **13**, 807–820.
[95] He M-Y, and Hutchinson JW (1989), Kinking of a crack out of an interface, *ASME J. Appl. Mech.* **56**, 270–278.
[96] Suo Z, and Hutchinson JW (1989), Sandwich test specimens for measuring interface crack toughness, *Mater. Sci. Eng., A* **A107**, 135–143.
[97] Malyshev BM, and Salganik RL (1965), The strength of adhesive joints using the theory of cracks, *Int. J. Fract. Mech.* **1**, 114–128.
[98] Comninou M (1990), An overview of interface cracks, *Eng. Fract. Mech.* **37**, 197–208.
[99] Knowles JK, and Pucik TA (1973), Uniqueness for plane crack problems in linear elastostatics, *J. Elast.* **39**, 223–236.
[100] Irwin GR (1960), Fracture mechanics, *Structural Mechanics, Proc of 1st Symp on Naval Structural Mechanics* JN Goodier and NJ Hoff (eds), Pergamon Press, Oxford, UK, 557–591.
[101] Rice JR (1968), Mathematical analysis in the mechanics of fracture, *Fracture, An Advanced Treatise* H Liebowitz (ed), Vol II, Academic Press, New York, NY 191–311.
[102] Erdogan F, and Sih GC (1963), On the crack extension in plates under plane loading and transverse shear, *ASME J. Basic Eng.* **85**, 519–527.
[103] Rice JR (1988), Elastic fracture mechanics concepts for interfacial cracks, *ASME J. Appl. Mech.* **55**, 98–103.
[104] Hutchinson JW, and Suo Z (1991), Mixed mode cracking in layered materials, *Adv. Appl. Mech.* **29**, 63–191.

[105] Rooke DP, and Cartwright DJ (1976), *Compendium of Stress Intensity Factors*, Hillingdon Press, Uxbridge, Middlesex, UK.
[106] Sih GC (1973), *Handbook of Stress Intensity Factors*, Vol 1, Inst of Fracture and Solid Mechanics, Lehigh Univ, Bethlehem PA.
[107] Murakami Y, Aoki S, Hasebe N, Itoh Y, Miyata H, Miyazaki N, Terada H, Tohgo K, Toya M, and Yuuki R (1987), *Stress Intensity Factors Handbook*, Vol 1, Pergamon Press, Oxford, UK.
[108] Murakami Y, Aoki S, Hasebe N, Itoh Y, Miyata H, Miyazaki N, Terada H, Tohgo K, Toya M, and Yuuki R (1990), *Stress Intensity Factors Handbook*, Vol 2, Revised Edition, Pergamon Press, Oxford, UK.
[109] Murakami Y, Hanson MT, Hasebe N, Itoh Y, Kishimoto K, Miyata H, Miyazaki N, Terada H, Tohgo K, and Yuuki R (1992), *Stress Intensity Factors Handbook*, Vol 3, Pergamon Press, Oxford, UK.
[110] Srawley JE, and Brown Jr, WF (1965), Fracture toughness testing methods, *Fracture Toughness Testing and Its Applications*, STP No 381, Am Soc for Testing and Materials, Philadelphia, PA 133–196.
[111] ASTM (1998), Standard test method for plane-strain fracture toughness of metallic materials, E399-90 (reapproved 1997), *1998 Annual Book of ASTM Standards*, Vol 3.01, Am Soc for Testing and Materials, Philadelphia PA, 413–443.
[112] Heyer RH, and McCabe DE (1970) Evaluation of a method of test for plane strain fracture toughness using a bend specimen, *Review of Developments in Plane Strain Fracture Toughness Testing*, STP No 463, Am Soc for Testing and Materials, Philadelphia PA, 22–41.
[113] McCabe DE (1972), Evaluation of the compact tension specimen for determining plane strain fracture toughness of high strength materials, *J. Mater.* **7**, 449–454.
[114] Underwood JH, and Kendall DP (1978), Cooperative plane strain fracture toughness tests with C-shaped specimens, *J. Test. Eval.* **6**, 296–300.
[115] Hudson CM, and Seward SK (1978), A compendium of sources of fracture toughness and fatigue-crack growth data for metallic alloys, *Int. J. Fract.* **14**, R151–R184.
[116] Hudson CM, and Seward SK (1982), A compendium of sources of fracture toughness and fatigue-crack growth data for metallic alloys—Part II, *Int. J. Fract.* **20**, R59–R117.
[117] Hudson CM, and Seward SK (1989), A compendium of sources of fracture toughness and fatigue-crack growth data for metallic alloys—Part III, *Int. J. Fract.* **39**, R43–R63.
[118] Hoysan SF, and Sinclair GB (1993), On the variability of fracture toughness, *Int. J. Fract.* **60**, R43–R49.
[119] Sinclair GB, and Chambers AE (1987), Strength size effects and fracture mechanics: What does the physical evidence say? *Eng. Fract. Mech.* **26**, 279–310.
[120] Sinclair GB, and Pieri RV (1990), On obtaining fatigue crack growth parameters from the literature, *Int. J. Fatigue* **12**, 57–62.
[121] Chamis CC (1969), Failure criteria for filamentary composites, NASA Tech Note D-5367, NASA, Washington DC.
[122] Valliappan S, Kjellberg S, and Svensson NL (1980), Finite element analysis of total hip prosthesis, *Proc of Int Conf on Finite Elements in Biomechanics*, Tucson AZ, Vol 2, 527–548.
[123] Belie RG, and Reddy JN (1980), Direct prediction of fracture for two-dimensional plane stress structures, *Comput. Struct.* **11**, 49–53.
[124] Kim YJ, and Hsu TR (1982), A numerical analysis on stable crack growth under increasing load, *Int. J. Fract.* **20**, 17–32.
[125] Chen C-N (1993), Nonlinear fracture assessment by using the finite element method, *Eng. Fract. Mech.* **46**, 57–77.
[126] Wells AA (1961), Unstable crack propagation in metals—Cleavage and fast fracture, *Proc of the Crack Propagation Symp*, Cranfield, UK, Vol 1, 210–230.
[127] Andersson H (1973), A finite-element representation of stable crack-growth, *J. Mech. Phys. Solids* **21**, 337–356.
[128] British Standards Inst (1979), Methods for crack opening displacement (COD) testing, BS 5762, British Standards Inst, London, UK.
[129] ASTM (1998), Standard test method for crack-tip opening displacement (CTOD) fracture toughness measurement, E1290-93, *1998 Annual Book of ASTM Standards*, Vol. 3.01, Am Soc for Testing and Materials, Philadelphia, PA, 814–823.
[130] Cottrell AH (1961), Theoretical aspects of radiation damage and brittle fracture in steels, *Steels for Reactor Pressure Circuits*, Special Report No 69, Iron and Steel Inst, London, UK, 281–296.
[131] Burdekin FM (1981), Assessment of defects: The C.O.D. approach, *Philos. Trans. R. Soc. London, Ser. A* **A299**, 155–167.
[132] Sinclair GB (1985), Some inherently unreliable practices in present day fracture mechanics, *Int. J. Fract.* **28**, 3–16.
[133] Williams ML (1951), Surface stress singularities resulting from various boundary conditions in angular corners of plates under bending, *Proc of 1st US Natl Congress of Appl Mech*, Illinois Inst of Tech, Chicago IL, 325–329.
[134] Kitover KA (1952), On the use of special systems of biharmonic functions for the solution of some problems in the theory of elasticity, *Prikl. Mat. Mekh.* **16**, 739–748 (in Russian).
[135] Huth JH (1953), The complex-variable approach to stress singularities, *ASME J. Appl. Mech.* **20**, 561–562.
[136] Williams ML (1956), The complex-variable approach to stress singularities—II, *ASME J. Appl. Mech.* **23**, 477–478.
[137] Bogy DB (1968), Edge-bonded dissimilar orthogonal elastic wedges under normal and shear loading, *ASME J. Appl. Mech.* **35**, 460–466.
[138] Tranter CJ (1948), The use of the Mellin transform in finding the stress distribution in an infinite wedge, *Q. J. Mech. Appl. Math.* **1**, 125–130.
[139] Coker EG, and Filon LNG (1931), *A Treatise on Photo-Elasticity*, Cambridge Univ Press, UK.
[140] Williams ML (1957), On the stress distribution at the base of a stationary crack, *ASME J. Appl. Mech.* **24**, 109–114.
[141] Bogy DB (1970), On the problem of edge-bonded elastic quarter-planes loaded at the boundary, *Int. J. Solids Struct.* **6**, 1287–1313.
[142] Bogy DB, and Wang KC (1971), Stress singularities at interface corners in bonded dissimilar isotropic elastic materials, *Int. J. Solids Struct.* **7**, 993–1005.
[143] Dempsey JP (1981), The wedge subjected to tractions: A paradox resolved, *J. Elast.* **11**, 1–10.
[144] Ting TCT (1984), The wedge subjected to tractions: A paradox re-examined, *J. Elast.* **14**, 235–247.
[145] Ting TCT (1996), Paradoxes puzzles, and dilemmas in mechanics, *Chinese J. Mech.* **12**, 25–32.
[146] Sinclair GB (1980), On the singular eigenfunctions for plane harmonic problems in composite regions, *ASME J. Appl. Mech.* **47**, 87–92.
[147] Ting TCT (1985), Asymptotic solution near the apex of an elastic wedge with curved boundaries, *Q. Appl. Math.* **42**, 467–476.
[148] Atkinson C (1979), Stress singularities and fracture mechanics, *Appl. Mech. Rev.* **32**, 123–135.
[149] Hwang KC, Yu SW, and Yang W (1990), Theoretical study of crack-tip singularity fields in China, *Appl. Mech. Rev.* **43**, 19–33.
[150] Murakami Y (1992), Stress singularity for notch at bimaterial interface, *Stress Intensity Factors Handbook*, Vol 3, Murakami *et al* Pergamon Press, Oxford, UK, Ch 18, 963–1062.
[151] Sinclair GB (1998), FEA of singular elasticity problems, *Proc of 8th Int ANSYS Conf*, Pittsburgh, PA, Vol 1, 225–236.
[152] Westergaard HM (1939), Bearing pressures and cracks, *ASME J. Appl. Mech.* **6**, A-49–A-53.
[153] Gallagher RH (1978), A review of finite element techniques in fracture mechanics, *Proc of 1st Int Conf on Numerical Methods in Fracture Mechanics*, AR Luxmoore and DRJ Owen (eds), Univ of Wales, Swansea UK, 1–25.
[154] Luxmoore AR, and Owen DRJ (eds) (1978), *Proceedings of the First International Conference on Numerical Methods in Fracture Mechanics*, Univ of Wales, Swansea, UK.
[155] Luxmoore AR, and Owen DRJ (eds) (1980), *Proceedings of the Second International Conference on Numerical Methods in Fracture Mechanics*, Univ of Wales, Swansea, UK.
[156] Luxmoore AR, and Owen DRJ (eds) (1984), *Proceedings of the Third International Conference on Numerical Methods in Fracture Mechanics*, Univ of Wales, Swansea, UK.
[157] Luxmoore AR, Owen DRJ, Rajapakse YPS, and Kanninen MF (eds) (1987), *Proceedings of the Fourth International Conference on Numerical Methods in Fracture Mechanics*, Southwest Research Institute, San Antonio, TX.
[158] Luxmoore AR, and Owen DRJ (eds) (1990), *Proceedings of the Fifth International Conference on Numerical Methods in Fracture Mechanics*, FhG Inst für Werkstoffmechnik, Freiburg, Germany.
[159] Henshell RD, and Shaw KG (1975), Crack tip finite elements are unnecessary, *Int. J. Numer. Methods Eng.* **9**, 495–507.
[160] Barsoum RS (1976), On the use of isoparametric finite elements in linear fracture mechanics, *Int. J. Numer. Methods Eng.* **10**, 25–37.
[161] Wait R (1978), Finite element methods for elliptic problems with singularities, *Comput. Methods Appl. Mech. Eng.* **13**, 141–150.
[162] Lim IL, Johnston IW, and Choi SK (1993), Application of singular quadratic distorted isoparametric elements in linear fracture mechanics, *Int. J. Numer. Methods Eng.* **36**, 2473–2499.
[163] Meda G, and Sinclair GB (1994), On the use of the H-integral to extract stress intensity factors, *Proc of 6th Int ANSYS Conf*, Pittsburgh PA, Vol 2, 6.39–6.60.
[164] Irwin GR (1958), Fracture, *Handbuch der Physik*, Springer-Verlag Ltd, Berlin, Germany, Vol VI, 551–590.

[165] Cooper DB, Meda G, and Sinclair GB (1995), A comparison of crack-flank displacement fitting for estimating *K* with a path independent integral, *Int. J. Fract.* **70**, 237–251.
[166] Chan SK, Tuba IS, and Wilson WK (1970), On the finite element method in linear fracture mechanics, *Eng. Fract. Mech.* **2**, 1–17.
[167] Parks DM (1974), A stiffness derivative finite element technique for determination of crack tip stress intensity factors, *Int. J. Fract.* **10**, 487–502.
[168] Rybicki EF, and Kanninen MF (1977), A finite element calculation of stress intensity factors by a modified crack closure integral, *Eng. Fract. Mech.* **9**, 931–938.
[169] Stern M (1973), A boundary integral representation for stress intensity factors, *Proc of 10th Anniversary Meeting of the Soc of Engineering Science*, Raleigh, NC, 125–132.
[170] Stern M, Becker EB, and Dunham RS (1976), A contour integral computation of mixed-mode stress intensity factors, *Int. J. Fract.* **12**, 359–368.
[171] Stern M, and Soni ML (1976), On the computation of stress intensities at fixed-free corners, *Int. J. Solids Struct.* **12**, 331–337.
[172] Hong C-C, and Stern M (1978), The computation of stress intensity factors in dissimilar materials, *J. Elast.* **8**, 21–34.
[173] Carpenter WC (1984), Calculation of fracture mechanics parameters for a general corner, *Int. J. Fract.* **24**, 45–58.
[174] Sinclair GB, Okajima M, and Griffin JH (1984), Path independent integrals for computing stress intensity factors at sharp notches in elastic plates, *Int. J. Numer. Methods Eng.* **20**, 999–1008 (see also (1985), *Int. J. Fract.* **27**, R81–R85).
[175] Okajima M, and Sinclair GB (1986), The C-integral: A path independent integral for computing singularity participation at a butt joint, *Proc of Int Conf on Computational Mech*, Tokyo, Japan, Vol 1, V11–V16.
[176] Carpenter WC, and Byers C (1987), A path independent integral for computing stress intensities for V-notched cracks in a bi-material, *Int. J. Fract.* **35**, 245–268.
[177] Banks-Sills L (1997), A conservative integral for determining stress intensity factors of a bimaterial strip, *Int. J. Fract.* **86**, 385–398.
[178] Banks-Sills L, and Sherman D (1986), Comparison of methods for calculating stress intensity factors with quarter-point elements, *Int. J. Fract.* **32**, 127–140.
[179] Pang HLJ (1993), Linear elastic fracture mechanics benchmarks: 2D finite element test cases, *Eng. Fract. Mech.* **44**, 741–751.
[180] Pang HLJ, and Leggat RH (1990), 2D test cases in linear elastic fracture mechanics, Report R0020, National Agency for Finite Element Methods and Standards, Glasgow, UK.
[181] Banks-Sills L (1991), Application of the finite element method to linear elastic fracture mechanics, *Appl. Mech. Rev.* **44**, 447–461.
[182] Meda G, Messner TW, Sinclair GB, and Solecki JS (1996), Path-independent *H* integrals for three-dimensional fracture mechanics, *Int. J. Fract.* **94**, 217–234.

Glenn Sinclair *received his undergraduate education from the University of Auckland in New Zealand. He graduated with a BS in Mathematics in 1967 and a BE in Engineering Science in 1969. He then attended Caltech, graduating with a PhD in Applied Mechanics in 1972. He has since served on the faculty of Yale University, the University of Auckland, Carnegie Mellon University, and Louisiana State University, where he is currently the Francis S Blummer Professor of Mechanical Engineering. His research is primarily concerned with fracture mechanics, tribology, and numerical methods. Recent interests focus on finding means of improving modeling so that stress and pressure singularities are removed from both solid and fluid mechanics problems, and submodeling procedures and verification techniques for finite element analysis.*